THE IDIOSYNCRATIC GROWTH OF THIN FILMS OF TETRACENE

A Dissertation

Presented to the Faculty of the Graduate School

of Cornell University

In Partial Fulfillment of the Requirements for the Degree of

Doctor of Philosophy

by

Rambert Kennith Nahm

20 August 2018

THE COMPLEXITIES OF THE THIN-FILM GROWTH OF TETRACENE REVEALED BY SYNCHROTRON X-RAY SCATTERING

Rambert Kennith Nahm, Ph. D.

Cornell University 2018

The thin-film growth of semiconducting organic molecules, and the molecular interactions and processes therein, for application in organic electronics has been a topic of great interest. Here, we will present our investigations on the thin-film growth of tetracene, a polyaromatic hydrocarbon, whose simple structure belies the complex nature of growth revealed by synchrotron X-ray scattering. Although tetracene is structurally very similar to pentacene, we find that the nature of the thin-film growth on SiO_2 of tetracene is quite different from that of pentacene. At a substrate temperature of $T_s \sim 30$ °C, we observe two unusual phenomena. First, using *in situ* X-ray reflectivity at the anti-Bragg condition, we observe a transition from 3D island growth to 2D layer-by-layer growth of tetracene as the growth rate is increased. We use *ex situ* atomic force microscopy to determine that upward transport drives 3D island growth. The transition from 3D growth to 2D growth occurs when the rate of admolecule attachment at the tetracene island/SiO_2 substrate edges, which is related to growth rate, effectively outcompetes the rate of upward step-edge transport. Second, using *in situ* grazing incidence X-ray diffraction, we observe a transition from growth of only a thin-film phase to growth of a bulk phase. We observe that the bulk phase appears at lower thickness and that there is a lower contribution of the thin-film phase for slower growth rate than for faster growth rates. This is due to significant reorganization at slower growth rates, resulting in molecules traversing upwards on

islands and escaping the influence of the substrate and relaxing into the bulk phase. Furthermore, we find that at $T_s \sim 0$ °C, the transition from 3D to 2D growth occurs at a much lower growth rate than at $T_s \sim 30$ °C, and we observe a lack of evidence for bulk-phase growth. This suggests that the rate of upward transport is suppressed at lower temperatures. Finally, we find that even by matching the surface energy of the substrate (with a pre-deposited layer of pentacene) and tetracene, there is still significant upward transport, although there is less than on pristine SiO_2.

BIOGRAPHICAL SKETCH

Rambert finished his K-12 education in Colorado, receiving his International Baccalaureate (IB) diploma after completing the IB program at Thornton High School in 2007. He remained in Colorado for his undergraduate studies at Colorado School of Mines (CSM), graduating magna cum laude with a B.S. in Chemical Engineering in 2010. While at CSM, he participated in research under Prof. Colin A. Wolden in Chemical Engineering, where he was exposed to the world of semiconductors and nanofabrication. Having no desire to work for oil companies and a keen interest in silicon-based technology, he decided to become a researcher in the field of microelectronics. To this end, Rambert chose to pursue a Ph. D. at Cornell University under the tutelage of Prof. James R. Engstrom, where he has studied the growth of thin films using a variety of techniques. He was awarded the Lester B. Knight Fellowship from 2010-2011 and the National Science Foundation IGERT Fellowship from 2011-2013. As an IGERT fellow, he was afforded the opportunity to spend part of the summer in 2012 in an externship in the lab of Prof. Dr. Frank Schreiber at Universität Tübingen in Germany. Rambert was also fortunate enough to have an internship during the summer of 2014 in the Components Research group at Intel Corp, in Hillsboro, Oregon. In addition to research, he enjoyed being a teaching assistant over the course of five semesters for three separate courses: CHEME 3720, 4840, and 6610. After his Ph. D., he will be starting as a module engineer in the Portland Technology Development (PTD) group at Intel Corp. in Hillsboro, Oregon.

To all who have made me smile, made me laugh.

Your warmth and support brought me here.

ACKNOWLEDGMENTS

There are many people who helped me get to where I am now that I would like to thank. First and foremost, I want to express my sincerest appreciation and gratitude for my advisor, Prof. James R. Engstrom. His fastidious approach to science and desire for excellence are qualities which have helped me become the researcher I am today and are qualities that will continue guiding me throughout the rest of my career. Jim, as the lab members call him, has not only made me a better scientist, but has also provided me with opportunities that have enriched my graduate career. He nominated me for an NSF IGERT fellowship and also provided the connection that led to my internship at Intel. I have also had the pleasure of being his teaching assistant for three semesters of CHEME 4840 and one semester of CHEME 3720. I will forever be thankful for his patience, support, and guidance. Because of him, I have had what I consider to be an enviable graduate career.

I would like to also express my thanks to my major and minor committee members, Prof. Tobias Hanrath and Prof. Darrell Schlom, for their input over the years. I especially want to thank my remaining committee member, Dr. Arthur Woll, for all of his assistance from when I started performing experiments at Cornell High Energy Synchrotron Source (CHESS) to now. His expertise in all things X-rays make him an invaluable resource, and he has been instrumental in setting up many of the experiments involving X-rays discussed in this dissertation. I am grateful to him for humoring me with discussion whenever I stopped by his office unannounced with questions.

The Engstrom Research Group is built upon strong teamwork, and I have been fortunate enough to have worked with exceptional people who I must thank as I would not be here without them. When I first started in the lab, Dr. Kevin Hughes and Dr.

Wenyu Zhang introduced me to the ultrahigh vacuum system in 312 Olin Hall and trained me on that system. While I did not overlap with Kevin for long, he provided helpful insight when I was writing proposals for fellowship applications and the qualifying exam. I worked closely with Wenyu for nearly 2 years, working on X-ray photoelectron spectroscopy and low energy ion scattering spectroscopy of inorganic thin films. I then worked with Dr. Edward Kish, who trained me on the G-line system, on investigating the thin-film growth of various organic molecules on various surfaces. Jade Noble assisted me with at least the first couple of CHESS runs where I was the project lead and helped me in our efforts to reboot our projects using scanning tunneling microscopy. I briefly worked with Jiun-Ruey Chen on designing a micro-reactor for studying ALD in the 312 chamber. The two newest members of our group, Hugh Bullen and Taewon Suh, have been extraordinary help for CHESS runs since early 2015. I am confident that all of the current junior members, Jiun-Ruey, Hugh, and Taewon, will have successful careers as they move forward. I cannot forget to also acknowledge the undergraduate researchers who have helped me along the way: Harris Karsch, Kevin Hung, Bryan Malecky, and James Dong.

In my personal life, I want to thank all of my friends I have made at Cornell for their support. They are too numerous to list here, but their encouragement and understanding pushed me through the difficult times. Some notables include some former roommates: Dr. Brian Koo, Dr. Lindsey Crawford, and Justin Rosch. Finally, I thank all of my friends and family back in Colorado for their unwavering support, encouragement, and love. I would not be the person I am today and would not have had the opportunities that led me here without them.

I am grateful to the following organizations for the financial support I have received: the Lester B. Knight Foundation, the National Science Foundation IGERT program, and Cornell University's Atkinson Center for a Sustainable Future.

TABLE OF CONTENTS

Abstract i
Biographical sketch iii
Dedication iv
Acknowledgements v
List of figures x
List of tables xvi
List of abbreviations xvii
List of symbols xviii

1. Introduction 1
1.1 Overview 1
1.2 Thin-film deposition of organic semiconductors 2
1.3 Tetracene 5
1.4 References 7
2. Experimental techniques 12
2.1 Overview 12
2.2 Substrate preparation 12
2.3 Organic thin film deposition and the G-line chamber 13
2.4 X-ray scattering techniques 17
2.4.1 Scattering at the anti-Bragg condition and the Trofimov model 18
2.4.2 Grazing incidence diffraction 22
2.5 Atomic force microscopy 24
2.6 References 25
3. Unexpected effects of the rate of deposition on the mode of growth and morphology of thin films of tetracene grown on silicon dioxide 27
3.1 Abstract 27
3.2 Introduction 28
3.3 Experimental Procedures 29
3.4 Results 31

3.5 Discussion 43
3.6 Conclusions 51
3.7 Acknowledgements 52
3.8 References 54

4. Who's on first? Tracking in real time the growth of multiple crystalline phases of an organic semiconductor: Tetracene on silicon dioxide 58

4.1 Abstract 58
4.2 Introduction 59
4.3 Experimental Procedures 60
4.4 Results 61
4.5 Discussion 74
4.6 Conclusions 81
4.7 Acknowledgements 82
4.8 References 83

5. Faster is smoother and so is lower temperature: The curious case of thin film growth of tetracene on silicon dioxide 87

5.1 Abstract 87
5.2 Introduction 88
5.3 Experimental Procedures 89
5.4 Results 90
5.5 Discussion 102
5.6 Conclusions 112
5.7 Acknowledgements 113
5.8 References 114

6. The role of surface energy in the growth of thin films of tetracene on thin films of pentacene on silicon dioxide 118

6.1 Abstract 118
6.2 Introduction 119
6.3 Experimental Procedures 120
6.4 Results and Discussion 121
6.5 Conclusions 129
6.6 Acknowledgements 132

6.7 References 133
7. Conclusions and future work 136

Appendix 140
A.1 Sample cooling in the G-line chamber..... 140
A.2 Fitting Pseudo-Voigt functional to GID in MATLAB 143

LIST OF FIGURES

Figure 1-1 Schematic representation of various processes during thin-film growth. Molecules are simply represented as circles, although many are anisotropic.

Figure 2-1 Photograph of the G-line table mounted on the diffractometer in the G3 hutch at CHESS.

Figure 2-2 A schematic cutaway of the inside of the chamber from CAD software.

Figure 2-3 **(a)** Scattered X-ray intensity at the anti-Bragg condition as a function of time for ideal 2D LbL growth (solid blue line, left ordinate). The solid black lines represent the layer coverages as a function of time (right ordinate). Similar figures are shown for a case with 2D LbL for 1 ML in **(b)** and for a case with 3D growth in **(c)**. The evolution of RMS roughness as a function of time for these cases are shown in **(d)**.

Figure 3-1 **(a)** Scattered X-ray intensity at the anti-Bragg condition as a function of time for thin films of tetracene grown on SiO_2 at 0.036 nm-s^{-1}, represented by the open circles (left ordinate, every 10^{th} data point shown for visibility). The solid blue line (left ordinate) represents a fit of the model to the data, and the solid black curves (right ordinate) represent predicted layer coverages of the individual layers. **(b)** Thickness (left ordinate), growth rate (right ordinate), and **(c)** RMS roughness as predicted by the fit of the data shown in **(a)**.

Figure 3-2 **(a)** A 20×20 μm^2 AF micrograph of a 22 nm thin film of tetracene grown on SiO_2 at 0.036 nm-s^{-1}. The line corresponds to the line scan shown in **(b)**, where the dashed line indicates nominal thickness. These figures are repeated for a 75 nm thin film of tetracene in **(c)** and **(d)**. For both micrographs, a height of zero represents the substrate, SiO_2.

Figure 3-3 **(a)** Scattered X-ray intensity at the anti-Bragg condition and the fit to the data (left ordinate, every 2^{nd} data point shown for visibility), and predicted layer coverages (right ordinate) for thin films of tetracene grown on SiO_2 at 0.091 nm-s^{-1}. **(b)** Thickness (left ordinate), growth rate (right ordinate), and **(c)** RMS roughness as predicted by the fit of the data shown in **(a)**.

Figure 3-4 **(a)** A 20×20 μm^2 AF micrograph of a 12.5 nm thin film of tetracene grown on SiO_2 at 0.091 nm-s^{-1}. The line corresponds to the line scan shown in **(b)**, where the dashed line indicates nominal thickness. These figures are repeated for a 25 nm thin film of tetracene in **(c)** and **(d)**. For both micrographs, a height of zero represents the substrate, SiO_2.

Figure 3-5 **(a)** Scattered X-ray intensity at the anti-Bragg condition and the fit to the data (left ordinate), and predicted layer coverages (right ordinate) for thin films of tetracene grown on SiO_2 at 0.61 nm-s^{-1}. **(b)** Thickness (left ordinate), growth rate (right ordinate), and **(c)** RMS roughness as predicted by the fit of the data shown in **(a)**.

Figure 3-6 **(a)** A 20×20 μm^2 AF micrograph of a 15.8 nm thin film of tetracene grown on SiO_2 at 0.61 nm-s^{-1}. The line corresponds to the line scan shown in **(b)**, where the dashed line indicates nominal thickness. A height of zero in **(a)** and **(b)** represents the substrate, SiO_2. These figures are repeated for a 210-280 nm thin film of tetracene in **(c)** and **(d)**. A height of zero in **(c)** and **(d)** represent the lowest points of the thin film.

Figure 3-7 **(a)** A zoomed view (5×5 μm^2) of the thin film of tetracene shown in Figure 2a. The line corresponds to the line scan shown in **(b)**. A height of zero in **(a)** and **(b)** represents the substrate, SiO_2. **(c)** A 5×5 μm^2 AF micrograph of a 29 nm thin film of pentacene grown on SiO_2 at 0.027 nm-s^{-1} at E_i = 2.5-2.6 eV. The line corresponds to the line scan shown in **(d)**. A height of zero in **(c)** and **(d)** represent the lowest points of the thin film.

Figure 3-8 RMS roughness and maximum RMS roughness from stochastic growth (left ordinate) represented by the solid and open circles, respectively (connected lines shown for ease of viewing), and fraction of exposed substrate (right ordinate) represented by the open squares (connected line shown for ease of viewing), for thin films of tetracene ~22 to ~29 nm thick on SiO_2 as a function of growth rate.

Figure 3-9 A schematic diagram of the molecular scale processes involved, including side-on and top views of an island, and the corresponding potential energy landscape. For simplicity, the adsorbed molecules are represented as spheres.

Figure 4-1 *Ex situ* XRR of a ~160 ML thin film of tetracene grown on SiO_2 at a nominal rate of 0.47 ML s^{-1}. The vertical lines (from left to right) indicate the expected positions from d_z = 12.93 Å (a thin-film phase), and 12.19 Å (the bulk phase). Inset on the bottom left is the chemical structure of tetracene.

Figure 4-2 *Ex situ* GID of a ~160 ML thin film of tetracene grown on SiO_2 at a nominal rate of 0.47 ML s^{-1}, same as that shown in Figure 4-1.

Figure 4-3 *In situ* real-time GID during the growth of the same thin film as in Figure 4-1 and Figure 4-2. Scattering data are shown for 20 s, 40 s, 60 s, 80 s, and 200 s from the start of growth.

Figure 4-4 (a) Integrated intensity of the $(021)_{TF}$ and $(021)_B$ peaks from Figure 4-3 displayed as a function of time. Every 4th data point is shown, and the data have been normalized to the maximum intensity observed for the bulk phase. (b) Numerical derivatives of the data shown in (a) as a function of time.

Figure 4-5 (a) Integrated intensity of the $(021)_B$ peaks at various rates of growth displayed as a function of time. Every 4th data point is shown. The same data from (a) displayed as a function of the total thickness.

Figure 4-6 (a) Integrated intensity of the $(021)_{TF}$ peaks at various rates of growth displayed as a function of time. Every 4th data point is shown. We also display, for this same $(021)_{TF}$ peak, (b) the out-of-plane FWHM, (c) $|q_{021}|$, and (d) the out-of-plane peak position at various rates of growth as a function of time. Every 4th data point is shown.

Figure 4-7 (a) Integrated intensity of the $(021)_{TF}$ peaks at various rates of growth displayed as a function of the total coverage. Every 4th data point is shown. We also display, for this same $(021)_{TF}$ peak, (b) the out-of-plane FWHM, (c) $|q_{021}|$, and (d) the out-of-plane peak position at various rates of growth as a function of the total coverage. Every 4th data point is shown.

Figure 4-8 (a) Thicknesses for the onset of the bulk phase (right ordinate, closed circles) and the thickness where the $(021)_{TF}$ intensity plateaus (left ordinate, open squares) as function of the rate of growth. (b) (a) Thicknesses for the onset of the bulk phase (right ordinate, closed circles) and the RMS roughness of ~ 19 ML thick films of tetracene on SiO_2 (left ordinate, open diamonds) as function of the rate of growth.

Figure 4-9 Schematic representation of the evolution of the two phases of tetracene, the thin-film phase (reddish tones) and the bulk phase (blueish tones). *Figure courtesy of James R. Engstrom.*

Figure 5-1 (a) Scattered X-ray intensity at the anti-Bragg condition as a function of time for a thin film of tetracene grown on SiO_2 at 0.144 ML-s^{-1} and T_s = 0 °C, represented by the open circles (left ordinate, every 2nd data point shown for visibility). The solid blue line (left ordinate) represents a fit of the model to the data, and the solid black curves (right ordinate) represent predicted layer coverages of the individual layers. (b) RMS roughness as predicted by the fit of the data shown in (a). A similar set of figures is shown for growth at 0.0266 ML-s^{-1} in (c) and (d).

Figure 5-2 (a) Scattered X-ray intensity at the anti-Bragg condition as a function of time for a thin film of tetracene grown on SiO_2 at 0.0141 ML-s^{-1} and T_s = 0 °C, represented by the open circles (left ordinate, every 5th data point shown for visibility). The solid blue line (left ordinate) represents a fit of the model to the data, and the solid black curves (right ordinate) represent predicted layer coverages of the individual layers. (b) RMS roughness as predicted by the fit of the data shown in (a). A similar set of figures is shown for growth at 0.00362 ML-s^{-1} in (c) and (d).

Figure 5-3 5 × 5 μm^2 AF micrographs of thin films of tetracene grown on SiO_2 at: (a) 0.144 ML-s^{-1} (12.1 ML); (b) 0.0266 ML-s^{-1} (10.4 ML), (c) 0.0141 ML-s^{-1} (10.7 ML), and (d) 0.00362 ML-s^{-1} (12.3 ML). All growths were conducted at T_s = 0 °C.

Figure 5-4 (a) Correlation length (left ordinate) and RMS roughness (right ordinate) as a function of growth rate, deduced from analysis of the images shown in Figure 5-3 and other similar ones. (b) Density of islands/characteristic features as a function of the rate of growth for conditions where 2D LbL growth is achieved.

Figure 5-5 Grazing incidence diffraction for thin films of tetracene: (a) 10 ML and (b) 20.7 ML thick thin films deposited at ~ 0.03 ML-s^{-1}, and (c) 10 ML and (d) 22.2 ML thick thin films deposited at ~ 0.003 ML-s^{-1}. All growths were conducted at T_s = 0 °C.

Figure 5-6 (a) Scattered X-ray intensity at the anti-Bragg condition, the fit to the data, and predicted layer coverages for a thin film of tetracene grown on SiO_2 at 30 °C at a rate of 0.467 ML-s^{-1}. Plotted in the same fashion

as those in Figures 5-1 and 5-2. (b) AF micrograph (20 × 20 μm^2) of a 12.2 ML thick thin film grown at the rate considered in (a). Similar figures for a growth rate of 0.0277 ML-s^{-1}, T_s = 30 °C, and a thickness of 17 ML are shown in (c) and (d).

Figure 5-7 Predicted layer coverages for growth of tetracene on SiO_2 at 0.0141 ML-s^{-1} and T_s = 0 °C (smooth black curves), and at 0.467 ML-s^{-1} and T_s = 30 °C (dashed blue curves).

Figure 5-8 A plot of the growth modes as a function of the rate of growth and the inverse substrate temperature. Open symbols represent fully 3D growth, half-filled represent a transition regime, and filled represent 2D LbL growth. The shaded areas represent the approximate regions of phase space for growth.

Figure 5-9 The minimum thickness for the appearance of the bulk phase as a function of the rate of growth and the substrate temperature for the growth of tetracene on SiO_2.

Figure 6-1 **(a)** Scattered X-ray intensity at the anti-Bragg condition as a function of time for a thin film of tetracene grown on **(a)** a nominally 1 ML pentacene on SiO_2 and **(b)** SiO_2, represented by the open circles (left ordinate). The solid blue line (left ordinate) represents a fit of the model to the data, and the solid black curves (right ordinate) represent predicted layer coverages of the individual layers. Data up to 80 s (of a total 172 s) shown for clarity.

Figure 6-2 RMS roughness as predicted by the fit to the data shown in **Figure 1(a,b)**.

Figure 6-3 **(a)** A 15×15 μm^2 AF micrograph of a ~17.9 ML thin film of tetracene grown on nominally 1 ML pentacene on SiO_2. **(b)** A line scan from **(a)**. **(c)** A 15×15 μm^2 AF micrograph of a ~14.4 ML thin film of tetracene grown on SiO_2. **(d)** A line scan from **(c)**.

Figure 6-4 Scattered X-ray intensity at the anti-Bragg condition as a function of time for thin films of tetracene grown on **(a)** nominally 2 ML pentacene on SiO_2 and **(b)** nominally 3 ML pentacene on SiO_2, represented by the open circles.

Figure 6-5 **(a)** A 15×15 μm^2 AF micrograph of a ~18.2 ML thin film of tetracene grown on nominally 2 ML pentacene on SiO_2. **(b)** A line scan from **(a)**. **(c)** A 15×15 μm^2 AF micrograph of a ~21.0 ML thin film of tetracene grown on SiO_2. **(d)** A line scan from **(c)**.

Figure 6-6 XRR of the thin films: **(a)** ~127 ML tetracene on 1 ML of pentacene, **(b)** ~140 ML tetracene on 2 ML of pentacene, **(c)** ~149 ML tetracene on 3 ML of pentacene. The colored, dashed lines represent the expected Bragg peaks (from left to right) for the thin-film phase of pentacene, the thin-film phase of tetracene, and the bulk phase of tetracene.

LIST OF TABLES

Table 4-1 Summary of the lattice parameters of the thin-film phase and bulk phase of both tetracene and pentacene.

Table 5-1 A tabulated summary of the rates of growth investigated here, thicknesses and roughnesses derived from the fits to the intensity at the anti-Bragg condition, and from AFM, and the correlation length from analysis of the 1D PSD.

LIST OF ABBREVIATIONS

1D	one-dimensional
2D	two-dimensional
3D	three-dimensional
AF	atomic force
AFM	atomic force microscopy (microscope)
CAD	computer-aided design
CHESS	Cornell High Energy Synchrotron Source
CNF	Cornell Nanoscience and Technology Facility
DIP	diindenoperylene
GID	grazing incidence (X-ray) diffraction
LbL	layer-by-layer
ML	monolayer
NBTC	Nanobiotechnology Center
PFP	perfluoropentacene
PSD	power spectral density
PTCDA	perylene-3,4,9,10-tetracarboxylic dianhydride
pBN	pyrolytic boron nitride
RMS	root mean square
SAM	self-assembled monolayer
STM	scanning tunneling microscopy (microscope)
UHV	ultra-high vacuum
XRR	X-ray reflectivity

LIST OF SYMBOLS

D	deposited thin-film thickness
E_i	incident kinetic energy
γ	surface energy
k	Boltzmann's constant
σ	root mean square roughness
ξ	correlation length

CHAPTER 1

INTRODUCTION

1.1 Overview

This dissertation is a compilation of our examinations on the growth of semiconducting organic thin films of tetracene. The present chapter begins with a general introduction to the field of organic semiconductors. Chapter 2 follows with a summary of the experimental techniques used in our investigations. These first two chapters will serve as a brief primer to the topic at hand. The next four chapters, representing already published or intended-to-be-published work (as of this writing), will describe our results, and interpretations thereof, from our experiments. Chapter 3 discusses the effect of growth rate on the growth mode and morphology of tetracene on silicon dioxide, or SiO_2, at a substrate temperature $T_s = 30$ °C. Chapter 4 details the effect of growth rate on the polymorphism of tetracene on SiO_2 at $T_s = 30$ °C. Chapter 5 describes the consequences of growing tetracene on SiO_2 at a lower substrate temperature $T_s = 0$ °C. Chapter 6 then pivots to the growth of heterostructures, and it explores the growth of thin films of tetracene on thin films of pentacene and the effect of the thickness of the pentacene layers on the growth of tetracene. Finally, Chapter 7 summarizes and concludes this dissertation. The appendices cover various experimental or analytical details concerning these results that may be of interest to the reader. There is also a brief appendix concerning the research group's scanning tunneling microscope (STM) and its usage.

1.2 Thin-film deposition of organic semiconductors

Organic semiconductors are attractive as candidates to replace traditional inorganic semiconductors like silicon in certain applications such as flexible electronics or solar cells.[1] In this dissertation, we consider small molecule organic semiconductors as opposed to semiconducting polymers. Furthermore, we will focus on the thin-film deposition of organic molecules *in vacuo*. Semiconducting organic molecules have been shown to exhibit a variety of behaviors during thin-film growth, such as: forming crystalline or amorphous thin films, growing in 2D or 3D modes, and also crystallizing into multiple polymorphs.[2–4] These phenomena are due, in part, to the anisotropic shapes of many molecules, and unlike in thin films of inorganic materials where atoms are held together by covalent, metallic, or ionic bonds, thin films of organic molecules are held together by weaker van der Waals interactions. Nevertheless, many of the classic principles and processes involved in inorganic thin-film growth apply to organic systems: adsorption, desorption, diffusion, nucleation, and growth. Such processes are shown schematically in Figure 1-1.

The Engstrom research group has investigated the effect of various factors on the thin-film growth of a wide variety of molecules, many of which grow in a 2D layer-by-layer fashion for one to several monolayers, including pentacene,[5–12] perfluoropentacene (PFP),[13] diindenoperylene (DIP),[11,14,15] and several perylene diimide derivatives (PTCDI-C_n).[12,16] In particular, the group has thoroughly studied the effect of incident kinetic energy, E_i, on the growth of organic molecules by employing a supersonic molecular beam as the source of the organic material. It was determined that hyperthermal growth had no appreciable effect on the nucleation density,[11] but E_i does affect the probability of adsorption, dependent on the nature of the surface.[14–16] A smooth decrease in the probability of adsorption with increasing E_i

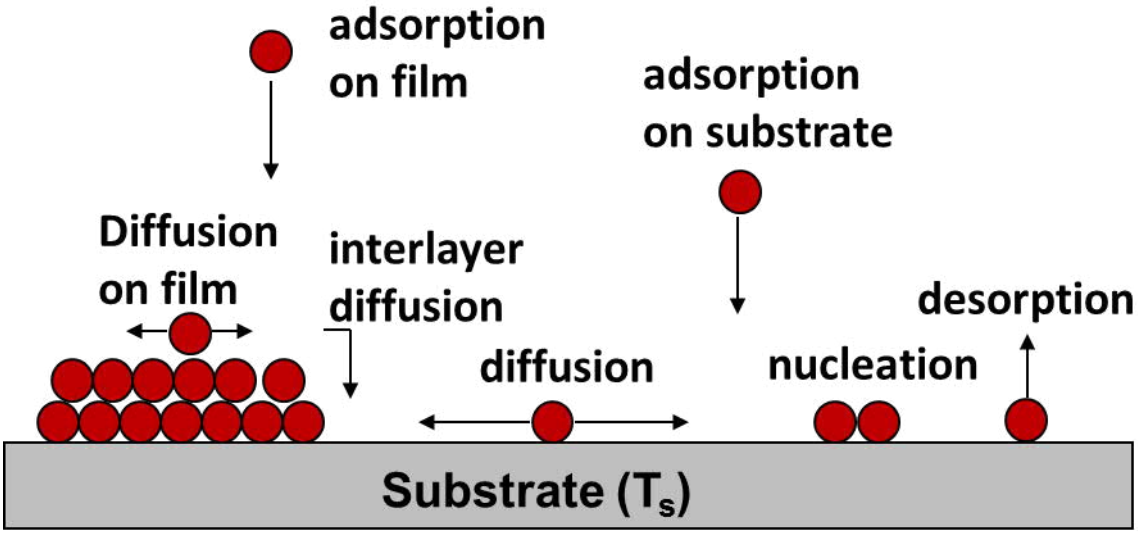

Figure 1-1 Schematic representation of various processes during thin-film growth. Molecules are simply represented as circles, although many are anisotropic.

observed for clean, unmodified SiO_2, indicative of trapping-mediated adsorption.[14] The group has also extensively explored the effect of surface energy on growth by way of modifying substrates with self-assembled monolayers (SAMs). Long SAMs like octyltrichlorosilane and octadecyltrichlorosilane more efficiently trap incident molecules, and the probability of adsorption on these surfaces exhibit little dependence on E_i, which is thought to be due to direct molecular insertion of the incident molecule into the SAM.[15,17] Moreover, the differences in surface termination and therefore surface energy impact growth during the first 1-2 MLs by changing how the molecules diffuse on the surface, nucleate, and ultimately incorporate into the growing thin film.[13,15,16,18] Increasing temperature has been demonstrated as a method to produce smoother organic thin films, thought to be a result of enhanced interlayer transport enabling molecules to more easily hop down step-edges[19] and also increased surface diffusivity leading to larger in-plane feature sizes.[18]

Many of the same aforementioned processes and effects must be considered when engineering organic-organic heterostructures. Heterostructures include two or more differing materials in various arrangements, such as a planar heterojunction or a distributed bulk heterojunction. The reader is encouraged to refer to a review of organic-organic heterostructures by Hinderhofer and Schreiber.[20] In this dissertation, we will focus on the formation of planar heterostructures. Many researchers have reported on the formation of such heterostructures, but a single theme becomes readily apparent: the nature of the firstly deposited organic thin film strongly influences the growth of the second thin film. Hinderhofer *et al.* have reported heterostructures of PFP on DIP, where the underlying DIP acted as a template for PFP – the degree of order in DIP determined the degree of order in PFP.[21] In another report, they additionally observe that depositing PFP on DIP can actually lead to initially smoothing of the overall thin film, as PFP fills in valleys present on the DIP surface.

They note a similar phenomenon with pentacene on PFP.[22] Others have also studied heterostructures of pentacene and PFP and have found that these two molecules can mix to form mixed phases akin to metal alloys.[23–25] Other examples of templating effects have been demonstrated in other systems: the growth of ordered C_{60} on DIP|SiO_2,[26] the growth of a standing-phase F_{16}CuPc at step-edges of pentacene and a lying-down phase of the same molecules on terraces of pentacene,[27] the formation of crystalline rubrene on top of a thin-film of α-quaterthiophene,[28] the growth of a lying-down phase of H_2Pc on PTCDA that can be disrupted by inserting an amorphous layer between them,[29] and others.[30–34]

We have also investigated the formation of heterostructures of pentacene and various perylene diimide derivatives (PTCDI-C_n). There, we find that depositing a low surface energy material on a high surface energy material will lead to smoothing of the surface. On the other hand, if a high surface energy material is deposited on a low surface energy material, then there exists a driving force for uphill transport and reorganization, causing rapid roughening of the surface.[12] Therefore, it is important to match the surface energies of organic materials in order to form smooth multilayers.

1.3 Tetracene

In this dissertation, we examine the growth of tetracene, a polycyclic aromatic hydrocarbon that is similar to pentacene (a prototypical organic semiconductor), but contains one fewer fused ring. Tetracene and pentacene both adopt triclinic crystals in their bulk form. The lattice parameters of tetracene (pentacene) are: a = 6.06 (7.9) Å, b = 7.84 (6.06) Å, c = 13.0 (16.01) Å, α = 77.1 (101.9)°, β = 72.1 (112.6)°, and γ = 85.8 (85.8)°.[35,36] Notably, it has been found that the carrier mobility of thin films

of tetracene depends on the rate at which the thin films were grown, where low growth rates yielded thin films with distinctly different morphology than those grown at higher growth rates.[37] Shi and Qin have also observed a similar dependence of morphology on growth rate for thin films grown on SiO_2.[38] Other groups have also noted that thin films of tetracene show poor coverage of the substrate and therefore poor carrier mobility.[39,40] While these previous studies have lent insight into the growth of tetracene, they have all utilized *ex situ* techniques for characterization, which potentially suffer from effects due to post-deposition thin film reorganization.[8]

Additionally, tetracene is an example of a molecule that exhibits multiple phases at room temperature in thin-film form.[41–44,39] Gompf *et al*. and Milita *et al*. have previously reported an effect of growth rate on the relative amounts of the two phases determined by *ex situ*, post-deposition techniques.[41,43] Both accounts reveal that lower growth rates incite more bulk phase with a smaller d_z-spacing while higher growth rates incite more thin-film phase with a larger d_z-spacing. However, whether the two phases grow simultaneously, mixed, or independently has remained unclear.

In this dissertation, we seek to reveal the nature of growth of tetracene. Our results shed insight into why there is a dependence of growth mode and morphology on growth rate and provide a better understanding of how and why the two aforementioned phases of tetracene arise during thin film growth. We present results from our investigations of the growth of tetracene, where we use *in situ* real-time synchrotron X-ray scattering techniques at Cornell High Energy Synchrotron Source (CHESS) to reveal the complexities that arise in the thin-film growth of tetracene. Major advantage of the work shown here include: we collect *in situ* and real-time data, providing us with many more data points than can be reasonably obtained with *ex situ* methods and the X-ray data avoids any potential post-deposition reorganization effects.

1.4 References

(1) Forrest, S. R. The Path to Ubiquitous and Low-Cost Organic Electronic Appliances on Plastic. *Nature* **2004**, *428* (6986), 911–918.

(2) Forrest, S. R. Ultrathin Organic Films Grown by Organic Molecular Beam Deposition and Related Techniques. *Chem. Rev.* **1997**, *97* (6), 1793–1896.

(3) Schreiber, F. Organic Molecular Beam Deposition: Growth Studies beyond the First Monolayer. *Phys. Status Solidi A* **2004**, *201* (6), 1037–1054.

(4) Witte, G.; Wöll, C. Growth of Aromatic Molecules on Solid Substrates for Applications in Organic Electronics. *J. Mater. Res.* **2004**, *19* (07), 1889–1916.

(5) Killampalli, A. S.; Schroeder, T. W.; Engstrom, J. R. Nucleation of Pentacene on Silicon Dioxide at Hyperthermal Energies. *Appl. Phys. Lett.* **2005**, *87* (3), 033110.

(6) Killampalli, A. S.; Engstrom, J. R. Nucleation of Pentacene Thin Films on Silicon Dioxide Modified with Hexamethyldisilazane. *Appl. Phys. Lett.* **2006**, *88* (14), 143125.

(7) Hong, S.; Amassian, A.; Woll, A. R.; Bhargava, S.; Ferguson, J. D.; Malliaras, G. G.; Brock, J. D.; Engstrom, J. R. Real Time Monitoring of Pentacene Growth on SiO2 from a Supersonic Source. *Appl. Phys. Lett.* **2008**, *92* (25), 253304/1–253301/3.

(8) Amassian, A.; Pozdin, V. A.; Desai, T. V.; Hong, S.; Woll, A. R.; Ferguson, J. D.; Brock, J. D.; Malliaras, G. G.; Engstrom, J. R. Post-Deposition Reorganization of Pentacene Films Deposited on Low-Energy Surfaces. *J. Mater. Chem.* **2009**, *19* (31), 5580–5592.

(9) Woll, A. R.; Desai, T. V.; Engstrom, J. R. Quantitative Modeling of in Situ X-Ray Reflectivity during Organic Molecule Thin Film Growth. *Phys. Rev. B* **2011**, *84* (7), 075479/1–075479/14.

(10) Desai, T. V.; Woll, A. R.; Engstrom, J. R. Thin Film Growth of Pentacene on Polymeric Dielectrics: Unexpected Changes in the Evolution of Surface Morphology with Substrate. *J. Phys. Chem. C* **2012**, *116* (23), 12541–12552.

(11) Kish, E. R.; Desai, T. V.; Greer, D. R.; Woll, A. R.; Engstrom, J. R. Nucleation of Diindenoperylene and Pentacene at Thermal and Hyperthermal Incident Kinetic Energies. *J. Vac. Sci. Technol. A* **2015**, *33* (3), 031511.

(12) Kish, E. R.; Nahm, R. K.; Woll, A. R.; Engstrom, J. R. When the Sequence of

Thin Film Deposition Matters: Examination of Organic-on-Organic Heterostructure Formation Using Molecular Beam Techniques and in Situ Real Time X-Ray Synchrotron Radiation. *J. Phys. Chem. C* **2016**, acs.jpcc.6b01717.

(13) Desai, T. V.; Woll, A. R.; Schreiber, F.; Engstrom, J. R. Nucleation and Growth of Perfluoropentacene on Self-Assembled Monolayers: Significant Changes in Island Density and Shape with Surface Termination. *J. Phys. Chem. C* **2010**, *114* (47), 20120–20129.

(14) Amassian, A.; Desai, T. V.; Kowarik, S.; Hong, S.; Woll, A. R.; Malliaras, G. G.; Schreiber, F.; Engstrom, J. R. Coverage Dependent Adsorption Dynamics in Hyperthermal Organic Thin Film Growth. *J. Chem. Phys.* **2009**, *130* (12), 124701/1–124701/9.

(15) Desai, T. V.; Hong, S.; Woll, A. R.; Hughes, K. J.; Kaushik, A. P.; Clancy, P.; Engstrom, J. R. Hyperthermal Organic Thin Film Growth on Surfaces Terminated with Self-Assembled Monolayers. I. The Dynamics of Trapping. *J. Chem. Phys.* **2011**, *134* (22), 224702/1–224702/13.

(16) Desai, T. V.; Kish, E. R.; Woll, A. R.; Engstrom, J. R. Hyperthermal Growth of N , N′ -Ditridecylperylene-3,4,9,10-Tetracarboxylic Diimide on Self-Assembled Monolayers: Adsorption Dynamics and Sub- and Multilayer Thin Film Growth. *J. Phys. Chem. C* **2011**, 18221–18234.

(17) Goose, J. E.; Killampalli, A. S.; Clancy, P.; Engstrom, J. R. Molecular-Scale Events in Hyperthermal Deposition of Organic Semiconductors Implicated from Experiment and Molecular Simulation. *J. Phys. Chem. C* **2009**, *113* (15), 6068–6073.

(18) Desai, T. V. Dissertation: In Situ Real-Time Studies of Organic Semiconductor Thin Film Growth, Cornell University, 2011.

(19) Krause, B.; Schreiber, F.; Dosch, H.; Pimpinelli, A.; Seeck, O. H. Temperature Dependence of the 2D-3D Transition in the Growth of PTCDA on Ag(111): A Real-Time X-Ray and Kinetic Monte Carlo Study. *Eur. Lett.* **2004**, *65* (3), 372–378.

(20) Hinderhofer, A.; Schreiber, F. Organic-Organic Heterostructures: Concepts and Applications. *Chemphyschem* **2012**, *13* (3), 628–643.

(21) Hinderhofer, A.; Hosokai, T.; Frank, C.; Novák, J.; Gerlach, A.; Schreiber, F. Templating Effect for Organic Heterostructure Film Growth: Perfluoropentacene on Diindenoperylene. *J. Phys. Chem. C* **2011**, *115* (32), 16155–16160.

(22) Hinderhofer, A.; Gerlach, A.; Kowarik, S.; Zontone, F.; Krug, J.; Schreiber, F. Smoothing and Coherent Structure Formation in Organic-Organic Heterostructure Growth. *Eur. Lett.* **2010**, *91* (5), 56002/1–56002/5.

(23) Breuer, T.; Witte, G. Thermally Activated Intermixture in Pentacene-Perfluoropentacene Heterostructures. *J. Chem. Phys.* **2013**, *138* (11), 114901.

(24) Hinderhofer, A.; Frank, C.; Hosokai, T.; Resta, A.; Gerlach, A.; Schreiber, F. Structure and Morphology of Coevaporated Pentacene-Perfluoropentacene Thin Films. *J. Chem. Phys.* **2011**, *134* (10), 104702.

(25) Salzmann, I.; Duhm, S.; Heimel, G.; Rabe, J. P.; Koch, N.; Oehzelt, M.; Sakamoto, Y.; Suzuki, T. Structural Order in Perfluoropentacene Thin Films and Heterostructures with Pentacene. *Langmuir* **2008**, *24* (14), 7294–7298.

(26) Hinderhofer, A.; Gerlach, A.; Broch, K.; Hosokai, T.; Yonezawa, K.; Kato, K.; Kera, S.; Ueno, N.; Schreiber, F. Geometric and Electronic Structure of Templated C 60 on Diindenoperylene Thin Films. *J. Phys. Chem. C* **2013**, *117* (2), 1053–1058.

(27) de Oteyza, D. G.; Barrena, E.; Sellner, S.; Ossó, J. O.; Dosch, H. Role of the Substrate Thickness for the Structural Properties of Organic–organic Heterostructures. *Surf. Sci.* **2007**, *601* (18), 4117–4121.

(28) Raimondo, L.; Fumagalli, E.; Moret, M.; Campione, M.; Borghesi, A.; Sassella, A. Epitaxial Interfaces in Rubrene Thin Film Heterostructures. *J. Phys. Chem. C* **2013**, *117* (27), 13981–13988.

(29) Heutz, S.; Cloots, R.; Jones, T. S. Structural Templating Effects in Molecular Heterostructures Grown by Organic Molecular-Beam Deposition. *Appl. Phys. Lett.* **2000**, *77* (24), 3938.

(30) So, F. F.; Forrest, S. R.; Shi, Y. Q.; Steier, W. H. Quasi-Epitaxial Growth of Organic Multiple Quantum Well Structures by Organic Molecular Beam Deposition. *Appl. Phys. Lett.* **1990**, *56* (7), 674.

(31) Lunt, R. R.; Benziger, J. B.; Forrest, S. R. Growth of an Ordered Crystalline Organic Heterojunction. *Adv. Mat.* **2007**, *19* (23), 4229–4233.

(32) Lunt, R. R.; Sun, K.; Kröger, M.; Benziger, J. B.; Forrest, S. R. Ordered Organic-Organic Multilayer Growth. *Phys. Rev. B* **2011**, *83* (6), 064114/1–064114/7.

(33) Sellam, F.; Schmitz-Hübsch, T.; Toerker, M.; Mannsfeld, S.; Proehl, H.; Fritz, T.; Leo, K.; Simpson, C.; Müllen, K. LEED and STM Investigations of Organic–organic Heterostructures Grown by Molecular Beam Epitaxy. *Surf.*

Sci. **2001**, *478* (1-2), 113–121.

(34) Schmitz-Hübsch, T.; Sellam, F.; Staub, R.; Törker, M.; Fritz, T.; Kübel, C.; Müllen, K.; Leo, K. Direct Observation of Organic–organic Heteroepitaxy: Perylene-Tetracarboxylic-Dianhydride on Hexa-Peri-Benzocoronene on Highly Ordered Pyrolytic Graphite. *Surf. Sci.* **2000**, *445* (2-3), 358–367.

(35) Holmes, D.; Kumaraswamy, S.; Matzger, A. J.; Vollhardt, K. P. C. On the Nature of Nonplanarity in the [N]Phenylenes. *Chem.-Eur. J.* **1999**, *5* (11), 3399–3412.

(36) Campbell, R. B.; Robertson, J. M.; Trotter, J. The Crystal Structure of Hexacene, and a Revision of the Crystallographic Data for Tetracene. *Acta Crystallogr.* **1962**, *15* (3), 289–290.

(37) Cicoira, F.; Santato, C.; Dinelli, F.; Murgia, M.; Loi, M. a.; Biscarini, F.; Zamboni, R.; Heremans, P.; Muccini, M. Correlation Between Morphology and Field-Effect-Transistor Mobility in Tetracene Thin Films. *Adv. Funct. Mater.* **2005**, *15* (3), 375–380.

(38) Shi, J.; Qin, X. Nucleation and Growth of Tetracene Films on Silicon Oxide. *Phys. Rev. B* **2008**, *78* (11), 115412.

(39) Moriguchi, N.; Nishikawa, T.; Anezaki, T.; Unno, A.; Tachibana, M.; Kojima, K. Carrier Mobility and Crystal Perfection of Tetracene Thin Film FET. *Phys. B* **2006**, *376-377*, 276–279.

(40) Bertolazzi, S.; Wünsche, J.; Cicoira, F.; Santato, C. Tetracene Thin Film Transistors with Polymer Gate Dielectrics. *Appl. Phys. Lett.* **2011**, *99* (1), 013301.

(41) Milita, S.; Servidori, M.; Cicoira, F.; Santato, C.; Pifferi, A. Synchrotron X-Ray Investigation of Tetracene Thin Films Grown at Different Deposition Fluxes. *Nucl. Instrum. Meth. B* **2006**, *246* (1), 101–105.

(42) Milita, S.; Santato, C.; Cicoira, F. Structural Investigation of Thin Tetracene Films on Flexible Substrate by Synchrotron X-Ray Diffraction. *Appl. Surf. Sci.* **2006**, *252* (22), 8022–8027.

(43) Gompf, B.; Faltermeier, D.; Redling, C.; Dressel, M.; Pflaum, J. Tetracene Film Morphology: Comparative Atomic Force Microscopy, X-Ray Diffraction and Ellipsometry Investigations. *Eur. Phys. J. B* **2008**, *27* (4), 421–424.

(44) Wünsche, J.; Tarabella, G.; Bertolazzi, S.; Bocoum, M.; Coppedè, N.; Barba, L.; Arrighetti, G.; Lutterotti, L.; Iannotta, S.; Cicoira, F.; Santato, C. The Correlation between Gate Dielectric, Film Growth, and Charge Transport in

Organic Thin Film Transistors: The Case of Vacuum-Sublimed Tetracene Thin Films. *J. Mater. Chem. C* **2013**, *1* (5), 967.

CHAPTER 2

EXPERIMENTAL TECHNIQUES

2.1 Overview

This dissertation makes use of various experimental techniques to investigate the growth of thin films of tetracene. All of the thin-film depositions have been carried out in one of the Engstrom Research Group's UHV chambers that has been custom-designed for use in the G3 hutch at CHESS. Details of this chamber are extensively detailed in previous dissertations by Drs. Todd Schroeder, Tushar Desai, and Edward Kish.[1–3] The design of the chamber enables *in situ* and real-time characterization by synchrotron X-ray scattering techniques at CHESS, which have been heavily employed throughout this work. Furthermore, *ex situ* techniques, such as atomic force microscopy (AFM) and X-ray characterization in the G2 hutch at CHESS, have been used to further probe thin films after growth. The intent of this chapter is to introduce the reader to the various experimental techniques used throughout this dissertation.

2.2 Substrate preparation

The substrates used for the experiments in this dissertation were thick silicon oxide pieces. The silicon dioxide, or SiO_2, was grown on 4" Si (100) wafers (Wacker-Siltronic, p-type, 500-550 μm, 38-63 Ω-cm) by wet thermal oxidation in the thermal oxide furnace at Cornell Nanofabrication Facility (CNF). Immediately before oxidation, the wafers were subjected to RCA Standard Clean 1, an oxide strip, and finally RCA Standard Clean 2. The oxide was grown to a thickness of 300 nm. To

ensure a consistent size (especially important for X-ray reflectivity), the SiO_2 wafers were diced using a dicing saw at CNF to dimensions of 4 mm × 30 mm. This size was used to ensure that the spot painted by the supersonic molecular beam was uniform across the substrate (*vide infra*).

The pieces of SiO_2 underwent further cleaning prior to any depositions. Properly cleaning is crucial to ensuring there is no residue or contamination from the dicing procedure nor from the ambient air. The substrates were cleaned by sequentially sonicating in chloroform and then deionized water, each for 20 minutes with rinsing in DI water between solvents, and finally drying with N_2. Utmost care must be taken to not cross-contaminate the solvents (no chloroform in water and vice versa). The substrates must be handled by the ends (of the long axis) with tweezers as to not scratch areas where thin films may be deposited. When drying, the substrates will need to be dried while holding one end, and then again while holding the other, to ensure thorough drying. (The tweezers should be dried in between). Extra care should be taken to make certain that the substrate is completely dried and there is no excess water on the edges. Samples should be inspected at this point for cleanliness and absence of any scratches. Samples with scratches should be discarded, and samples that exhibit residue should be cleaned again. The substrates were then subjected to UV/ozone cleaning with a Samco UV-1 (SAMCO, Inc.), located in the Nanobiotechnology Center (NBTC) cleanroom facilities, for 20 minutes.

2.3 Organic thin film deposition and the G-line chamber

The Engstrom group makes use of a custom UHV chamber that was designed for growth of organic semiconductors *via* a supersonic molecular beam and *in situ*

characterization by synchrotron X-rays at CHESS. It is fitted with Be windows to allow for X-rays to pass into the chamber (Be is a low-Z material and does not strongly absorb X-rays), scatter off of the sample, and be collected by a detector. The chamber was designed for easy transfer onto and off of a diffractometer in the G3 station. A picture of the chamber mounted on the diffractometer is shown in Figure 2-1. A cutaway of the inside of the chamber generated by computer-aided design (CAD) software is shown in Figure 2-2.

There are two sources for organic molecules currently on the chamber: a supersonic molecular beam source and a more conventional effusive beam source (thermal evaporator). A supersonic beam is generated by expanding a stream of carrier gas such as He through a small nozzle or orifice at high pressure into a volume with a sufficiently low pressure to cause isentropic, supersonic expansion. Before expansion, this carrier can be seeded with heavier molecules such as the organics considered here. The lighter molecules like He will accelerate the heavier molecules to high velocities and thus, high kinetic energies. In the G-line chamber, the carrier is passed through an *in situ* heated vessel containing a powder of the organic molecule of interest. The temperature of the vessel is controlled to produce a desired vapor pressure of the organic molecule. The seeded carrier then expands through a 150 μm nozzle into a UHV source chamber with a typical base pressure of $\sim 5\times10^{-9}$ Torr. The expanded beam then passes through a trump-shaped skimmer, a differentially pumped ante-chamber with an optional LN2 trap, and finally passing through a beam-defining aperture before entering the main growth chamber and striking the substrate. Owing to the well-defined shape of the beam and high beam-to-background ratio, multiple spots may be grown on a single sample by simply translating it. More details can be found in Dr. Todd Schroeder's , Dr. Tushar Desai's, or Dr. Edward Kish's dissertations.[1–3]

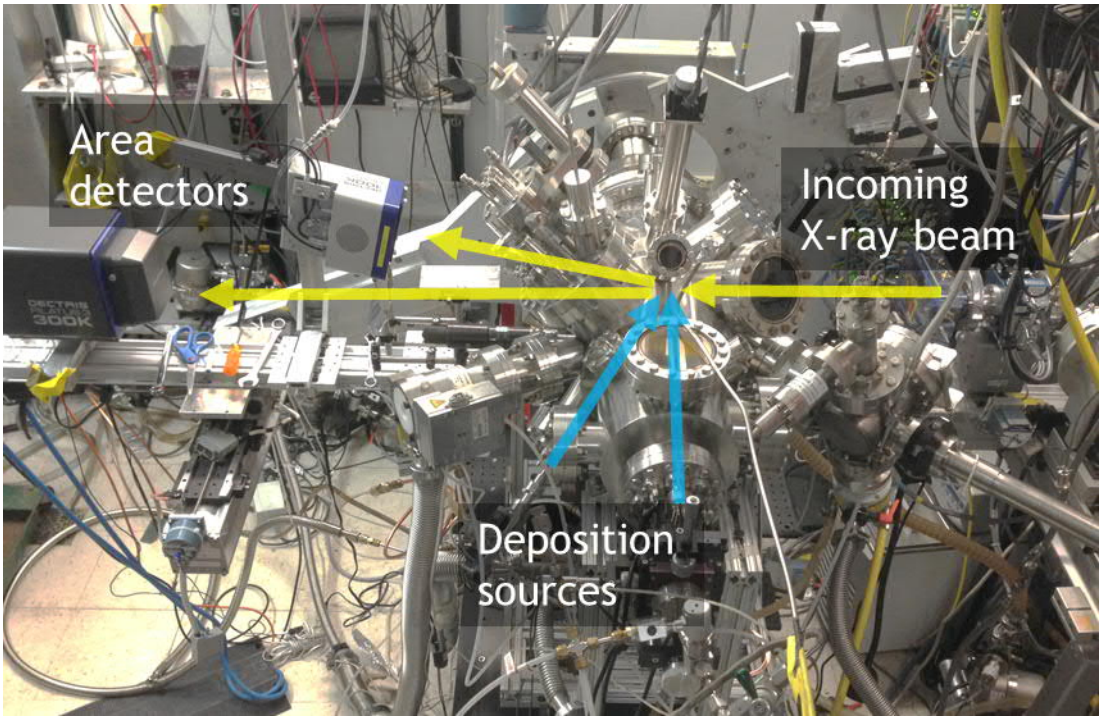

Figure 2-1 Photograph of the G-line table mounted on the diffractometer in the G3 hutch at CHESS.

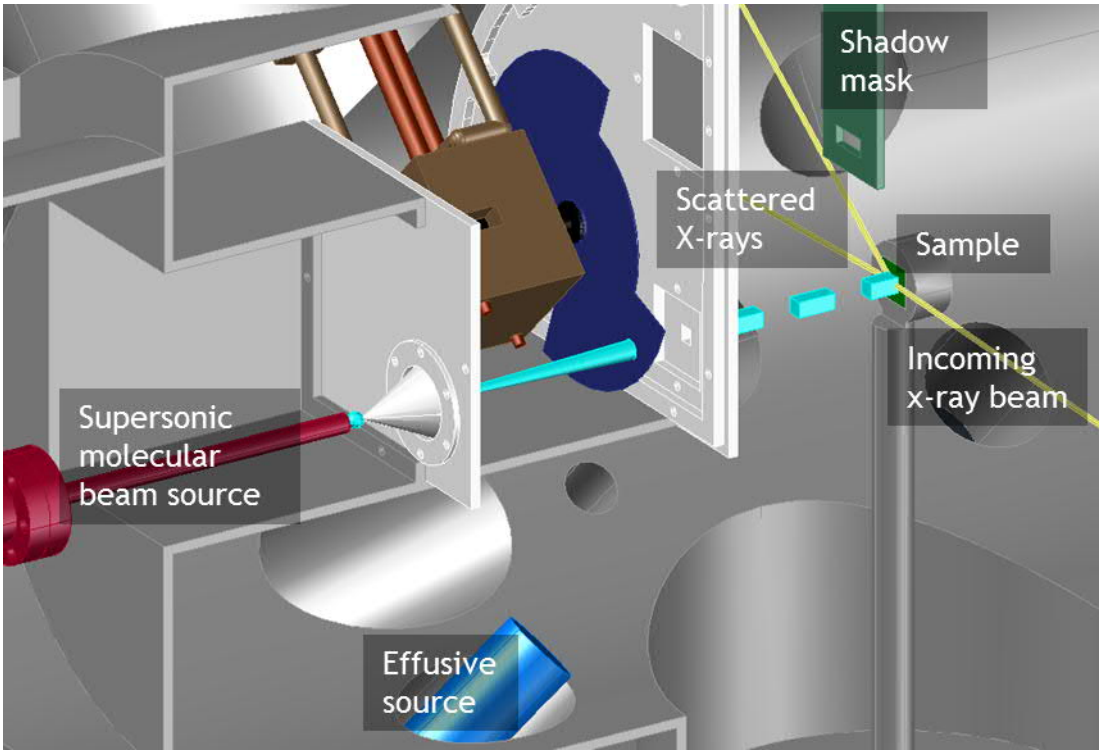

Figure 2-2 A schematic cutaway of the inside of the chamber from CAD software.

While the supersonic source produces a beam possessing hyperthermal kinetic energy, the effusive source produces beams with kinetic energy on the order of ~kT, where k is Boltzmann's constant. The effusive source consists of a 10 cc tapered, cylindrical pyrolytic boron nitride (pBN) crucible, and heating elements with feedback control using a thermocouple input. The crucible contains the molecule of interest and is heated to a controlled temperature to produce a vapor pressure of the organic material. The molecules in the beam have a high probability of adsorption on any surface and will coat anything in the line-of-sight of the beam. A shutter is used to block the beam from the substrate and the majority of the chamber. Further, a translatable shadow mask is employed to define a beam-spot on the sample. With this, we can sequentially deposit organic molecules from either source on the same area on the sample to form heterostructures. More details can be found in Dr. Tushar Desai's or Dr. Edward Kish's dissertations.[2,3]

2.4 X-ray scattering techniques

X-rays can be a powerful, non-invasive tool to probe many kinds of samples in many different ways. For example, X-rays can be used to produce real-space "images" or tomograms, such as in computed tomographic (CT) scanners found in many hospitals. X-rays can be used to reveal the chemical composition and nature of a sample through techniques such as X-ray photoelectron spectroscopy, Auger electron spectroscopy, X-ray fluorescence, and X-ray absorption spectroscopy. The aforementioned techniques arise from the inelastic (Compton) scattering or photoabsorption of X-rays. This dissertation focuses on techniques that exploit the elastic (Rayleigh) scattering of X-rays scattering. More specifically, this dissertation

considers X-ray diffraction, where X-rays, scattered off of crystalline solids, constructively interfere according to Bragg's Law:

$$2d \sin\theta = n\lambda$$

where d is the spacing between lattice planes of the crystal, θ is the angle of incidence between the X-rays and the lattice plane, n is a positive integer, and λ is the wavelength of the X-rays. For a more detailed description of X-ray diffraction, the reader is encouraged to seek out any of the many available texts concerning this topic, such as B. E. Warren's X-ray Diffraction or B. D. Cullity's Elements of X-ray Diffraction. This dissertation makes use of an interesting phenomenon that occurs at the so-called anti-Bragg condition.

2.4.1 Scattering at the anti-Bragg condition and the Trofimov model

In this section, the concept of scattering at the anti-Bragg condition is introduced. For a detailed review of this, the reader is referred to papers by Woll *et al.* and Kowarik *et al.*[4,5] This section, adapted from Woll *et al.*,[4] serves to put the rest of the dissertation into context.

X-rays primarily interact with electrons, and the intensity of the scattered X-rays is proportional to the square of the scattering amplitude, $|F(\boldsymbol{q})|^2$, where the scattering amplitude is the Fourier transform of the electron density:

$$A(\boldsymbol{q}) = \int_V \rho(\boldsymbol{r}) e^{-i\boldsymbol{q}\boldsymbol{r}} d\boldsymbol{r}$$

where $f(\boldsymbol{r})$ is the electron density, $\boldsymbol{q}$ is the momentum transfer vector, and $\boldsymbol{r}$ is the real-space vector within the crystal. This scattering amplitude is a complex number and can be alternatively represented by its magnitude and phase:

$$A(\boldsymbol{q}) = |A(\boldsymbol{q})|e^{i\phi(q)}$$

This may be adapted for the case of thin-film growth, or in the context of this dissertation: growth of an organic thin film on SiO_2, where the substrate can be assumed to be unchanging. Treated in this manner, the scattering amplitude can be split into components representing the substrate and the growing thin film:

$$A(\boldsymbol{q_z}, \boldsymbol{t}) = A_{\text{sub}}e^{i\phi_{\text{sub}}} + A_{\text{film}}\sum_{n=1}\theta_n(t)e^{-q_z d_z(n-1)}$$

where the first term represents the substrate and the second term includes the summation of all of the layers of the growing thin film. θ_n represents the coverage of layer n, q_z is the momentum transfer vector normal to the substrate surface, and d_z is the interlayer spacing between layers of the organic thin film.

Organic thin films such as thin films of tetracene, pentacene, and others, form with their *c*-planes, or (001) planes, parallel to the substrate. The *q*-space representation of the spacing of these planes is given by:

$$q_{001} = \frac{2\pi}{d_{001}}$$

Here, d_{001} is the spacing between the (001) planes and is equivalent to d_z mentioned earlier. At the so-called anti-Bragg condition, q_z is equal to half of the value of q_{001}, so

$$q_{00\frac{1}{2}} = \frac{1}{2} q_{001} = \frac{\pi}{d_{001}} = \frac{\pi}{d_z}$$

Therefore, the scattering amplitude can be simplified to:

$$A(\boldsymbol{q}, t) = A_{\text{sub}} e^{i\phi_{\text{sub}}} + A_{\text{film}} \sum_{n=1} \theta_n(t) e^{-\pi(n-1)}$$

From this, it is clear that there will be an oscillation in $A(\boldsymbol{q},t)$ and also the intensity of the scattered X-rays because the layers of the growing thin film will alternate between causing destructive and constructive interference. In this dissertation, the intensity of the scattered X-rays at the anti-Bragg condition is measured *in situ* and in real time during the course of a deposition in the G3 station at CHESS using a PILATUS area detector.

The layer coverages, θ_n, can be modeled by several approaches, detailed by Woll *et al.*[4] These include a modified version of a model proposed by Cohen *et al.*,[6–8] a model by Braun *et al.*,[9] and a simplified version of a model by Trofimov *et al.*[10] This dissertation focuses on the last of these, which will be referred to as the Trofimov model. In this model, the rate of change of the coverage of each layer *n* is described by:

$$\frac{d\theta_n}{dt} = \begin{cases} R_1(1-\theta_1) + R_{n>1}(\theta_1 - \xi_1) & n = 1 \\ R_{n>1}(\xi_{n-1} - \xi_n) & n > 1 \end{cases}$$

where

$$\xi_n = \begin{cases} 0 & \theta_n < \theta_{n,cr} \\ 1 - e^{-\left[\sqrt{-\ln(1-\theta_n)} - \sqrt{-\ln(1-\theta_{n,cr})}\right]^2} & \theta_n \geq \theta_{n,cr} \end{cases}$$

Here, R_1 represents the growth rate for layer 1, and $R_{n>1}$ represents the growth rate for all subsequent layers. The distinction between R_1 and $R_{n>1}$ is included explicitly in the model to account for any coverage dependent adsorption dynamics due to deposition from a hyperthermal source (*i.e.*, a supersonic molecular beam).[8] ξ_n represents a so-called "feeding zone" of layer n. If an atom or molecule land in this feeding zone, then they will contribute to the growth of layer n+1. If instead they land outside of this zone, then they will diffuse downward and contribute to the growth of layer n. $\theta_{n,cr}$ represents a critical coverage of layer n that is required for layer n+1 to nucleate and begin growing. In practice, $\theta_{1,cr}$ and $\theta_{2,cr}$ are independently specified and fit. The critical coverage for all subsequent layers n>2 are defined by an asymptotic approach from $\theta_{2,cr}$ to $\theta\infty_{,cr}$, modified by a parameter N_0:

$$\theta_{\infty,cr} = \theta_{2,cr} + \left(\theta_{\infty,cr} - \theta_{2,cr}\right)\left(1 - e^{\frac{n-2}{N_0}}\right)$$

For the case of 2D layer-by-layer (LbL) growth, the critical coverage of each layer is unity. That is, each layer completes before the next layer begins to grow. This behavior will manifest itself as sharp oscillations in the scattered X-ray intensity as shown in Figure 2-3(a). If growth is 2D LbL for 1 ML and then becomes 3D in nature, these oscillations dampen out with time, as displayed in Figure 2-3(b). Finally, if growth is completely 3D in nature, there is a monotonic decrease in the scattered X-ray intensity with no oscillations, as depicted in Figure 2-3(c). Also shown in these figures are the associated layer coverages. In Figure 2-3(d), the evolution of the RMS roughness is displayed. It is clear that thin films that grow in a 3D manner become rougher than those that grow in a 2D LbL fashion.

It is important to note that any fits of the above model to the data are most reliable around critical features in the data, which constrain the possible solutions. For

the case of 3D growth where there is only a decay in the intensity, the fits are likely unreliable. In the case where growth begins as 2D LbL but then becomes 3D (similar to Stranski-Krastanov growth),[11] the critical features may only extend to the first few monolayers, after which the intensity either decays or becomes flat/featureless, adding considerable uncertainty to the fit after the critical features. Additionally, it is important to recognize that the Trofimov model (*vide supra*) only accounts for net downward transport; it does not account for upward transport, a topic which will be explored through the course of this dissertation.

2.4.2 Grazing incidence diffraction

Grazing incidence X-ray diffraction, or grazing incidence diffraction (GID) is a diffraction method that is surface sensitive due to the grazing incidence of the X-ray beam with the sample. The angle is chosen such that there is more diffraction from the thin film than there is from the bulk substrate. To achieve this, the angle is typically chosen to be just underneath the critical angle of the substrate. Underneath the critical angle, there is total external reflection of the X-rays from the substrate, so diffraction comes largely from the thin film of interest. At grazing incidence, only a small fraction of the incoming photons from the X-ray beam scatter off of the sample, so the intensity of the scattered X-rays is low. Using a synchrotron X-ray source is thus advantageous to achieve a much higher flux than a conventional tabletop X-ray source. The reader is encouraged to refer to a review of grazing incidence scattering techniques by Renaud *et al.*[12] In this dissertation, *in situ* and real-time GID measurements were also taken in G3 by making use of PILTAUS area detectors. *Ex situ* GID has been performed exclusively in the G2 station at CHESS.

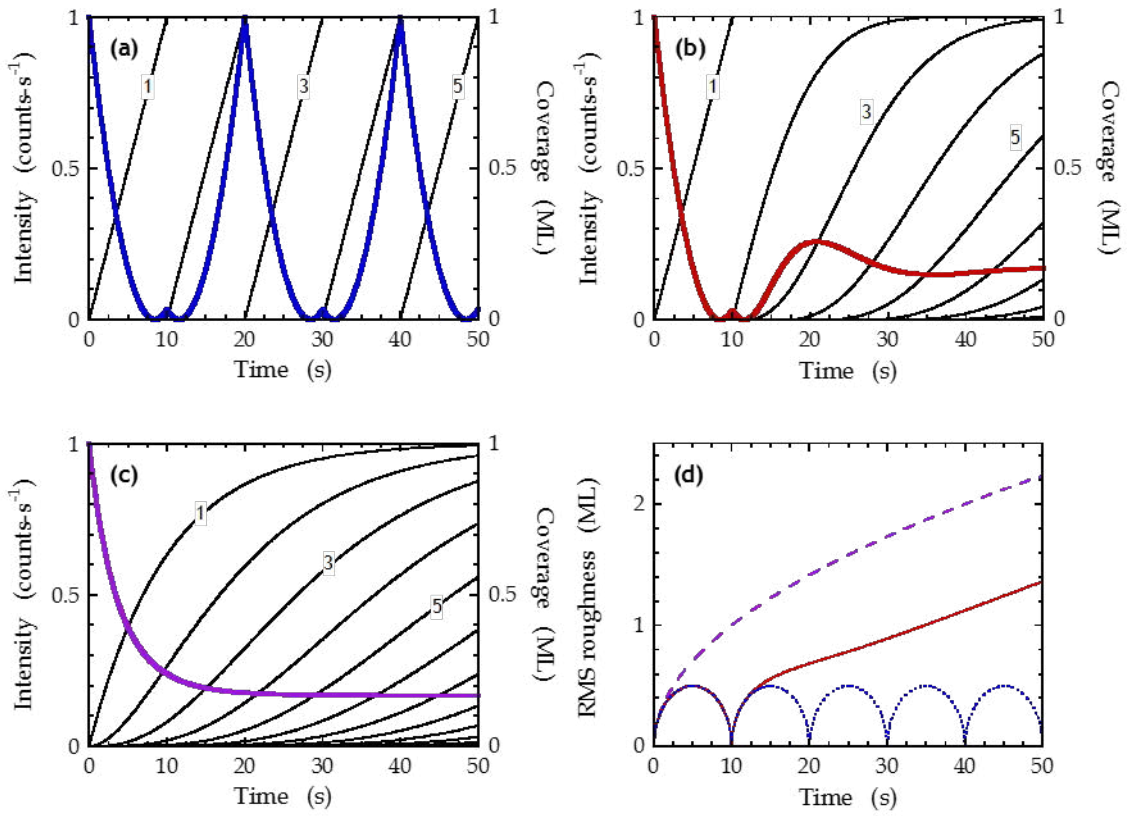

Figure 2-3 **(a)** Scattered X-ray intensity at the anti-Bragg condition as a function of time for ideal 2D LbL growth (solid blue line, left ordinate). The solid black lines represent the layer coverages as a function of time (right ordinate). Similar figures are shown for a case with 2D LbL for 1 ML in **(b)** and for a case with 3D growth in **(c)**. The evolution of RMS roughness as a function of time for these cases are shown in **(d)**.

2.5 Atomic force microscopy

Atomic force microscopy (AFM) was used as an *ex situ* characterization technique for the work contained within this dissertation. AFM is a type of scanning probe microscopy (SPM) which indirectly produces a topographic map of the surface being scanned. In the following work, we used a Bruker Innova AFM (Bruker Corp.), operated in tapping mode, at CHESS, using Olympus AC160TS-R3 microcantilevers (Olympus Corp.), to characterize thin films *ex situ* and examine the morphology of the thin films of interest. Due to the nature of being used as an *ex situ* technique (although there do exist *in situ* AFMs), thin films are subject to possibly deleterious effects, such as post-deposition reorganization,[13] which may alter the microstructure between growth and characterization. The atomic force (AF) micrographs were analyzed using Gwyddion (freeware software for SPM data, available online at http://gwyddion.net). Pre-processing of micrographs in Gwyddion typically involved: leveling the data by mean plane subtraction, removing a polynomial background, aligning the rows by their medians, and then correcting horizontal scars. Gwyddion was then used to determine root mean square (RMS) roughness, extract line scans, and perform 1D power-spectral density (PSD) analysis to determine correlation lengths on the surfaces of the examined thin films.[14,15]

2.6 References

(1) Schroeder, T. W. Dissertation: Thin Film Deposition Employing Supersonic Molecular Beams: Nucleation and Growth of Silicon, Silicon Germanium and Pentacene, Cornell University, 2004.

(2) Desai, T. V. Dissertation: In Situ Real-Time Studies of Organic Semiconductor Thin Film Growth, Cornell University, 2011.

(3) Kish, E. R. Dissertation: Real Time in Situ X-Ray Studies of Organic Heterostructure Formation, Cornell University, 2014.

(4) Woll, A. R.; Desai, T. V.; Engstrom, J. R. Quantitative Modeling of in Situ X-Ray Reflectivity during Organic Molecule Thin Film Growth. *Phys. Rev. B* **2011**, *84* (7), 075479/1–075479/14.

(5) Kowarik, S.; Gerlach, A.; Skoda, M. W. A.; Sellner, S.; Schreiber, F. Real-Time Studies of Thin Film Growth: Measurement and Analysis of X-Ray Growth Oscillations beyond the Anti-Bragg Point. *Eur. Phys. J. Spec. Top.* **2009**, *167* (1), 11–18.

(6) Cohen, P. I.; Petrich, G. S.; Pukite, P. R.; Whaley, G. J.; Arrott, A. S. Birth-Death Models of Epitaxy: I. Diffraction Oscillations from Low Index Surfaces. *Surf. Sci.* **1989**, *216* (1-2), 222–248.

(7) Hong, S.; Amassian, A.; Woll, A. R.; Bhargava, S.; Ferguson, J. D.; Malliaras, G. G.; Brock, J. D.; Engstrom, J. R. Real Time Monitoring of Pentacene Growth on SiO2 from a Supersonic Source. *Appl. Phys. Lett.* **2008**, *92* (25), 253304/1–253301/3.

(8) Amassian, A.; Desai, T. V.; Kowarik, S.; Hong, S.; Woll, A. R.; Malliaras, G. G.; Schreiber, F.; Engstrom, J. R. Coverage Dependent Adsorption Dynamics in Hyperthermal Organic Thin Film Growth. *J. Chem. Phys.* **2009**, *130* (12), 124701/1–124701/9.

(9) Braun, W.; Jenichen, B.; Kaganer, V. M.; Shtukenberg, A. G.; Däweritz, L.; Ploog, K. H. Layer-by-Layer Growth of GaAs(001) Studied by in Situ Synchrotron X-Ray Diffraction. *Surf. Sci.* **2003**, *525* (1-3), 126–136.

(10) Trofimov, V. I.; Mokerov, V. G.; Shumyankov, A. G. Kinetic Model for Molecular Beam Epitaxial Growth on a Singular Surface. *Thin Solid Films* **1997**, *306* (1), 105–111.

(11) Venables, J. A.; Spiller, G. D. T.; Hanbucken, M. Nucleation and Growth of

Thin Films. *Rep. Prog. Phys.* **1984**, *47* (4), 399–459.

(12) Renaud, G.; Lazzari, R.; Leroy, F. Probing Surface and Interface Morphology with Grazing Incidence Small Angle X-Ray Scattering. *Surf. Sci. Rep.* **2009**, *64* (8), 255–380.

(13) Amassian, A.; Pozdin, V. A.; Desai, T. V.; Hong, S.; Woll, A. R.; Ferguson, J. D.; Brock, J. D.; Malliaras, G. G.; Engstrom, J. R. Post-Deposition Reorganization of Pentacene Films Deposited on Low-Energy Surfaces. *J. Mater. Chem.* **2009**, *19* (31), 5580–5592.

(14) Collins, G. W.; Letts, S. A.; Fearon, E. M.; McEachern, R. L.; Bernat, T. P. Surface Roughness Scaling of Plasma Polymer Films. *Phys. Rev. Lett.* **1994**, *73* (5), 708–711.

(15) Biscarini, F.; Samorí, P.; Greco, O.; Zamboni, R. Scaling Behavior of Anisotropic Organic Thin Films Grown in High Vacuum. *Phys. Rev. Lett.* **1997**, *78* (12), 2389–2392.

CHAPTER 3

UNEXPECTED EFFECTS OF THE RATE OF DEPOSITION ON THE MODE OF GROWTH AND MORPHOLOGY OF THIN FILMS OF TETRACENE GROWN ON SILICON DIOXIDE[*]

3.1 Abstract

We have examined the growth of thin films of tetracene on SiO_2 using *in situ* real time X-ray synchrotron radiation and *ex situ* atomic force microscopy. Using *in situ* X-ray reflectivity, we observe a transition from 3D island growth to 2D layer-by-layer growth of thin films of tetracene on SiO_2 as the deposition rate of tetracene is increased. This unusual phenomenon has not been observed in previous work with pentacene, despite the similarities between these two molecules. Atomic force microscopy suggests that tetracene may tend to quickly traverse "upwards" on thin film features such as the edges of islands, making these thin films susceptible to reorganization during and/or after growth. We determine that upward transport during growth drives 3D island growth. Furthermore, the transition from 3D growth to 2D growth results when the rate of admolecule attachment at the tetracene island/SiO_2 substrate edges effectively outcompetes the rate of upward step-edge transport. Increasing the growth rate, and consequently this rate of admolecule attachment, suppresses upward step-edge transport, leading to 2D growth.

---

[*] Nahm, R. K.; Engstrom, J. R. Unexpected Effects of the Rate of Deposition on the Mode of Growth and Morphology of Thin Films of Tetracene Grown on SiO_2. *J. Phys. Chem. C* **2016**, *120* (13), 7183–7191.

3.2 Introduction

Organic semiconductors have been an area of great interest owing to their ability to form crystalline thin films at room temperature, which also exhibit good electrical properties. These diverse materials are promising in applications such as flexible electronic and photovoltaic devices, and are even poised to allow for roll-to-roll fabrication of said devices.[1,2] However, there is a multitude of factors affecting the performance of these organic-based devices that need to be better understood for these materials to be successfully applied in these areas. One of these factors is, of course, the choice of the organic semiconductor, as this will set the upper limit for performance. In addition, irrespective of the chosen material, its electrical properties in a thin film format are also linked to the morphology of the material. The evolution of thin film morphology is complex and is affected by many factors, including some as simple as the composition of the substrate and the conditions of growth.[3–7] Therefore, understanding the assembly of thin films of organic semiconductors is crucial to creating better devices.

In this paper, we examine the growth of tetracene, a polycyclic aromatic hydrocarbon that is similar to pentacene (a prototypical organic semiconductor), but contains one fewer fused ring. Notably, it has been found that the carrier mobility of thin films of tetracene depends on the rate at which the thin films were grown, where low growth rates yielded thin films with distinctly different morphology than those grown at higher growth rates.[8] Shi and Qin have also observed a similar dependence of morphology on growth rate for thin films grown on SiO_2.[9] Other studies have found that two distinct phases of tetracene, a thin film phase and a bulk phase, form during deposition and that the volume fraction of each phase are dependent on deposition rate and substrate.[10–13] While these previous studies have lent insight into

the growth of tetracene, they have all utilized *ex situ* techniques for characterization, which potentially suffer from effects due to post-deposition thin film reorganization.[14]

Here, we present results on the growth of thin films of tetracene on SiO_2, which we have acquired in real time using *in situ* X-ray scattering. We use synchrotron X-ray radiation at Cornell High Energy Synchrotron Source (CHESS) to probe the deposition of tetracene to gain insight concerning the interactions between molecules of tetracene and the substrate. Synchrotron radiation has been successfully used in a similar manner to study the deposition of a variety of organic molecules on different surfaces.[15–26] Coupled with results from atomic force microscopy (AFM), we will show definitively that tetracene behaves quite differently from pentacene and that the morphological evolution of the thin films displays an unusual dependence on growth rate.

3.3 Experimental Procedures

The experiments involving thin film deposition were performed in a custom-designed UHV chamber fitted with Be windows, detailed elsewhere,[27] in the G3 station at CHESS. A supersonic beam of tetracene was generated by passing the carrier gas, He, over a heated vessel containing tetracene powder (99.99%, Sigma-Aldrich) and then expanding the tetracene-seeded gas into a UHV source chamber (base pressure ~ 5×10^{-9} Torr) through a 150 μm diameter nozzle. The beam then passes through a trumpet-shaped skimmer, a differentially-pumped antechamber, and then through an aperture which defines the beam to strike the sample in the main scattering chamber. A remotely-controlled shutter allows for control over the exposure of the substrate to the beam. The growth rate of tetracene was varied by

changing the temperature of the vessel containing tetracene. Using correlations based on time-of-flight measurements of the kinetic energy of a supersonic molecular beam of pentacene,[27,28] also seeded in He, we estimate that the incident kinetic energy (E_i) of tetracene for all experiments was 2.5-2.6 eV. Multiple experiments can be run on a single substrate by translating the sample perpendicular to the supersonic beam, which has a high beam-to-background flux ratio. The substrates were Si(100) wafers with 300 nm of thermal oxide held at a nominal temperature of T_s = 30 °C. Prior to deposition, the substrates were cleaned by sequentially sonicating the substrates in chloroform and then DI water, each for 20 min. with rinsing in DI water between solvents, and finally drying with N_2. The substrates were then subjected to UV/ozone cleaning with a Samco UV-1 (SAMCO, Inc.) for 20 min.

During deposition, thin film growth was monitored *in situ* with real-time X-ray reflectivity (XRR) at the so-called anti-Bragg condition, where $q_z = ½\ q_{(001)}$, which has been shown to be a powerful technique to provide insight into the nature of growth, i.e., 2D layer-by-layer (LbL) vs. 3D islanded growth.[19,20] Specifically, we monitor growth at q_z = 0.242 Å^{-1}, the anti-Bragg condition for the thin film phase of tetracene where the interlayer spacing, d = 12.96 Å. The X-ray beam energy was 10.06 keV with a flux of ~ 10^{15} photons-cm^{-2}-s^{-1} (often attenuated). Measurements of the intensity of the scattered X-ray beam were made using a DECTRIS Pilatus 100K area detector (DECTRIS, Ltd.). Following deposition, thin films were characterized *ex situ* with a Bruker Innova AFM (Bruker Corp.) operated in tapping mode using Olympus AC160TS-R3 micro-cantilevers (Olympus Corp.).

3.4 Results

In Figure 3-1(a), we display the intensity of the scattered X-ray beam collected at the anti-Bragg condition vs. time for the growth of tetracene on SiO_2. From *ex situ* AFM (*vide infra*) we estimate a nominal growth rate of 0.036 nm-s^{-1}. We observe here that, for these conditions of growth, the scattered X-ray intensity decreases monotonically. If tetracene grew in a 2D LbL fashion, oscillations in the intensity would be expected.[19,20] Instead, the lack of oscillations is demonstrative of 3D growth, as opposed to the 2D LbL growth exhibited by pentacene at similar conditions (growth rate and T_s).[15,18,21] We fit this data to a simplified version of a mean-field rate-equation model developed by Trofimov *et al*.[29–32] We have found this model to accurately describe the growth of pentacene on SiO_2 and other small molecule organic semiconductors on a variety of surfaces, correctly predicting layer coverages, thin film thickness, and roughness, verified by independent measurements using AFM.[20] The fit of the scattered intensity and the layer coverages predicted by the model are also shown in Figure 3-1(a). The fit describes the data well, albeit to a set of results that lacks critical features such as local extrema.

In Figure 3-1(b) we display the thin film thickness (D) and the growth rate predicted by the model. In Figure 3-1(c) we also display the RMS roughness (σ) predicted by the model. In all cases we assume 1 ML = 12.96 Å. As may be seen, the model predicts there is an acceleration in the rate of growth. We have observed similar behavior concerning the kinetics of growth of several other small molecule organic semiconductors,[22–25] and this effect is due to the coverage dependence of the probability of adsorption. At the high incident kinetic energies for tetracene examined here, the trapping probability is much less on clean SiO_2 than on pre-existing layers of tetracene. A direct consequence is that growth rate is not constant until the substrate is

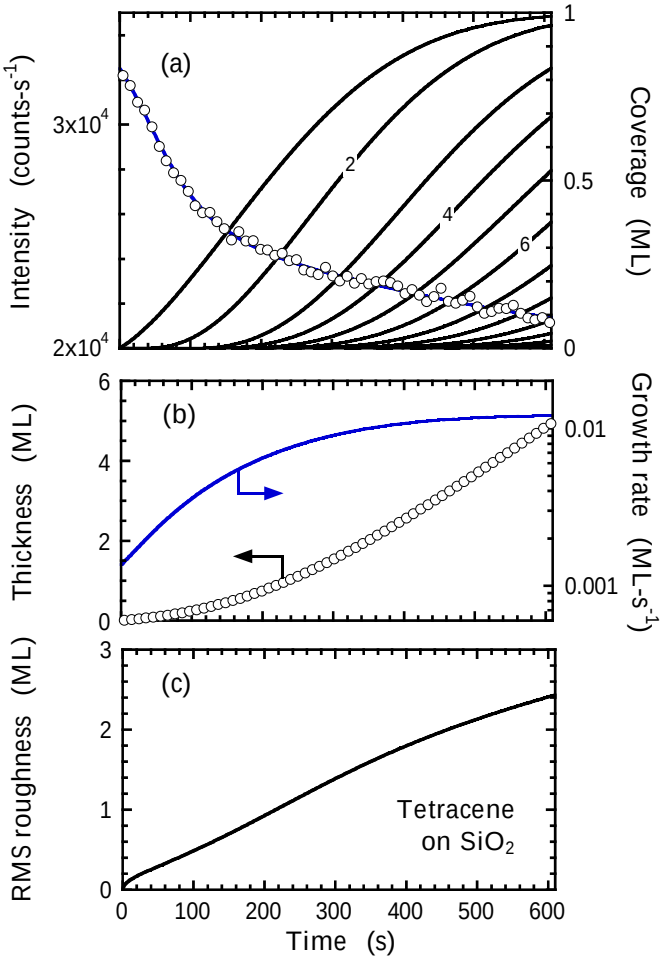

Figure 3-1: **(a)** Scattered X-ray intensity at the anti-Bragg condition as a function of time for thin films of tetracene grown on SiO_2 at 0.036 nm-s^{-1}, represented by the open circles (left ordinate, every 10^{th} data point shown for visibility). The solid blue line (left ordinate) represents a fit of the model to the data, and the solid black curves (right ordinate) represent predicted layer coverages of the individual layers. **(b)** Thickness (left ordinate), growth rate (right ordinate), and **(c)** RMS roughness as predicted by the fit of the data shown in **(a)**.

fully covered by tetracene such that tetracene is growing on itself. The RMS roughness predicted by the model increases monotonically, which is expected with 3D growth. Again, since the data lack critical features, the uncertainty of the model in predicting the RMS roughness likely increases with increasing thickness.

In Figure 3-2(a), we present a 20 × 20 μm^2 atomic force (AF) micrograph representing the thin film of tetracene formed at the end of the experiment (t = 612 s) we considered in Figure 3-1. Based on the results shown in Figure 3-1, this thin film is predicted by the model to have a nominal thickness of D = 6.5 nm and a roughness of σ = 3.2 nm. The morphology clearly exhibits large 3D islands, and while the model predicts that the substrate should be entirely covered, the large flat areas that are visible are only consistent with that of the bare substrate. The islands are dendritic and are on the order of microns in size in the plane of the substrate. Upon closer inspection, the edges of the islands are also significantly taller than the interior portions of the islands, an observation which is exemplified by the line profile we display in Figure 3-2(b). The edges are as high as ~ 60 nm tall whereas the center of the island is ~30 nm tall. From analysis of this image we determine the mean thickness of this thin film is D = 22 nm, while the RMS roughness is σ = 23 nm. In comparison these values are, respectively, factors of ~ 3.4 and ~ 7.2 larger than those predicted by the fit to the X-ray intensity at the anti-Bragg point.

Why are there such large differences between the results from AFM and the predictions of the fit to the anti-Bragg data? First, as indicated above, the absence of critical features in the latter make the uncertainty in predictions of the model significant. Independent of this fact, the monotonic decay in intensity is an unambiguous signature of 3D growth. Concerning the roughness measured by AFM, the value determined here is much greater than the roughness that would be predicted by stochastic roughening (where the roughness scales as $n^{1/2}$, where n is the number of

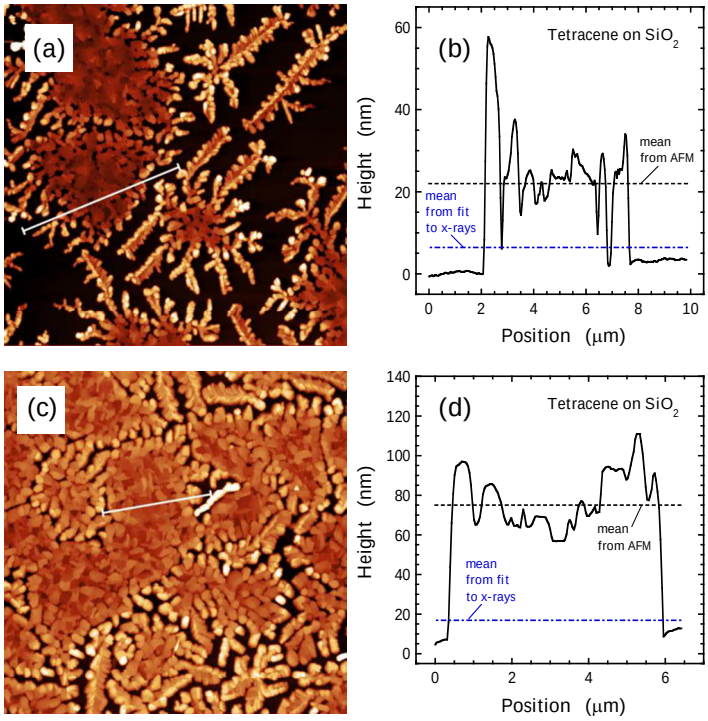

Figure 3-2: **(a)** A 20×20 μm^2 AF micrograph of a 22 nm thin film of tetracene grown on SiO_2 at 0.036 nm-s^{-1}. The line corresponds to the line scan shown in **(b)**, where the dashed line indicates nominal thickness. These figures are repeated for a 75 nm thin film of tetracene in **(c)** and **(d)**. For both micrographs, a height of zero represents the substrate, SiO_2.

monolayers). For example, using the thickness of D = 22 nm (~ 17 ML) measured from AFM, a roughness of σ = 5.3 nm (~ 4.1 ML) is expected from stochastic roughening, assuming a perfectly smooth substrate (from AFM the RMS for SiO_2 is < 0.2 nm). Here, the roughness measured by AFM is σ = 23 nm (~ 18 ML), a factor of 4.3 greater than stochastic roughening, which implicates significant reorganization during and/or after thin film growth. Our model for growth does not allow for "upward" transport of tetracene, thus, a fit to X-ray data cannot produce a result comparable to what we observe in *ex situ* AFM.

Do these features persist for longer times of exposure/thicker thin films? In Figure 3-2(c), we present an AF micrograph of another thin film grown at the same rate but for a longer time (t = 1277 s). We observe that, as the thin film gets thicker, the islands begin to coalesce, but the tall edges persist, as shown by the line profile in Figure 3-2(d). In addition, even for a mean coverage of ~ 58 ML (D = 75 nm) the substrate is still visible. Based on these results from AFM and those from modeling the X-ray intensity at the anti-Bragg condition, 3D growth is dominant at this growth rate.

In Figure 3-3, we consider a set of results similar to those shown in Figure 3-1 for the growth of tetracene on SiO_2, but at a higher growth rate. Based solely on the expected change in the vapor pressure of tetracene in this case compared to the conditions in Figure 3-1, the growth rate should be a factor of ~ 2 larger. From *ex situ* AFM (*vide infra*) we estimate a nominal growth rate of 0.091 nm-s^{-1}, or about 2-½ times that for the experiment we considered in Figure 3-1. Here in Figure 3-3(a), we clearly observe one oscillation in the X-ray intensity, with a maximum at ~ 45 s, suggesting a possible change to 2D LbL growth at these conditions. Qualitatively, one oscillation could indicate one or two MLs of LbL growth,[20] but this can be discriminated more clearly with modeling. Again, we fit this data to the model and

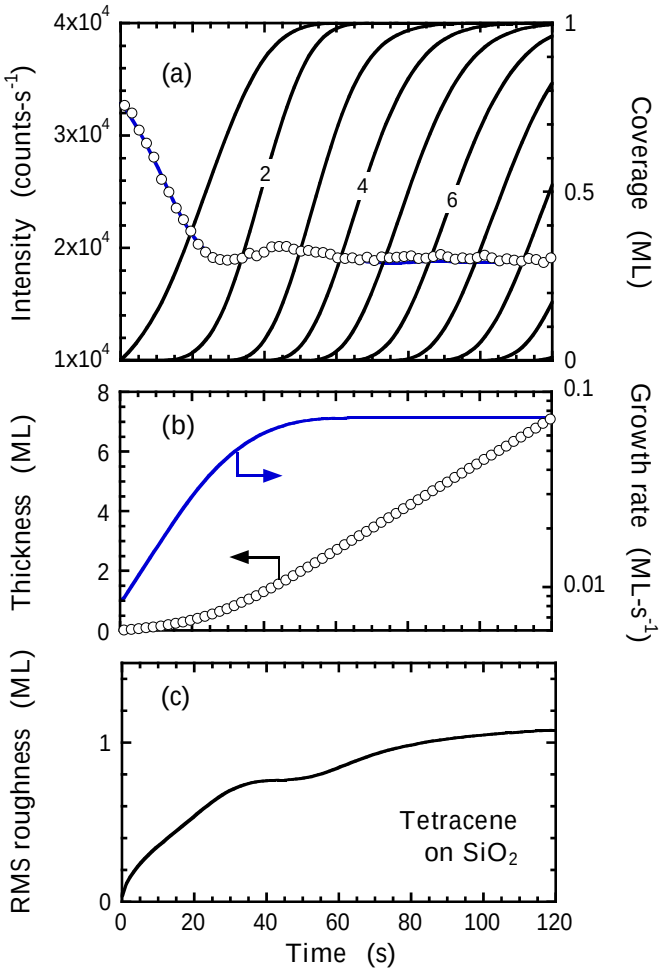

Figure 3-3: **(a)** Scattered X-ray intensity at the anti-Bragg condition and the fit to the data (left ordinate, every 2nd data point shown for visibility), and predicted layer coverages (right ordinate) for thin films of tetracene grown on SiO_2 at 0.091 nm-s^{-1}. **(b)** Thickness (left ordinate), growth rate (right ordinate), and **(c)** RMS roughness as predicted by the fit of the data shown in **(a)**.

show the result in Figure 3-3(a). We see that the fit to the intensity captures the oscillation and matches the data well, and that the single oscillation represents the completion of two MLs of 2D LbL growth before the thin film begins to transition to a 3D mode of growth.

In Figure 3-3(b), we display the thin film thickness and the growth rate predicted by the model. In Figure 3-3(c), we also display the RMS roughness predicted by the model. We see that acceleration in the rate of growth is predicted until $t \sim 50$ s, or the point at which the first monolayer completely covers the substrate. The RMS roughness predicted by the model exhibits a plateau at t = 30-50 s, consistent with much smoother LbL growth for the first 2 MLs.

As before, we can compare the predictions of the model to the results from AFM. In Figure 3-4 we show two sets of results for thin films of tetracene grown at the same nominal rate we considered in Figure 3-3 but for exposure times of (a,b) 172 s and (c,d) 276 s. Based on the fit to the X-ray data, the thin film thicknesses should be $D \sim 15$ nm (11 ML) and ~ 25 nm (19 ML), respectively, and we would expect both thin films to completely cover the substrate. Both thin films do not completely cover the substrate, although the thicker thin film is closer to doing so. Instead, we see large islands, some with dendritic features [*cf*. Figure 3-4(a)], and tall edges are apparent as with the case of the slower growth rate considered in Figure 3-2. From the line profiles shown in Figures 4(b) and 4(d) the edges are as much as twice the height of the middle of the islands.

From the AFM data, we can calculate the thicknesses of the two thin films we consider in Figure 3-4 and we find them to be D = 12.5 nm (9.7 ML) and 25 nm (19 ML), which are in good to excellent agreement with the predictions of the model based on the fit to the X-ray intensity at the anti-Bragg condition. This agreement is indicated by the dashed lines shown in the line scans given in Figures 4(b) and 4(d).

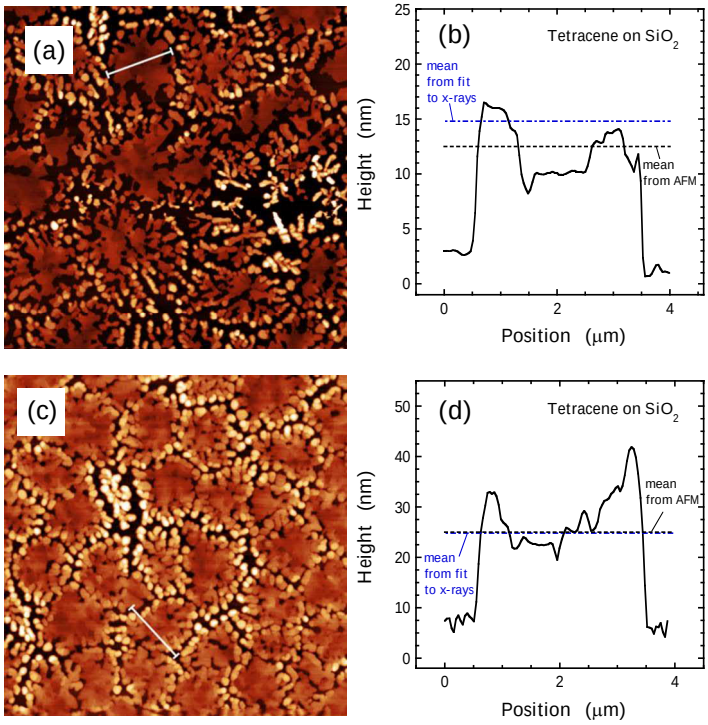

Figure 3-4: **(a)** A 20×20 μm^2 AF micrograph of a 12.5 nm thin film of tetracene grown on SiO_2 at 0.091 nm-s^{-1}. The line corresponds to the line scan shown in **(b)**, where the dashed line indicates nominal thickness. These figures are repeated for a 25 nm thin film of tetracene in **(c)** and **(d)**. For both micrographs, a height of zero represents the substrate, SiO_2.

From AFM, we find values for the RMS roughness of (a,b) σ = 11.9 nm (9.2 ML) and (c,d) 11.5 nm (8.9 ML). Both of these values are much larger than those predicted by a fit to the X-ray data, reflecting the inability of the model to predict layer occupancies once the growth becomes fully 3D. If we compare these values to what stochastic growth would produce, they are also larger: (a,b) a measured value of σ = 9.2 ML vs. 3.1 ML for stochastic growth; and (c,d) a measured value of σ = 8.9 ML vs. 4.4 ML for stochastic growth. Interestingly, the thinner of the two thin films is also slightly rougher. This could be a consequence of upward transport during growth and/or post-deposition reorganization that is facilitated at island edges, which we discuss further below.

In Figure 3-5, we present a set of results similar to those shown in Figures 1 and 3 for an even higher growth rate. Here, the growth rate should be a factor of ~ 7 (11) larger compared to the conditions in Figure 3-3 (Figure 3-1) based on the expected change in the vapor pressure of tetracene. From *ex situ* AFM (*vide infra*) we estimate a nominal growth rate of 0.61 nm-s^{-1}, or about 6.7 times larger than that for the experiment in Figure 3-3. In Figure 3-5(a), we observe rather clearly two oscillations in the scattered X-ray intensity with maxima at ~ 2.5 s and ~ 5 s. The shape of this oscillation is quite similar to 2D LbL growth observed for pentacene on SiO_2.[15,20,21,33] As before, we fit this data to the model and the result is shown in Figure 3-5(a). In this case, the first and second maxima represent the completion of the first and second ML of growth, respectively, after which there is a transition to a 3D mode of growth.

In Figure 3-5(b), we display the thin film thickness and the growth rate predicted by the model. In Figure 3-5(c), we also display the RMS roughness predicted by the model. Again, we note there is acceleration in the rate of growth until t ~ 4 s where the first monolayer completely covers the substrate. The RMS

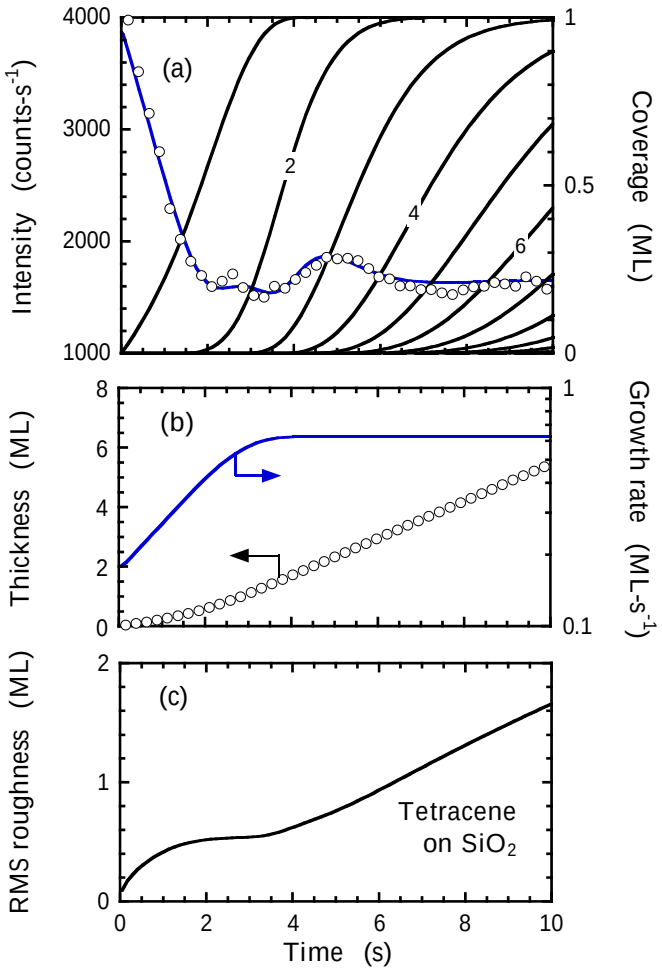

Figure 3-5: **(a)** Scattered X-ray intensity at the anti-Bragg condition and the fit to the data (left ordinate), and predicted layer coverages (right ordinate) for thin films of tetracene grown on SiO_2 at 0.61 nm-s^{-1}. **(b)** Thickness (left ordinate), growth rate (right ordinate), and **(c)** RMS roughness as predicted by the fit of the data shown in **(a)**.

roughness predicted by the model increases with thickness for the regime of growth considered here.

Again, we compare the predictions of the model to the results from AFM. In Figure 3-6 we show results for two thin films of tetracene grown at the same nominal rate shown in Figure 3-5 but for exposure times of (a,b) 26 s and (c,d) 347 s. Based on the fit to the X-ray data, the thin film shown in Figure 3-6(a) should possess a thickness of $D \sim 20.1$ nm (15.5 ML) and the roughness should be $\sigma \sim 4.6$ nm (3.6 ML), and we would expect this thin film to completely cover the substrate. In contrast to the thin films grown at slower growth rates [*cf*. Figures 2(a), 2(b) and Figures 4(a), 4(b)], where there were large islands with tall edges, this surface is comprised of many small grains or islands that have merged into each other, but not necessarily formed a continuous thin film. The line profile shown in Figure 3-6(b) displays islands rising ~ 20 nm or higher above the lowest point, which is likely the underlying SiO_2 substrate. In Figure 3-6(c) we present an AF micrograph of another thin film grown at the same rate for a significantly longer time (t = 347 s). Notably, the substrate appears to be entirely covered by tetracene, and many small grains are present. The line profile in Figure 3-6(d) shows the coarse grains.

From the AFM data, we calculate the thickness of the thin film considered in Figure 3-6(a) to be D = 15.8 nm (12.2 ML), which is in good agreement with the predictions of the model based on the fit to the X-ray intensity at the anti-Bragg condition. This agreement is indicated by the dashed lines shown in the line scans presented in Figure 3-6(b). From AFM we determine the roughness of (a,b) to be σ = 9.0 nm (7.0 ML). Again, we observe that this thin film is rougher than that predicted by the model owing to the model being unable to predict layer occupancies accurately once the growth becomes 3D. This value for roughness is also greater than that for stochastic growth: (a,b) a measured value of σ = 7.0 ML vs. 3.5 ML for stochastic

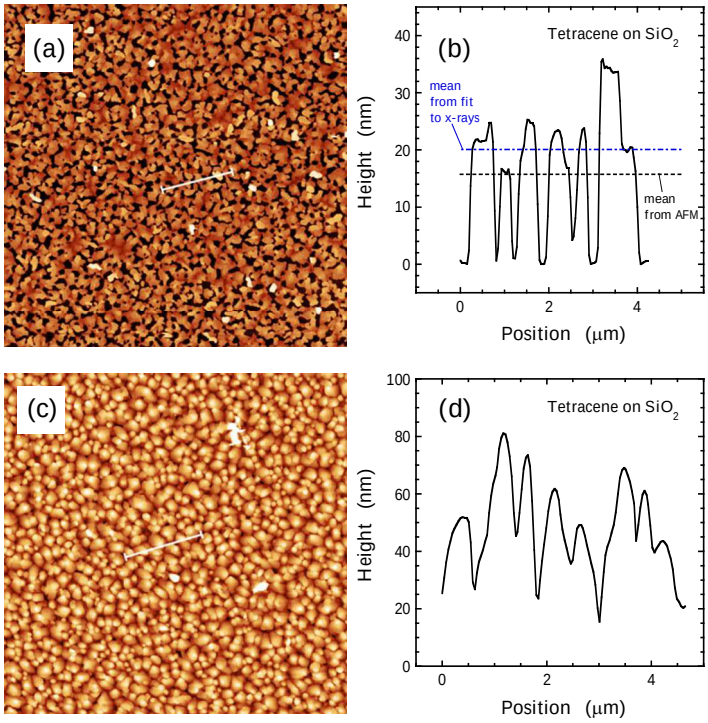

Figure 3-6: **(a)** A 20×20 μm^2 AF micrograph of a 15.8 nm thin film of tetracene grown on SiO_2 at 0.61 nm-s^{-1}. The line corresponds to the line scan shown in **(b)**, where the dashed line indicates nominal thickness. A height of zero in **(a)** and **(b)** represents the substrate, SiO_2. These figures are repeated for a 210-280 nm thin film of tetracene in **(c)** and **(d)**. A height of zero in **(c)** and **(d)** represent the lowest points of the thin film.

growth. For the thicker thin film shown in Figure 3-6(c), the roughness is measured to be σ = 15.0 nm (11.6 ML), which is greater than for the results shown in Figures 6(a) and 6(b). Based on the growth rates determined for the thinner film, the film displayed in Figure 3-6(d) could be D ~ 210-280 nm (162-216 ML) thick. Using these thicknesses, stochastic growth would give a RMS roughness of σ ~ 13-15 ML – larger than what is measured. Thus, for this particular thin film, we need not necessarily invoke the presence of upward transport during growth and/or post-deposition reorganization.

3.5 Discussion

We have examined the thin film growth of tetracene on SiO_2, focusing on the dependence of the growth mode on the growth rate. The data in the previous section demonstrate an unexpected dependence of morphology on growth rate: at low deposition rates, tetracene grows in a 3D mode, whereas at high deposition rates, tetracene initially grows 2D LbL before eventually growing 3D. Is this phenomenon exhibited by similar molecules? Concerning pentacene, we previously investigated the thin film growth of pentacene from a supersonic molecular beam source on SiO_2 at room temperature and at various rates and did not find such a transition. Using *in situ* synchrotron X-ray scattering and *ex situ* AFM, we observed that pentacene grew in a 2D LbL mode over a wide range of growth rates (0.009-0.137 ML-s^{-1}),[21] which overlap the rates of growth considered here for tetracene (0.028-0.467 ML-s^{-1}).

In Figure 3-7, we present a direct comparison of the morphology of thin films of (a,b) tetracene and (c,d) pentacene grown on SiO_2 at similar growth conditions (T_s, E_i, growth rate, thickness). Here, tetracene (E_i = 2.5-2.6 eV) was grown at a rate of

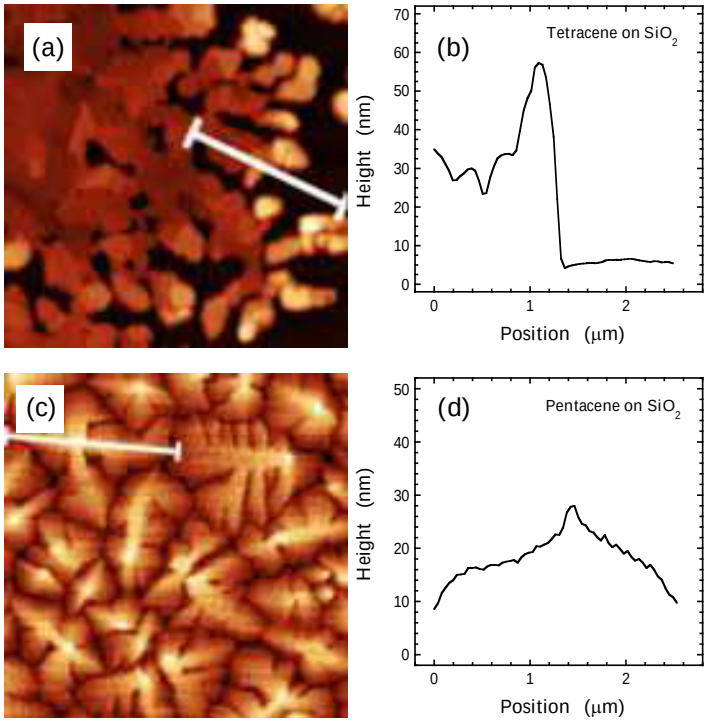

Figure 3-7 **(a)** A zoomed view (5×5 μm^2) of the thin film of tetracene shown in Figure 3-2(a). The line corresponds to the line scan shown in **(b)**. A height of zero in **(a)** and **(b)** represents the substrate, SiO_2. **(c)** A 5×5 μm^2 AF micrograph of a 29 nm thin film of pentacene grown on SiO_2 at 0.027 nm-s^{-1} at E_i = 2.5-2.6 eV. The line corresponds to the line scan shown in **(d)**. A height of zero in **(c)** and **(d)** represent the lowest points of the thin film.

0.036 nm-s^{-1} (0.028 ML-s^{-1}) to a thickness of 22 nm (~ 17 ML), and pentacene (E_i = 2.7 eV) was grown at a rate of 0.027 nm-s^{-1} (0.017 ML-s^{-1}) to a thickness of 29 nm (~ 19 ML).[34] Both thin films were grown at room temperature. In Figures 7(a) and 7(b), we show a close-up AF micrograph of a thin film of tetracene shown earlier [*cf*. Figure 3-2(a)] and a corresponding line-scan. As observed above, this thin film exhibited large areas of bare substrate. These data clearly show the primary features of the island: edges taller than the interior, with relatively steep sidewalls. In Figures 7(c) and 7(d), we present an AF micrograph of a thin film of pentacene and a corresponding line-scan. In Figure 3-7(c), we observe a drastically different morphology than tetracene, and instead see pyramid-shaped islands with dendritic features. The line-scan in Figure 3-7(d) shows that the islands are always tallest in the interior, unlike in the case of tetracene.

Why is the morphology of thin films of tetracene so different from that of thin films of pentacene? As noted previously, the data suggest upward transport during and/or after thin film deposition of tetracene. Concerning pentacene, we have previously observed post-deposition reorganization of thin films of pentacene less than ~ 5 ML thick grown on low energy surfaces, namely on SiO_2 terminated with self-assembled monolayers (SAMs).[14] In this work we did *not* observe re-organization on *clean*, unmodified SiO_2. Interestingly, even for cases that showed post-deposition re-organization/de-wetting, we observed intensity oscillations at the anti-Bragg point during growth, consistent with 2D LbL growth. Finally, thin films greater than ~ 5 ML in thickness were stable on all surfaces, and did not undergo post-deposition re-organization. As a whole, these results pointed to the importance of surface energy as a driving force for re-organization, and island edges as regions that can facilitate upward transport.

We first consider the thermodynamic driving force for thin film reorganization: surface energies. Clean, unmodified SiO_2 has been reported to have a surface energy lying between 50 and 60 mJ-m^{-2}.[35,36] (We note that the aforementioned work on pentacene on low-energy surfaces involved SAMs with much lower surface energies of 12-36 mJ-m^{-2}.)[14] The (001) facets of tetracene and pentacene, which represent the preferred orientation during growth, have been predicted to have similar surface energies of 84 mJ-m^{-2} and 82-91 mJ-m^{-2}, respectively.[37] These values are larger than the surface energy of SiO_2 (indicating a driving force for dewetting), but their similarity does not predict significantly different behavior between tetracene and pentacene.

Even in the presence of a driving force for upward transport and reorganization, the kinetics of transport will determine whether or not such events will occur with significant frequency. Stated another way, the driving force determines the irreversibility of the process, while the kinetics determines the rate. One can expect that the barriers to transport across step edges may scale with the strength of the intermolecular potential. The enthalpy of sublimation of the crystal can give us some insight: for tetracene it is ~ 32 kcal-mol^{-1}, for pentacene it is ~ 40 kcal-mol^{-1}.[38] If the barriers to transport scale with these energies, then transport will be faster for tetracene vis-à-vis pentacene. In one study of acenes using empirical molecular mechanics (MM3π) potentials,[39] it was found that the binding energy of molecules on the (001) facet, and the barrier for "downward" step-edge crossing scaled with the cohesive energy nearly linearly among anthracene, tetracene and pentacene. In addition, given the orientation of the islands and the crystal structure, the enthalpy of sublimation (~ cohesive energy) can be used to estimate the binding energy of a molecule at the step edge. Thus, one can also compute the barrier for "*upward*" transport given these three quantities. Doing so, we find that the computed barrier for

upward transport scales with the cohesive energy nearly linearly among these three acenes. Moreover, the predicted barrier for upward transport is ~ 17.7 and 22.5 kcal-mol^{-1} for tetracene and pentacene, respectively. Employing a reasonable attempt frequency of 10^{13} s^{-1} and T_s = 30 °C, we predict a rate coefficient for upward step-edge crossing of $k \sim 2$ s^{-1} and 6×10^{-4} s^{-1} for tetracene and pentacene, or a factor of 3,000 difference.

An order of magnitude estimate for the rate at which molecules impact the edge of an island can be made using the growth rate, the spacing between island edges, and the size of the unit cell. The AF micrograph displayed in Figure 3-6(a) gives us some guidance, and a reasonable order of magnitude value for the spacing between island edges is ~ 100 nm. Using this number and the growth rates observed for the 3 cases considered here (0.028, 0.070 and 0.47 ML-s^{-1}), we estimate impingement rates of molecules at the island edge of ~ 2, 5 and 30 site^{-1}-s^{-1}. The latter two impingement rates exceed what we have estimated for the rate coefficient for upward transport. Thus, it seems that for the conditions examined here the two processes, attachment at the island edge and upward transport, are occurring at rates that are competitive with each other.

In the scenario we have just introduced, there is a competition between island reorganization, via upward interlayer transport, and island growth, via admolecule attachment at edges. The latter, of course, depends on the rate of growth. We can find additional evidence for this effect if we examine the morphology of thin films of similar thicknesses grown at different growth rates using *ex situ* AFM. In Figure 3-8, we plot the RMS surface roughness of thin films of tetracene (all ~ 22-29 nm thick) as a function of the growth rate. We also show the roughness expected solely from stochastic growth. As may be seen there is a strong dependence of the RMS surface roughness on the rate of growth. At the lowest rate of growth (*cf*. Figures 1-2) the

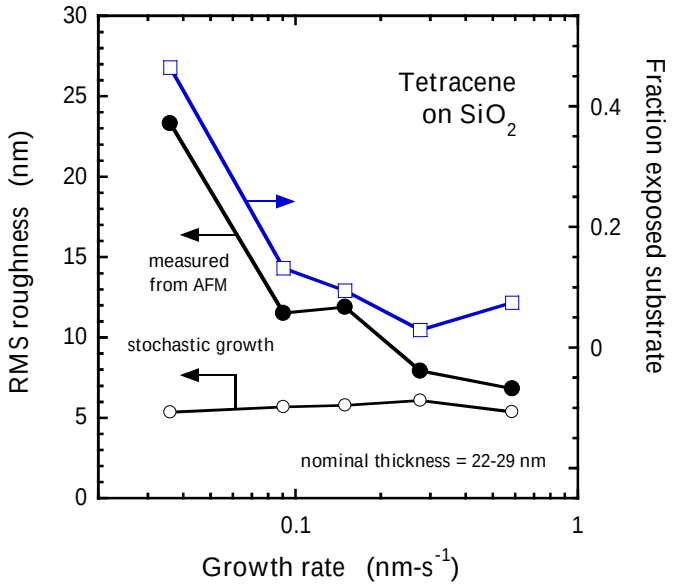

Figure 3-8 RMS roughness and maximum RMS roughness from stochastic growth (left ordinate) represented by the solid and open circles, respectively (connected lines shown for ease of viewing), and fraction of exposed substrate (right ordinate) represented by the open squares (connected line shown for ease of viewing), for thin films of tetracene ~22 to ~29 nm thick on SiO_2 as a function of growth rate.

roughness is very large, whereas at the highest rate of growth (*cf*. Figures 5-6) the roughness is much smaller and approaches that expected from stochastic growth. In Figure 3-8 we also display the fraction of the substrate surface that is exposed after growth, based on *ex situ* AFM. As may be seen there is a strong correlation between the surface roughness and the fraction of surface that is exposed. Since the edges of islands, or the interface between areas of covered and uncovered substrate act as the most likely regions for upward transport and reorganization, this correlation is expected. The fact that the islands formed at lower growth rates are highest near their edges (the source of molecules traversing upwards) is also consistent with this picture.

In Figure 3-9, we consider a schematic diagram of the molecular scale processes involved in results we have observed here, including side-on and top views of an island, and the corresponding potential energy landscape. For simplicity we have chosen to represent the adsorbed molecules as spheres. First, we expect lateral transport of the admolecules across the surfaces of the substrate and the terraces of the thin film to be facile, with very little energetic corrugation. This is due to the fact that a molecule like tetracene will lay flat to maximize its van der Waals interaction, before binding in a mostly standing up fashion in an island. What is important are the processes occurring at the edge of an island. As an admolecule approaches an island edge, there will be a strong attraction to bind to the island, but there may be a barrier to this process associated with the change in the molecule's orientation from laying down to standing up. Once attached to an island edge, the molecule will encounter a barrier to upward transport. Competing with the rate of upward transport will be the rate at which additional admolecules arrive at the step edge. If a molecule at an island edge site is covered by another attaching admolecule, it becomes a molecule representing the interior of the island where upward transport is energetically strongly disfavored. At sufficiently high rates of growth, the flux of molecules arriving at

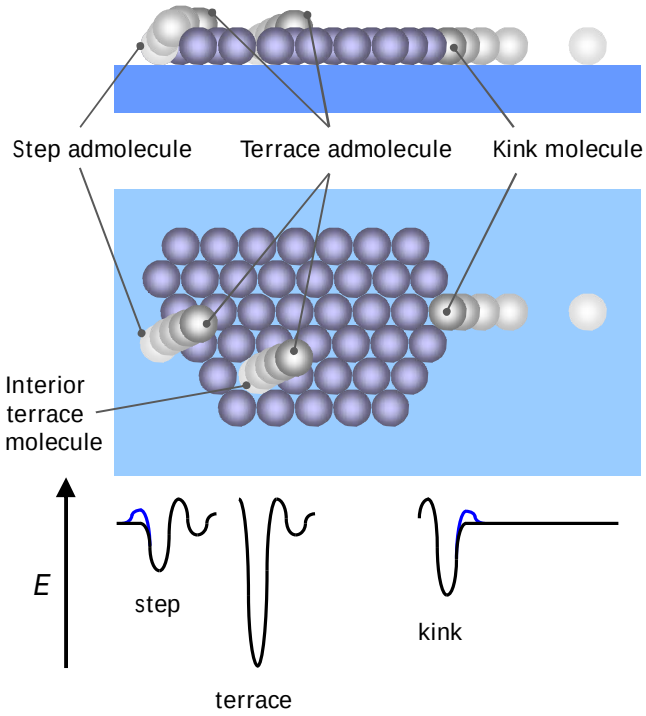

Figure 3-9 A schematic diagram of the molecular scale processes involved, including side-on and top views of an island, and the corresponding potential energy landscape. For simplicity, the adsorbed molecules are represented as spheres. *Figure courtesy of James R. Engstrom.*

island edges is sufficient to compete with the rate of upward transport, and we observe 2D LbL growth. Furthermore, it is conceivable that 2D LbL growth could be promoted by decreasing the temperature of the substrate and hence the rate of upward transport. In a similar vein, Forrest and co-workers previously observed smoother films following growth at lower temperatures and large 3D islands at higher temperatures during the thin film growth of perylene-3,4,9,10-tetracarboxylic dianhydride (PTCDA) on Au(111).[40] Our observations should apply to any system that possesses an energetic driving force for reorganization/dewetting, and where the barrier for upward transport is such that the rate of this process is on the order of the rate at which admolecules arrive at a step edge.

3.6 Conclusions

We have examined the effect of the growth rate on the mode of growth and the morphology of thin films of tetracene that are deposited on SiO_2 at room temperature. From *in situ* X-ray reflectivity, we find that tetracene forms polycrystalline thin films for the conditions we examined here. From measurements made *in situ* and in real time with X-rays at the anti-Bragg condition, we find that tetracene grows in a 3D mode at low growth rates (< 0.05 nm-s^{-1}) but then transitions to grow in a 2D LbL fashion at higher growth rates (> 0.1 nm-s^{-1}). At low growth rates the features that are formed after the deposition of many layers (> 10 MLs) are characterized by islands that are, in general, much higher at their edges than at their interior regions, possessing edges that are also steep. In addition, significant regions of the substrate remain uncovered even for a nominal thickness in excess of 15 MLs. The RMS surface

roughness of these thin films is also much greater than what would be expected from random, stochastic growth.

These results for tetracene have been compared to results for pentacene found at similar rates of growth on SiO_2 at room temperature. In particular, pentacene exhibits 2D LbL growth at low coverages for all growth rates, and the morphology of islands formed at higher coverages are consistent with 3D growth produced by limited downward step-edge transport. In contrast significant upward step-edge transport occurs during the growth of tetracene thin films, which is likely due to a smaller barrier for step-edge crossing for tetracene compared to pentacene. Upward step-edge transport, driven by differences in surface energies between tetracene and the SiO_2 surface, leads to thin films that do not cover the substrate, exhibiting the aforementioned morphology. Upward transport and 3D growth can be suppressed by increasing the growth rate sufficiently, where admolecule attachment at island edges can effectively compete with upward admolecule transport. Our work makes clear that thin films of very similar organic molecules can grow very differently, even if their surface energies are similar. This is important to consider when engineering organic-organic heterostructures for application in areas such as optoelectronic devices.

3.7 Acknowledgements

We would like to thank Arthur R. Woll for invaluable technical contributions. This work was supported in part by Cornell University's David R. Atkinson Center for a Sustainable Future (ACSF). This work made use of the Nanobiotechnology Center shared research facilities at Cornell, and is based upon research conducted at the

Cornell High Energy Synchrotron Source (CHESS), which is supported by the National Science Foundation under NSF award DMR-1332208.

3.8 References

(1) Forrest, S. R. The Path to Ubiquitous and Low-Cost Organic Electronic Appliances on Plastic. *Nature* **2004**, *428*, 911–918.

(2) Mei, J.; Diao, Y.; Appleton, A. L.; Fang, L.; Bao, Z. Integrated Materials Design of Organic Semiconductors for Field-Effect Transistors. *J. Am. Chem. Soc.* **2013**, *135*, 6724–6746.

(3) Schreiber, F. Organic Molecular Beam Deposition: Growth Studies beyond the First Monolayer. *Phys. Status Solidi A* **2004**, *201*, 1037–1054.

(4) Kowarik, S.; Gerlach, A.; Schreiber, F. Organic Molecular Beam Deposition: Fundamentals, Growth Dynamics, and in Situ Studies. *J. Phys.-Condens. Mat.* **2008**, *20*, 184005.

(5) Fenter, P.; Eisenberger, P.; Burrows, P.; Forrest, S. R.; Liang, K. S. Epitaxy at the Organic-Inorganic Interface. *Phys. B* **1996**, *221*, 145–151.

(6) Forrest, S. R.; Burrows, P. E. Growth Modes of Organic Semiconductor Thin Films Using Organic Molecular Beam Deposition: Epitaxy, van Der Waals Epitaxy, and Quasi-Epirtaxy. *Supramol. Sci.* **1997**, *4*, 127–139.

(7) Li, H.; Giri, G.; Tok, J. B.-H.; Bao, Z. Toward High-Mobility Organic Field-Effect Transistors: Control of Molecular Packing and Large-Area Fabrication of Single-Crystal-Based Devices. *MRS Bull.* **2013**, *38*, 34–42.

(8) Cicoira, F.; Santato, C.; Dinelli, F.; Murgia, M.; Loi, M. a.; Biscarini, F.; Zamboni, R.; Heremans, P.; Muccini, M. Correlation Between Morphology and Field-Effect-Transistor Mobility in Tetracene Thin Films. *Adv. Funct. Mater.* **2005**, *15*, 375–380.

(9) Shi, J.; Qin, X. Nucleation and Growth of Tetracene Films on Silicon Oxide. *Phys. Rev. B* **2008**, *78*, 115412.

(10) Milita, S.; Servidori, M.; Cicoira, F.; Santato, C.; Pifferi, A. Synchrotron X-Ray Investigation of Tetracene Thin Films Grown at Different Deposition Fluxes. *Nucl. Instrum. Meth. B* **2006**, *246*, 101–105.

(11) Milita, S.; Santato, C.; Cicoira, F. Structural Investigation of Thin Tetracene Films on Flexible Substrate by Synchrotron X-Ray Diffraction. *Appl. Surf. Sci.* **2006**, *252*, 8022–8027.

(12) Gompf, B.; Faltermeier, D.; Redling, C.; Dressel, M.; Pflaum, J. Tetracene Film Morphology: Comparative Atomic Force Microscopy, X-Ray Diffraction and

Ellipsometry Investigations. *Eur. Phys. J. B* **2008**, *27*, 421–424.

(13) Wünsche, J.; Tarabella, G.; Bertolazzi, S.; Bocoum, M.; Coppedè, N.; Barba, L.; Arrighetti, G.; Lutterotti, L.; Iannotta, S.; Cicoira, F.; et al. The Correlation between Gate Dielectric, Film Growth, and Charge Transport in Organic Thin Film Transistors: The Case of Vacuum-Sublimed Tetracene Thin Films. *J. Mater. Chem. C* **2013**, *1*, 967.

(14) Amassian, A.; Pozdin, V. A.; Desai, T. V.; Hong, S.; Woll, A. R.; Ferguson, J. D.; Brock, J. D.; Malliaras, G. G.; Engstrom, J. R. Post-Deposition Reorganization of Pentacene Films Deposited on Low-Energy Surfaces. *J. Mater. Chem.* **2009**, *19*, 5580–5592.

(15) Mayer, A. C.; Ruiz, R.; Headrick, R. L.; Kazimirov, A.; Malliaras, G. G. Early Stages of Pentacene Film Growth on Silicon Oxide. *Org. Electron.*, 2004, *5*, 257–263.

(16) Krause, B.; Schreiber, F.; Dosch, H.; Pimpinelli, A.; Seeck, O. H. Temperature Dependence of the 2D-3D Transition in the Growth of PTCDA on Ag(111): A Real-Time X-Ray and Kinetic Monte Carlo Study. *Eur. Lett.* **2004**, *65*, 372–378.

(17) Kowarik, S.; Gerlach, A.; Sellner, S.; Schreiber, F.; Cavalcanti, L.; Konovalov, O. Real-Time Observation of Structural and Orientational Transitions during Growth of Organic Thin Films. *Phys. Rev. Lett.* **2006**, *96*, 1–4.

(18) Kowarik, S.; Gerlach, A.; Leitenberger, W.; Hu, J.; Witte, G.; Wöll, C.; Pietsch, U.; Schreiber, F. Energy-Dispersive X-Ray Reflectivity and GID for Real-Time Growth Studies of Pentacene Thin Films. *Thin Solid Films* **2007**, *515*, 5606–5610.

(19) Kowarik, S.; Gerlach, A.; Skoda, M. W. A.; Sellner, S.; Schreiber, F. Real-Time Studies of Thin Film Growth: Measurement and Analysis of X-Ray Growth Oscillations beyond the Anti-Bragg Point. *Eur. Phys. J. Spec. Top.* **2009**, *167*, 11–18.

(20) Woll, A. R.; Desai, T. V.; Engstrom, J. R. Quantitative Modeling of in situ X-Ray Reflectivity during Organic Molecule Thin Film Growth. *Phys. Rev. B* **2011**, *84*, 075479/1–075479/14.

(21) Hong, S.; Amassian, A.; Woll, A. R.; Bhargava, S.; Ferguson, J. D.; Malliaras, G. G.; Brock, J. D.; Engstrom, J. R. Real Time Monitoring of Pentacene Growth on SiO_2 from a Supersonic Source. *Appl. Phys. Lett.* **2008**, *92*, 253304/1–253301/3.

(22) Amassian, A.; Desai, T. V.; Kowarik, S.; Hong, S.; Woll, A. R.; Malliaras, G. G.; Schreiber, F.; Engstrom, J. R. Coverage Dependent Adsorption Dynamics in Hyperthermal Organic Thin Film Growth. *J. Chem. Phys.* **2009**, *130*, 124701/1–124701/9.

(23) Desai, T. V.; Woll, A. R.; Schreiber, F.; Engstrom, J. R. Nucleation and Growth of Perfluoropentacene on Self-Assembled Monolayers: Significant Changes in Island Density and Shape with Surface Termination. *J. Phys. Chem. C* **2010**, *114*, 20120–20129.

(24) Desai, T. V.; Hong, S.; Woll, A. R.; Hughes, K. J.; Kaushik, A. P.; Clancy, P.; Engstrom, J. R. Hyperthermal Organic Thin Film Growth on Surfaces Terminated with Self-Assembled Monolayers. I. The Dynamics of Trapping. *J. Chem. Phys.* **2011**, *134*, 224702/1–224702/13.

(25) Desai, T. V.; Kish, E. R.; Woll, A. R.; Engstrom, J. R. Hyperthermal Growth of N,N′-Ditridecylperylene-3,4,9,10-Tetracarboxylic Diimide on Self-Assembled Monolayers: Adsorption Dynamics and Sub- and Multilayer Thin Film Growth. *J. Phys. Chem. C* **2011**, 18221–18234.

(26) Desai, T. V.; Woll, A. R.; Engstrom, J. R. Thin Film Growth of Pentacene on Polymeric Dielectrics: Unexpected Changes in the Evolution of Surface Morphology with Substrate. *J. Phys. Chem. C* **2012**, *116*, 12541–12552.

(27) Schroeder, T. W. Thin Film Deposition Employing Supersonic Molecular Beams: Nucleation and Growth of Silicon, Silicon Germanium and Pentacene. Ph.D. Thesis, Cornell University, 2004.

(28) Killampalli, A. S.; Schroeder, T. W.; Engstrom, J. R. Nucleation of Pentacene on Silicon Dioxide at Hyperthermal Energies. *Appl. Phys. Lett.* **2005**, *87*, 033110.

(29) Trofimov, V. I.; Mokerov, V. G.; Shumyankov, A. G. Kinetic Model for Molecular Beam Epitaxial Growth on a Singular Surface. *Thin Solid Films* **1997**, *306*, 105–111.

(30) Trofimov, V. I.; Mokerov, V. G. Rate Equations Model for Layer Epitaxial Growth Kinetics. *Thin Solid Films* **2003**, *428*, 66–71.

(31) Trofimov, V. I.; Kim, J.; Bae, S. Influence of Two Different Adatom Mobilities on the Initial Heteroepitaxial Growth Kinetics. *Surf. Sci.* **2007**, *601*, 4465–4469.

(32) Trofimov, V. I.; Kim, J.; Bae, S. Temperature Behavior of the Growth Mechanism during Layer Epitaxial Growth. *J. Phys. Conf. Ser.* **2008**, *100*, 082005.

(33) Ruiz, R.; Choudhary, D.; Nickel, B.; Toccoli, T.; Chang, K.-C.; Mayer, A. C.; Clancy, P.; Blakely, J. M.; Headrick, R. L.; Iannotta, S.; et al. Pentacene Thin Film Growth. *Chem. Mater.* **2004**, *16*, 4497–4508.

(34) Killampalli, A. S. Interface Formation and Thin Film Deposition for Molecular and Organic Electronics. Ph.D. Thesis, Cornell University, 2006.

(35) Knieling, T.; Lang, W.; Benecke, W. Gas Phase Hydrophobisation of MEMS Silicon Structures with Self-Assembling Monolayers for Avoiding in-use Sticking. *Sens. Actuat. B-Chem.* **2007**, *126*, 13–17.

(36) Kawai, A.; Kawakami, J. Characterization of SiO_2 Surface Treated by HMDS Vapor and O_2 Plasma with AFM Tip. *J. Photopolym. Sci. Tec.* **2003**, *16*, 665–668.

(37) Ambrosch-Draxl, C.; Nabok, D.; Puschnig, P.; Meisenbichler, C. The Role of Polymorphism in Organic Thin Films: Oligoacenes Investigated from First Principles. *New J. Phys.* **2009**, *11*, 125010.

(38) Roux, M. V.; Temprado, M.; Chickos, J. S.; Nagano, Y. Critically Evaluated Thermochemical Properties of Polycyclic Aromatic Hydrocarbons. *J. Phys. Chem. Ref. Data* **2008**, *37*, 1855.

(39) Goose, J. E.; First, E. L.; Clancy, P. Nature of Step-Edge Barriers for Small Organic Molecules. *Phys. Rev. B* **2010**, *81*, 10–12.

(40) Forrest, S. R. Ultrathin Organic Films Grown by Organic Molecular Beam Deposition and Related Techniques. *Chem. Rev.* **1997**, *97*, 1793–1896.

CHAPTER 4

WHO'S ON FIRST? TRACKING IN REAL TIME THE GROWTH OF MULTIPLE CRYSTALLINE PHASES OF AN ORGANIC SEMICONDUCTOR: TETRACENE ON SILICON DIOXIDE*

4.1 Abstract

We have examined the effect of growth rate on the evolution of two polymorphs of thin films of tetracene on SiO_2 using synchrotron X-ray radiation and molecular beam techniques. *Ex situ* X-ray reflectivity shows that tetracene forms two phases on SiO_2: a thin-film phase and a bulk phase. We have used *in situ*, real-time grazing incidence diffraction during growth to reveal the nature of growth concerning these two phases. We observe that there is initially growth of only the thin-film phase, up to a thickness of several monolayers. This is followed by the nucleation of the bulk phase, growth of both phases, and finally growth of only the bulk phase. We find that the deposited thickness when the bulk phase nucleates increases with increasing growth rate. Similarly, we find that the deposited thickness at which the thin-film phase saturates also increases with increasing growth rate. These apparent dependencies on growth rate are actually a consequence of the local coverage, which depends on growth rate, particularly for the former effect. At low growth rates, there is 3D growth resulting

---

* Nahm, R. K.; Engstrom, J. R. Who's on First? Tracking in Real Time the Growth of Multiple Crystalline Phases of an Organic Semiconductor: Tetracene on SiO2. *J. Chem. Phys.* **2017**, *146* (5), 52815.

from upward transport of tetracene at island edges, resulting in tall features where molecules escape the influence of the substrate and form into the bulk phase. Increasing the growth rate leads to growth that is more 2D and uniform in coverage, delaying the formation of the bulk phase.

4.2 Introduction

The growth of thin films of organic molecules for application in organic electronics has been a topic of great interest as researchers search for effective combinations of materials and explore the complex behaviors that arise from the breadth of these combinations.[1–3] Organic molecules can assemble into crystalline thin films, but they interact *via* relatively weak van der Waals interactions compared to covalent/ionic/metallic bonds in inorganic systems. In addition, due to their often complex, low-symmetry shapes, thin films of organic molecules can form a variety of polymorphs,[4,5] sometimes influenced by the presence of a substrate.[6] Even relatively simple molecules have been shown to exhibit multiple polymorphs, such as perylenetetracarboxylic dianhydride (PTCDA),[7,8] pentacene,[9–12] perfluoropentacene,[13] and diindenoperylene (DIP).[14,15] These different polymorphs naturally have different properties, and one particular structure may be more desirable than another.[11,16] Therefore, it is of critical importance to understand how these polymorphs arise during thin film growth to obtain the desired properties.

Tetracene is another example of a molecule that exhibits multiple phases at room temperature in thin-film form.[17–21] Gompf *et al*. and Milita *et al*. have observed the formation of two phases, and have reported their relative amounts as determined by *ex situ*, post-deposition techniques.[17,18] Both studies found that lower growth rates

produced more bulk phase while higher growth rates produced more thin-film phase. Lacking in these works was a determination of the evolution of the two phases, and why might the growth rate affect the relative proportion of the two crystalline structures. Here, we seek to provide a better understanding of how and why these phases arise during thin film growth. We will present the results from our investigation on the formation of the thin-film phase and the bulk phase of tetracene on SiO_2, where we use *in situ* real-time grazing incidence diffraction (GID) at Cornell High Energy Synchrotron Source (CHESS) to monitor the evolution of these crystalline phases. We will show that this technique allows us to determine when each of the phases begins to grow, which will also lend insight into the dynamics of the growth of thin films of tetracene.

4.3 Experimental Procedures

Thin films of tetracene were grown on clean SiO_2 using a supersonic molecular beam source in a custom-designed UHV chamber fitted with Be windows, detailed elsewhere,[22] in the G3 station at CHESS. Briefly, a supersonic beam of tetracene is generated by passing He carrier gas over a heated vessel containing tetracene (99.99%, Sigma-Aldrich) and then expanding this gas through a 150 μm diameter nozzle into a source chamber. This beam then passes through a trumpet-shaped skimmer, a differentially pumped ante-chamber, and then a beam-defining aperture before striking the sample, which is at a nominal T_s = 30 °C, in the main scattering chamber (base pressure ~ 5×10^{-9} Torr). We vary the growth rate by controlling the temperature of the heated vessel containing the tetracene. Further details regarding the estimated incident kinetic energy (2.5-2.6 eV) and sample preparation are given elsewhere.[23]

Growth rate was estimated by *ex situ* atomic force microscopy (AFM) by calculating the volume over a given area (the scan size) to find thickness.[23] AFM was also used to measure RMS roughness.

During deposition, thin-film growth was monitored *in situ* with real-time GID. The X-ray beam was incident on the substrate at an angle of 0.13°, and the energy of the X-ray beam was 10.06 keV. The intensity of the scattered X-ray beam was measured continuously using a PILATUS 100K area detector (DECTRIS, Ltd.) with a dwell time of one second. In this manner, we collect scattering data throughout the duration of growth, as compared to approaches using *ex situ* analysis, which can only characterize the thin film post-deposition. Fitting of in-plane diffraction peaks was performed using an approximate 2D Voigt function (product of a Gaussian and a Lorentzian function). Post-deposition X-ray reflectivity (XRR) and GID were measured *ex situ* in the G2 station at CHESS. *Ex situ* GID data were indexed using previously developed methods.[24,25]

4.4 Results

In Figure 4-1, we display the *ex situ* XRR of a thin film of tetracene (~ 160 ML) grown on SiO_2 at a nominal rate of 0.47 ML s^{-1}. Here, we observe two sets of peaks, indicating two distinct phases of tetracene. One phase displays peaks at q_z = 0.487, 0.971, and 1.456 $Å^{-1}$, giving an average d_z-spacing of 12.93 ± 0.016 Å. The other phase displays peaks at q_z = 0.516, 1.031, and 1.547 $Å^{-1}$, giving an average d_z-spacing of 12.19 ± 0.0025 Å. The latter matches well with the bulk-phase structure of tetracene reported by Campbell and co-workers (d_z-spacing of 12.26 Å)[26] and by Holmes and co-workers (d_z-spacing of 12.10 Å).[27] The former, with the larger

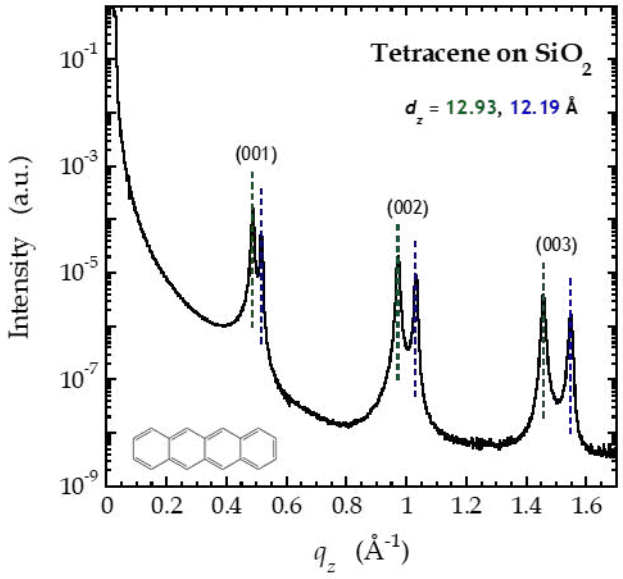

Figure 4-1: *Ex situ* XRR of a ~160 ML thin film of tetracene grown on SiO_2 at a nominal rate of 0.47 ML s^{-1}. The vertical lines (from left to right) indicate the expected positions from d_z = 12.93 Å (a thin-film phase), and 12.19 Å (the bulk phase). Inset on the bottom left is the chemical structure of tetracene.

d_z-spacing is a thin-film phase, which was reported in a previous study of thin films of tetracene on SiO_2 by Gompf and co-workers.[17] Pentacene, a molecule very similar to tetracene, has also been observed to form both a thin-film phase and a bulk phase for a variety of growth conditions.[10,12,28,29]

We display in Figure 4-2 *ex situ* GID from the same thin film examined by XRR in Figure 4-1. We also show the results from indexing the two phases. The lattice parameters for the bulk phase, indicated by the red symbols and text, were refined from the parameters given by Holmes and co-workers.[27] The lattice parameters for the thin-film phase, indicated by the green symbols and text, were iterated upon starting with a shift in parameters analogous to that seen for the bulk phase and thin-film phase of pentacene.[29] The lattice parameters are summarized in Table 4-1. Given that tetracene and pentacene possess very similar crystal structures, we unsurprisingly observe a similarity between these data and GID for thin films of pentacene.[29–31] These data, collected *ex situ*, tell us nothing about time evolution of the two phases. Namely, it is not yet clear if these two phases begin forming at the same time, or does one phase grow after the other, and is this transition one that is smooth or abrupt? We can use *in situ*, real-time GID to interrogate the evolution of these two phases during thin-film growth.

In Figure 4-3, we present a subset of data that was collected by the area detector during growth of the same thin film examined in Figure 4-1 and Figure 4-2. While data is recorded effectively every second, we display data for five times during growth: 20, 40, 60, 80, and 200 s. At 20 s of thin film growth, it is clear that the only phase that exists at this point is the thin-film phase. At 40 s of thin film growth, the (021) peak of the bulk phase becomes faintly visible. Beyond 40 s of thin film growth, peaks belonging to the bulk phase become more apparent. At 200 s of thin

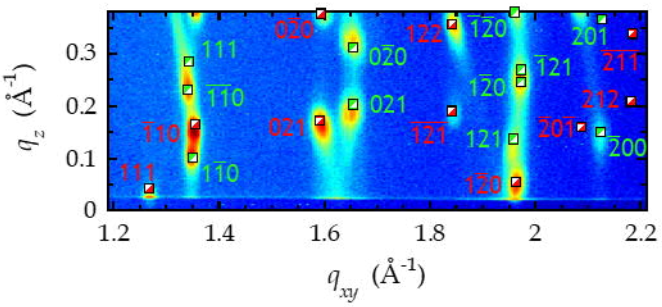

Figure 4-2: *Ex situ* GID of a ~160 ML thin film of tetracene grown on SiO_2 at a nominal rate of 0.47 ML s^{-1}, same as that shown in Figure 4-1.

Table 4-1: Summary of the lattice parameters of the thin-film phase and bulk phase of both tetracene and pentacene.

Phase	***a* (nm)**	***b* (nm)**	***c* (nm)**	**α (°)**	**β (°)**	**γ (°)**
Tetracene						
Thin-film (this work)	0.592	0.76	1.32	79.8	86.4	89.6
Bulk (this work)	0.604	0.792	1.31	76.6	72	86
Bulk[a]	0.606	0.784	1.301	77.1	72.1	85.8
Pentacene						
Thin-film[b]	0.592	0.754	1.563	81.5	87.2	89.9
Bulk[c]	0.606	0.79	1.501	81.6	77.2	85.8

[a]Holmes, *et al*. (ref. 27)

[b]Nabok, *et al*. (ref. 29)

[c]Campbell, *et al*. (ref. 26)

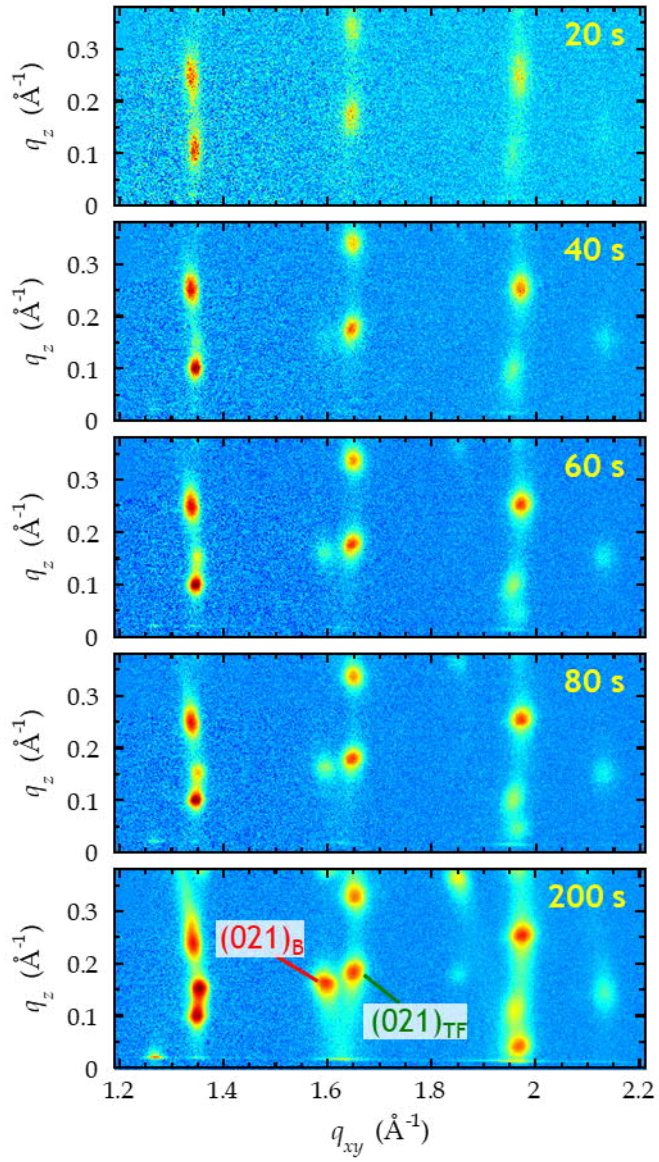

Figure 4-3: *In situ* real-time GID during the growth of the same thin film as in Figure 4-1 and Figure 4-2. Scattering data are shown for 20 s, 40 s, 60 s, 80 s, and 200 s from the start of growth.

film growth, the intensity of the (021) peak of the bulk phase is similar in magnitude to the (021) peak of the thin-film phase.

To track the formation of both phases, we have used approximate 2D Voigt functions to fit simultaneously the $(021)_{TF}$ and $(021)_{B}$ Bragg peaks for every frame of data. We can extract the intensity, position, and the full-width-at-half-maximum (FWHM) of the peaks. Due to low signal-to-noise at early times, we use a threshold of three times the standard error, 3σ, of the counts above zero to determine the appearance of a diffraction peak. The intensity of either peak before this time is considered to be zero. The integrated intensities of the $(021)_{TF}$ and $(021)_{B}$ peaks, which are directly proportional to the volume of these phases, for the same experiment shown in Figure 4-3 are shown in Figure 4-4(a). These data reveal several important facts concerning the evolution of the two crystalline phases. First, at short times, *only the thin-film phase is observed*, where the integrated intensity of the diffraction peak from the thin-film phase begins to rise immediately, but that of the bulk phase does not begin rising for some time after growth has begun. Second, once the bulk phase has appeared, we observe that there is growth of both phases for significant period of time. We also note that there is clear acceleration in the rate of growth of the bulk phase and possibly also, to a lesser extent, with the thin film phase. Third, at longer times the bulk phase eventually dominates the growth, as the growth of the thin-film phase decelerates, and the thickness/amount of the thin-film phase plateaus.

This behavior is made somewhat clearer in Figure 4-4(b), where we have used numerical differentiation of the data given in Figure 4-4(a) to estimate that rates of growth of the two phases. We see that these data reveal four stages of growth: (*i*) initially, we only have growth of the thin film phase; followed by (*ii*) growth of both phases, where there is strong acceleration in the rate of growth of the bulk phase;

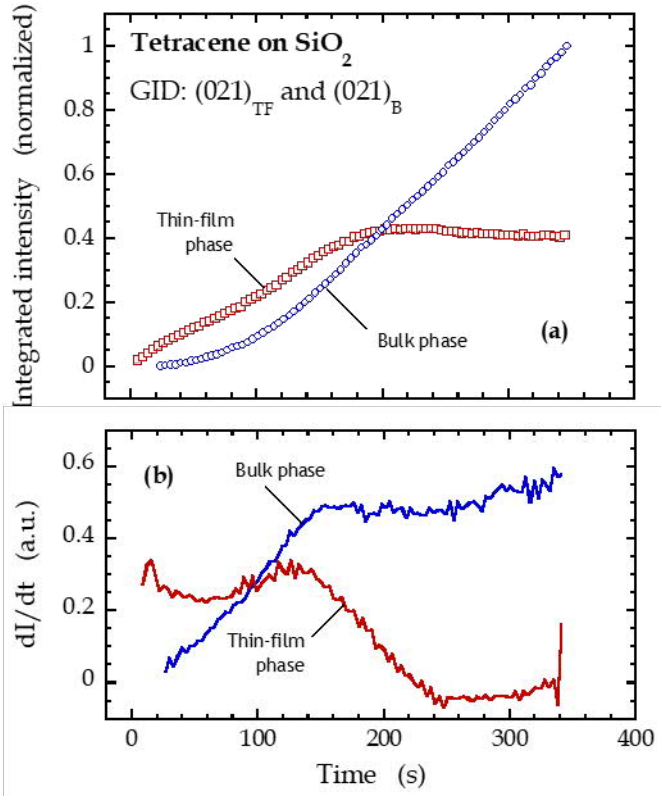

Figure 4-4: (a) Integrated intensity of the $(021)_{TF}$ and $(021)_B$ peaks from Figure 4-3 displayed as a function of time. Every 4th data point is shown, and the data have been normalized to the maximum intensity observed for the bulk phase. (b) Numerical derivatives of the data shown in (a) as a function of time.

followed by (*iii*) deceleration of the rate of growth of the thin film phase; followed by (*iv*) only growth of the bulk phase.

Is this behavior observed for other growth rates? In Figure 4-5(a), we display the integrated intensity of the $(021)_B$ Bragg peak as a function of time for several growth rates. For all cases, there is time delay in the formation of the bulk phase, and the diffraction feature does not rise as soon as growth begins. Furthermore, the slope of the intensity increases until there is an approximately constant slope, consistent with the results we showed Figure 4-4(b). Thus, for all cases, there is a delay in nucleation of the bulk phase, followed by a period where the growth accelerates, and eventually becomes constant. In Figure 4-5(b) we plot the integrated intensity vs. the total thickness based on the estimated growth rates from AFM. As may be seen, these curves do not overlap. This can be interpreted as a consequence of the amounts of the two phases that are present as a function of the growth rate. Namely, these data indicate that the fraction of the thin film that is in the bulk phase at a particular total thickness decreases as the rate of growth increases.

We can gain additional insight into the evolution of the two phases if we consider similar results for the thin-film phase. As before with the $(021)_B$ peak, we can also fit the $(021)_{TF}$ Bragg peak to an approximate 2D Voigt function. In Figure 4-6(a), we display the integrated intensity of the $(021)_{TF}$ peak as a function of time. This diffraction feature begins to grow essentially immediately after the substrate is exposed to the molecular beam of tetracene. At long times, we can again see that the intensity of this feature plateaus, indicating that the growth of the thin-film phase eventually stops. We also observe that the intensity reached at the plateau (proportional to the amount of the thin-film phase) appears to scale with the rate of growth.

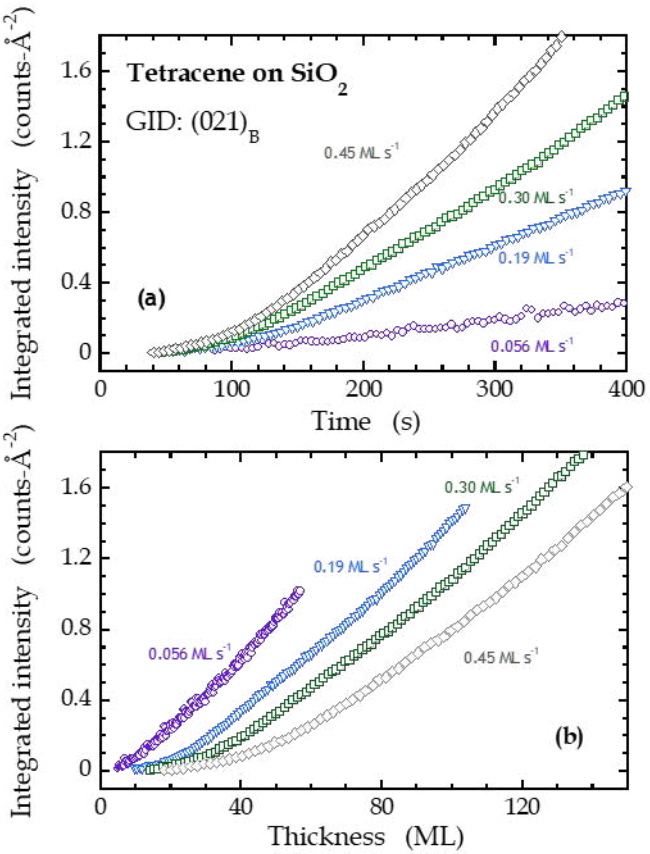

Figure 4-5: (a) Integrated intensity of the $(021)_B$ peaks at various rates of growth displayed as a function of time. Every 4th data point is shown. The same data from (a) displayed as a function of the total thickness.

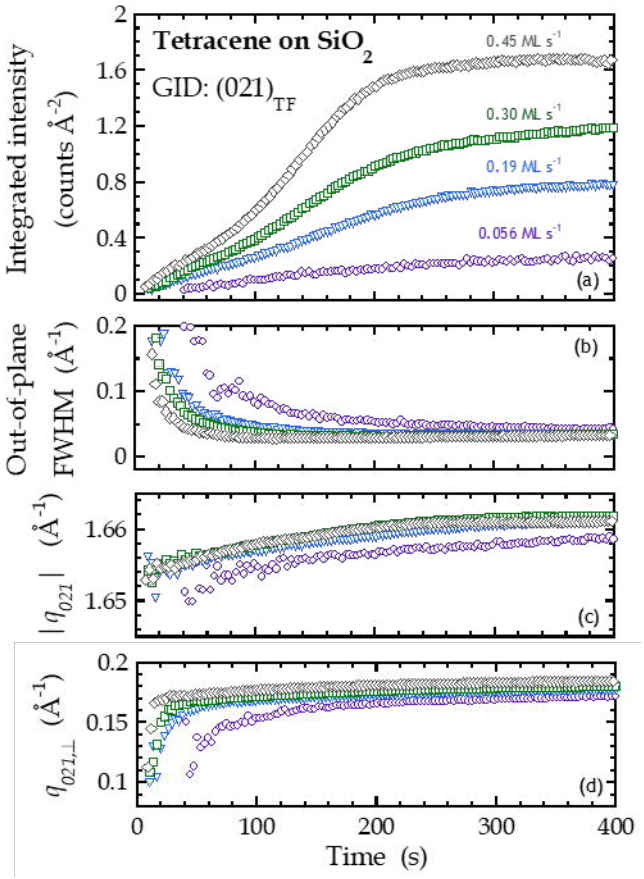

Figure 4-6: (a) Integrated intensity of the $(021)_{TF}$ peaks at various rates of growth displayed as a function of time. Every 4th data point is shown. We also display, for this same $(021)_{TF}$ peak, (b) the out-of-plane FWHM, (c) $|q_{021}|$, and (d) the out-of-plane peak position at various rates of growth as a function of time. Every 4th data point is shown.

Similar to the analysis presented above for the bulk phase, in Figure 4-7(a) we plot the integrated intensity for the thin-film phase vs. the total thickness based on the estimated growth rates from AFM. Here we see that there is considerable overlap between these sets of data, reflecting the dominance of the thin-film phase at smaller thickness. Deviations become apparent at larger thicknesses where the amount of the thin-film phase plateaus, and this plateau become larger at higher growth rates.

Additional information concerning the nature of the thin film that is grown can be found from an analysis of the width of the Bragg peak for the thin-film phase. We display the out-of-plane full-width-at-half-maximum (FWHM) as a function of time in Figure 4-6(b), and as a function of the total coverage in Figure 4-7(b). We can expect that the out-of-plane FWHM will be larger for thinner films and smaller for thicker films because of the crystallites being a finite size, as described by the Scherrer equation. As expected, the out-of-plane FWHM is initially larger before decaying to a smaller value as the thin film becomes thicker. This width becomes nearly equivalent for all growth rates (~0.03 $Å^{-1}$) at large thicknesses, and this value is greater than the expected smearing of the diffraction spot due to the size of the sample and the beam (Δq_z ~ 0.002 $Å^{-1}$). This observation implies that the out-of-plane size of the crystallites may be similar for all cases. We note in passing that analysis of the in-plane width of the peaks (not shown here) gave results where the deviations were below the threshold for smearing of the diffraction spots due to the size of the sample and the beam (Δq_{xy} ~ 0.02 $Å^{-1}$). Thus, we will not comment further on those results.

Analysis of the position of the in-plane diffraction peak for the thin-film phase is of interest, however. We display the magnitude of the vector defining the position of the $(021)_{TF}$ peak, $|q_{021}|$, as a function of time in Figure 4-6(c), and as a function of the total coverage in Figure 4-7(c). Here, there is a modest change in $|q_{021}|$ from

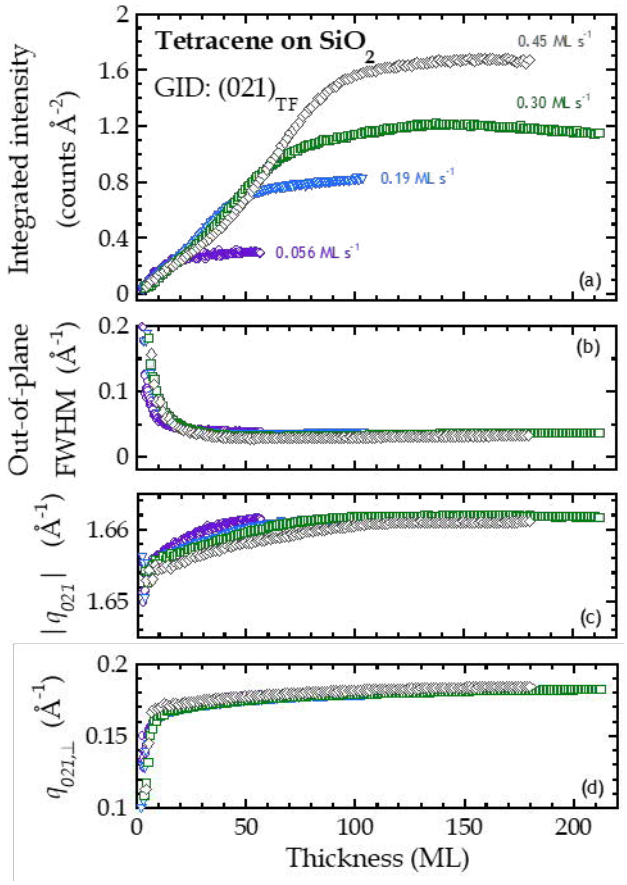

Figure 4-7: (a) Integrated intensity of the $(021)_{TF}$ peaks at various rates of growth displayed as a function of the total coverage. Every 4th data point is shown. We also display, for this same $(021)_{TF}$ peak, (b) the out-of-plane FWHM, (c) $|q_{021}|$, and (d) the out-of-plane peak position at various rates of growth as a function of the total coverage. Every 4th data point is shown.

~ 1.65 $Å^{-1}$ to ~ 1.66 $Å^{-1}$, representing a shift of less than 1%. As a function of total coverage, the results are quite similar for the different rates of growth. We display the out-of-plane position (q_z) for this same $(021)_{TF}$ peak as a function of time in Figure 4-6(d), and as a function of the total coverage in Figure 4-7(d). Here we observe an unexpected, yet significant, change in the position of this peak. For all cases, the peak appears first at $q_{021,\perp}$ ~ 0.1 $Å^{-1}$, and then increases and plateaus at a value of $q_{021,\perp}$ ~ 0.17 $Å^{-1}$. As a function of total coverage, the results are quite similar for the different rates of growth. We note that the entire peak shifts instead of the formation of multiple peaks, suggesting that every portion of the thin film that is thin-film phase is changing in concert. Kowarik and co-workers observed a similar phenomenon during the growth of DIP on SiO_2.[14,15]

4.5 Discussion

We have examined *in situ* and in real time the evolution of two polymorphs, a thin-film phase and a bulk phase, during the thin-film growth of tetracene on SiO_2. We have also examined the effect of the rate of growth on the evolution of these two phases. GID revealed that these two phases of tetracene do not begin growing simultaneously and that there is not an abrupt transition between the growth of the two phases. Instead, there are four regimes of growth: (*i*) growth initially of only the thin-film phase; (*ii*) a regime where the bulk phase nucleates, and there is a rapid rate of acceleration in the rate of growth of that phase, while the thin-film phase continues to grow, (*iii*) a regime where the growth of the thin-film phase decelerates, and (iv) a regime where the thin film phase stops growing and only the bulk phase continues to grow. We note here that a significant difference between the two phases is their

d_z-spacing, where a transition from the thin-film to the bulk phase will involve tilting of the molecules of tetracene further from the surface normal, decreasing the d_z-spacing. Such a transition from a larger d_z-spacing to a smaller one has also previously been reported for pentacene and DIP.[15,32] Given the fact that we observe growth of both phases for a significant period of time, there must be portions of the thin film which contain regions of both phases. This creates a diffuse interface between the phases, where initially the thin film is comprised of only the thin-film phase, while eventually only the bulk phase is grown. We will discuss how this transition from growth of the thin-film phase to growth of the bulk phase occurs, and how it depends on the rate of growth.

When does the bulk phase begin to grow? A previous study on pentacene reported that growth must exceed a critical thickness of at least 100 nm of pentacene on SiO_2 (at room temperature) before the bulk phase begins to grow,[9] and another argued that surface energy was the driving force for this transition.[33] Watanabe *et al.* observed the rise of the bulk phase of pentacene after ~6.5 ML of growth of the thin-film phase using *in situ* GID.[34] In another study, Mayer *et al.* used *in situ* X-ray reflectivity and argued that both the thin-film and bulk phase of pentacene nucleate at nearly the same thin-film thickness (~1 ML).[12] However, these measurements were of poor time resolution (each scan took 65-90 s) and conclusions were drawn from fitting a model to data that did not *begin* until the thin film of pentacene was already thicker than 60 nm (~ 40 ML).

Our results lack the uncertainties of these previous studies due to high signal-to-noise ratio data, short acquisition times (1 s), and the use of *in situ*, real time techniques. The results we have presented here clearly show that, for tetracene, *the bulk phase does not nucleate in the first monolayer*. This is very likely also true for pentacene, as it is a very similar molecule, and the observations by Bouchoms *et al.*

concerning the critical thickness for the transition from bulk to thin-film phase corroborate this.[9] Is there also a critical thickness for tetracene at which a similar transition from the thin-film phase to the bulk phase occurs? Moreover, is this concept of a critical thickness even valid for the case of tetracene grown on SiO_2?

Using the intensities of the bulk phase shown in Figure 4-5 (*vide supra*), we can determine the time at which diffraction from the bulk phase becomes apparent and use that time and the mean growth rate to determine an onset thickness. More specifically, we use the time at which the counts were above zero by 3σ, as described earlier. We display the results from this analysis in Figure 4-8(a). The onset thickness shows a strong dependence on growth rate, varying from ~ 5 ML at 0.056 ML-s^{-1} to ~ 17 ML at 0.45 ML-s^{-1}. We recall that the intensity of the plateau for the thin-film phase also displayed a dependence on growth rate [*cf*. Figures 4-6(a) and 4-7(a)]. To quantify this effect, we have fit straight lines to the linear portion of the rising intensity of the thin-film phase, and another to the plateaued region, to find the intersection of these two lines and determine a thickness. In Figure 4-8(a), we display these (total) thicknesses as a function of the rate of growth. We see that these thicknesses increase with growth rate from ~16 ML at 0.056 ML-s^{-1} to ~ 92 ML at 0.45 ML-s^{-1}. These results unambiguously indicate that the amount of the thin-film phase present in the thin films is greater for higher growth rates. This agrees with a report from Gompf and co-workers, where they observe that increasing growth rate from 0.2 nm-s^{-1} (0.15 ML-s^{-1}) to 1.7 nm-s^{-1} (1.3 ML-s^{-1}) results in a greater amount of the thin-film phase.[17] Similarly, Milita and co-workers have also previously studied the formation of two phases of tetracene on SiO_2 and reported an increase in the amount of the phase with higher d_z-spacing (note: their value was 13.2 Å) as the growth rate was increased from 0.025 nm-s^{-1} (0.019 ML-s^{-1}) to 0.2 nm-s^{-1} (0.15 ML-s^{-1}).[18]

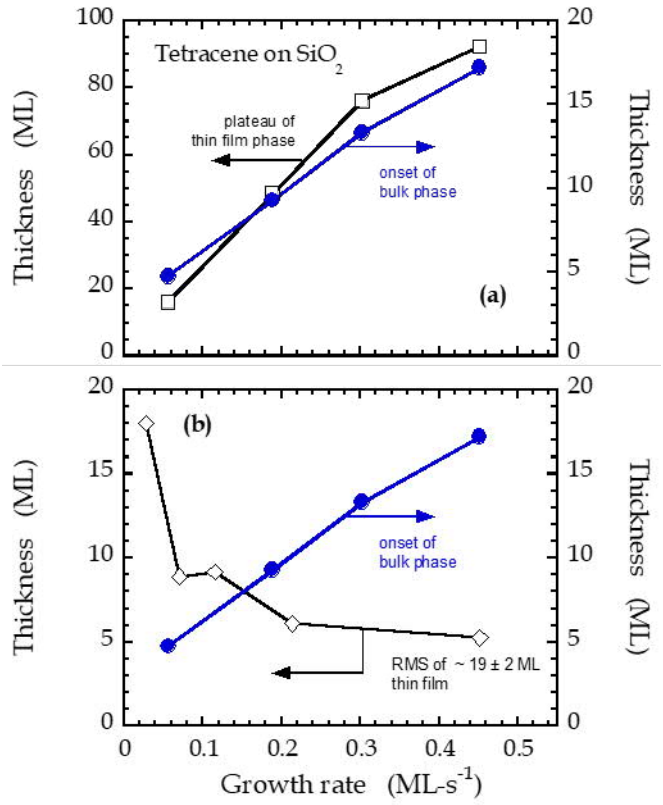

Figure 4-8: (a) Thicknesses for the onset of the bulk phase (right ordinate, closed circles) and the thickness where the $(021)_{TF}$ intensity plateaus (left ordinate, open squares) as function of the rate of growth. (b) (a) Thicknesses for the onset of the bulk phase (right ordinate, closed circles) and the RMS roughness of ~ 19 ML thick films of tetracene on SiO_2 (left ordinate, open diamonds) as function of the rate of growth.

One more factor to consider in interpreting our results concerns the morphology/topography of the deposited thin films. As we have shown in previous work, the topography of tetracene exhibits an unusual dependence on the rate of growth—3D islanded growth is favored at low growth rates, while 2D layer-by-layer and smoother growth occurs at high growth rates.[22] In Figure 4-8(b) we plot the RMS roughness for thin films of tetracene grown on SiO_2 under the same conditions we consider here These films were all 19 ± 2 ML in thickness, placing them near the upper limit of values we found for the thickness of the onset of the bulk phase. Interestingly, we see that for the lowest growth rate considered here, the RMS roughness approaches the nominal thickness, which can only occur if the film is discontinuous, and possesses regions that are much thicker than what one would observe from, say, stochastic, random deposition.

Do any diffraction features *from the thin-film phase* provide clues as to the onset of nucleation of the bulk phase? The most relevant data are provided in Figure 4-7. Of the three sets of results concerning peak positions and FWHMs, the set most in line with the observed appearance of the bulk phase (at ~ 5-17 MLs) would be the results for the position of the out-of-plane component for the $(021)_{TF}$ peak. We note that the initial increase in $q_{021,\perp}$ corresponds to a decrease in the d_z-spacing. We determine the thickness at which the out-of-plane position of the $(021)_{TF}$ peak begins to plateau by fitting a line to the early-time rising data, fitting a line to the long-time plateau, and finding the intersection. Interestingly, this thickness exhibits no apparent trend with growth rate and has an average of ~ 8 ± 2 ML. Thus, it is unclear if these data indicate an evolution of the thin-film phase unit cell towards one that is more like the bulk phase, and might initiate nucleation.

We have addressed *when* the bulk phase begins to grow, and now examine *why* it begins to grow. First, we discard the notion that the bulk phase will form on clean

SiO_2, at least for the conditions we consider here. The thin-film phase forms because of the interface between the tetracene thin film and SiO_2, and the interfacial energy associated with it. This interfacial interaction is sufficient to overcome the energetic cost of forming the thin-film phase over the bulk phase. Why would a bulk phase form on some regions of SiO_2, but not others? The most logical explanation for the appearance of the bulk phase is that the influence of the substrate has dissipated sufficiently. The presence of the thin-film phase is the entity that of course changes the effect of the substrate. The two likely factors concerning the thin film phase that might affect nucleation of the bulk phase are its thickness and topography.

Let us assume that a critical thickness does exist for the nucleation of the bulk phase, perhaps similar to the value (~ 8 ML) suggested by the analysis of the data in Figure 4-7(d). This, by itself, would not predict a dependence on growth *rate*, which we clearly observe here. We must recognize, however, that what likely is important is the *local* thickness, and not the mean thickness. As shown in Figure 4-8(b) we find for the lowest growth rates that we can expect that the RMS roughness can be significant, i.e., on the order of or even exceeding that of the mean thickness. Thus, in this scenario, the critical thickness is reached at the smallest mean coverage at the lowest rate of growth, while it requires a larger mean coverage at the higher rates of growth where the thin films are smoother. This is a compelling argument, but it may not tell the complete story. Surface roughness itself may also play a role in nucleation. It is known for many thin film/substrate combinations, that nucleation is often facilitated at step edges, single-layer or multiple-layer steps. In this case, the thin films deposited at lower rates of growth might also be expected to provide a higher density of steps sites (due to greater roughness) than those grown at higher rates.

To summarize our observations we consider the schematic diagram in Figure 4-9. Here we display the four stages of growth, indicating how the two phases may

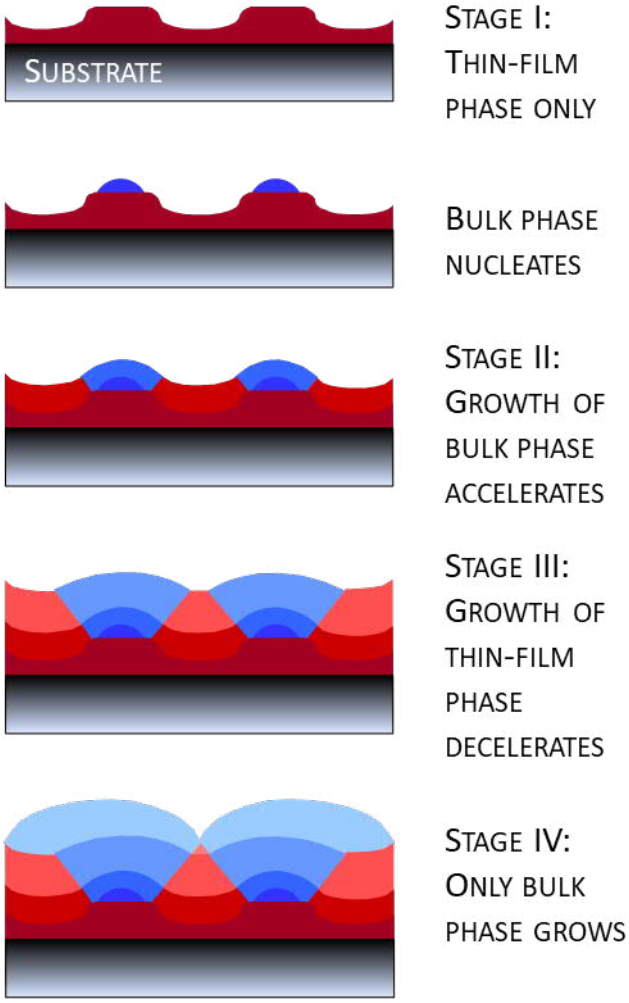

Figure 4-9: Schematic representation of the evolution of the two phases of tetracene, the thin-film phase (reddish tones) and the bulk phase (blueish tones). *Figure courtesy of James R. Engstrom.*

evolve as a function of time and/or thickness. First, there is an initial period, Stage I, where only the thin film phase is formed. Even for relatively high rates of thin-film growth there is significant roughness, as indicated. Second, as we have argued above, at some point the local thickness exceeds the critical thickness and the bulk phase nucleates. If this phase grows in a 3D islanded mode, we expect its rate to accelerate as we have observed for Stage II of growth. In Stage III, the bulk phase continues to grow, while growth of the thin-film phase begins to decelerate. Finally, in Stage IV, growth of the thin-film phase has ceased, the bulk phase covers the surface, and only the bulk phase is subsequently grown.

4.6 Conclusions

We have examined the effect of growth rate on the evolution of two polymorphs of thin films of tetracene that are grown on SiO_2 at room temperature. From *ex situ* X-ray reflectivity, we find that tetracene forms two phases on SiO_2—a thin-film phase with d_z = 12.93 Å, and the bulk phase with d_z = 12.19 Å. We use *in situ*, real-time grazing incidence diffraction to determine directly the evolution of the two phases with time and thin film thickness. Initially, up to several monolayers of deposition, only the thin-film phase is grown. We find no evidence for formation of the bulk phase in the monolayer regime, rather, there is a significant delay in the onset of growth of the bulk phase. At a growth rate of 0.056 ML-s^{-1}, the bulk phase begins growing at ~ 5 ML, while the thin-film phase saturates after the growth of ~ 16 ML (total) of deposited thin film. As growth rate is increased, both of these thicknesses marking changes in the stage of growth increase. At a growth rate of 0.45 ML-s^{-1}, the bulk phase begins growing at ~ 17 ML, while the growth of the thin-film phase

persists until ~ 88 ML total of deposited thin film. We propose that the delay, in terms of a thin film thickness, in the formation of the bulk phase at the higher growth rates is associated with the formation of smoother thin films at these rates. At lower growth rates, due to the effects of upward transport of tetracene at island edges, the thin films are rougher, and a smaller total coverage is able to produce thin films where the critical thickness is exceeded, enabling the growth of the bulk phase. The bulk phase is more likely to form on tall features, of which there are many at low growth rates where there is 3D growth. Increasing the growth rate kinetically traps molecules from moving upwards and promotes more sustained growth of the thin-film phase. From this work, it is clear that the influence of the substrate on growth may dictate what the initial growing phase of organic thin film is, but the kinetics of thin-film reorganization can play a significant role in determining when and what phase ultimately becomes the dominant contributor to growth.

4.7 Acknowledgements

We would like to thank Dr. Arthur R. Woll for invaluable technical contributions, as well as James Dong and Jade M. Noble for technical assistance. We also thank Detlef-M. Smilgies for his assistance on indexing GID data. This work was supported in part by Cornell University's David R. Atkinson Center for a Sustainable Future (ACSF). This work made use of the Nanobiotechnology Center shared research facilities at Cornell, and is based upon research conducted at the Cornell High Energy Synchrotron Source (CHESS), which is supported by the National Science Foundation under NSF award DMR-1332208.

4.8 References

(1) Witte, G.; Wöll, C. Growth of Aromatic Molecules on Solid Substrates for Applications in Organic Electronics. *J. Mater. Res.* **2004**, *19* (7), 1889–1916.

(2) Forrest, S. R. The Path to Ubiquitous and Low-Cost Organic Electronic Appliances on Plastic. *Nature* **2004**, *428* (6986), 911–918.

(3) Dimitrakopoulos, C. D.; Malenfant, P. R. L. Organic Thin Film Transistors for Large Area Electronics. *Adv. Mat.* **2002**, *14* (2), 99–117.

(4) Diao, Y.; Lenn, K. M.; Lee, W.; Blood-Forsythe, M. A.; Xu, J.; Mao, Y.; Kim, Y.; Reinspach, J. A.; Park, S.; Aspuru-Guzik, A.; Xue, G.; Clancy, P.; Bao, Z.; Mannsfeld, S. C. B. Understanding Polymorphism in Organic Semiconductor Thin Films through Nanoconfinement. *J. Am. Chem. Soc.* **2014**, *136* (49), 17046–17057.

(5) Mas-Torrent, M.; Rovira, C. Role of Molecular Order and Solid-State Structure in Organic Field-Effect Transistors. *Chem. Rev.* 2011, pp 4833–4856.

(6) Jones, A. O. F.; Chattopadhyay, B.; Geerts, Y. H.; Resel, R. Substrate-Induced and Thin-Film Phases: Polymorphism of Organic Materials on Surfaces. *Adv. Funct. Mater.* **2016**, *26* (14), 2233–2255.

(7) Krause, B.; Dürr, A. C.; Ritley, K.; Schreiber, F.; Dosch, H.; Smilgies, D. Structure and Growth Morphology of an Archetypal System for Organic Epitaxy: PTCDA on Ag(111). *Phys. Rev. B* **2002**, *66* (23), 235404.

(8) Forrest, S. R. Ultrathin Organic Films Grown by Organic Molecular Beam Deposition and Related Techniques. *Chem. Rev.* **1997**, *97* (6), 1793–1896.

(9) Bouchoms, I. P. M.; Schoonveld, W. A.; Vrijmoeth, J.; Klapwijk, T. M. Morphology Identification of the Thin Film Phases of Vacuum Evaporated Pentacene on SIO2 Substrates. *Synth. Met.* **1999**, *104* (3), 175–178.

(10) Knipp, D.; Street, R. A.; Völkel, A. R.; Ho, J. Pentacene Thin Film Transistors on Inorganic Dielectrics: Morphology, Structural Properties, and Electronic Transport. *J. Appl. Phys.* **2003**, *93* (1), 347.

(11) Ambrosch-Draxl, C.; Nabok, D.; Puschnig, P.; Meisenbichler, C. The Role of Polymorphism in Organic Thin Films: Oligoacenes Investigated from First Principles. *New J. Phys.* **2009**, *11* (12), 125010.

(12) Mayer, A.; Kazimirov, A.; Malliaras, G. Dynamics of Bimodal Growth in Pentacene Thin Films. *Phys. Rev. Lett.* **2006**, *97* (10), 105503.

(13) Hinderhofer, A.; Hosokai, T.; Frank, C.; Novák, J.; Gerlach, A.; Schreiber, F. Templating Effect for Organic Heterostructure Film Growth: Perfluoropentacene on Diindenoperylene. *J. Phys. Chem. C* **2011**, *115* (32), 16155–16160.

(14) Kowarik, S.; Gerlach, A.; Sellner, S.; Cavalcanti, L.; Konovalov, O.; Schreiber, F. Real-Time X-Ray Diffraction Measurements of Structural Dynamics and Polymorphism in Diindenoperylene Growth. *Appl. Phys. A-Mater.* **2009**, *95* (1), 233–239.

(15) Kowarik, S.; Gerlach, A.; Sellner, S.; Schreiber, F.; Cavalcanti, L.; Konovalov, O. Real-Time Observation of Structural and Orientational Transitions during Growth of Organic Thin Films. *Phys. Rev. Lett.* **2006**, *96* (12), 125504.

(16) Cheng, H.-L.; Mai, Y.-S.; Chou, W.-Y.; Chang, L.-R.; Liang, X.-W. Thickness-Dependent Structural Evolutions and Growth Models in Relation to Carrier Transport Properties in Polycrystalline Pentacene Thin Films. *Adv. Funct. Mater.* **2007**, *17* (17), 3639–3649.

(17) Gompf, B.; Faltermeier, D.; Redling, C.; Dressel, M.; Pflaum, J. Tetracene Film Morphology: Comparative Atomic Force Microscopy, X-Ray Diffraction and Ellipsometry Investigations. *Eur. Phys. J. E* **2008**, *27* (4), 421–424.

(18) Milita, S.; Servidori, M.; Cicoira, F.; Santato, C.; Pifferi, A. Synchrotron X-Ray Investigation of Tetracene Thin Films Grown at Different Deposition Fluxes. *Nucl. Instrum. Meth. B* **2006**, *246* (1), 101–105.

(19) Milita, S.; Santato, C.; Cicoira, F. Structural Investigation of Thin Tetracene Films on Flexible Substrate by Synchrotron X-Ray Diffraction. *Appl. Surf. Sci.* **2006**, *252* (22), 8022–8027.

(20) Wünsche, J.; Tarabella, G.; Bertolazzi, S.; Bocoum, M.; Coppedè, N.; Barba, L.; Arrighetti, G.; Lutterotti, L.; Iannotta, S.; Cicoira, F.; Santato, C. The Correlation between Gate Dielectric, Film Growth, and Charge Transport in Organic Thin Film Transistors: The Case of Vacuum-Sublimed Tetracene Thin Films. *J. Mater. Chem. C* **2013**, *1* (5), 967.

(21) Moriguchi, N.; Nishikawa, T.; Anezaki, T.; Unno, A.; Tachibana, M.; Kojima, K. Carrier Mobility and Crystal Perfection of Tetracene Thin Film FET. *Phys. B* **2006**, *376–377*, 276–279.

(22) Schroeder, T. W. Dissertation: Thin Film Deposition Employing Supersonic Molecular Beams: Nucleation and Growth of Silicon, Silicon Germanium and Pentacene, Cornell University, 2004.

(23) Nahm, R. K.; Engstrom, J. R. Unexpected Effects of the Rate of Deposition on the Mode of Growth and Morphology of Thin Films of Tetracene Grown on SiO 2. *J. Phys. Chem. C* **2016**, *120* (13), 7183–7191.

(24) Smilgies, D.-M.; Blasini, D. R. Indexation Scheme for Oriented Molecular Thin Films Studied with Grazing-Incidence Reciprocal-Space Mapping. *J. Appl. Crystallogr.* **2007**, *40* (4), 716–718.

(25) Busch, P.; Rauscher, M.; Smilgies, D.-M.; Posselt, D.; Papadakis, C. M. Grazing-Incidence Small-Angle X-Ray Scattering from Thin Polymer Films with Lamellar Structures – the Scattering Cross Section in the Distorted-Wave Born Approximation. *J. Appl. Crystallogr.* **2006**, *39* (3), 433–442.

(26) Campbell, R. B.; Robertson, J. M.; Trotter, J. The Crystal Structure of Hexacene, and a Revision of the Crystallographic Data for Tetracene. *Acta Crystallogr.* **1962**, *15* (3), 289–290.

(27) Holmes, D.; Kumaraswamy, S.; Matzger, A. J.; Vollhardt, K. P. C. On the Nature of Nonplanarity in the [N]Phenylenes. *Chem.-Eur. J.* **1999**, *5* (11), 3399–3412.

(28) Dimitrakopoulos, C. D.; Brown, A. R.; Pomp, A. Molecular Beam Deposited Thin Films of Pentacene for Organic Field Effect Transistor Applications. *J. Appl. Phys.* **1996**, *80* (4), 2501.

(29) Nabok, D.; Puschnig, P.; Ambrosch-Draxl, C.; Werzer, O.; Resel, R.; Smilgies, D.-M. Crystal and Electronic Structures of Pentacene Thin Films from Grazing-Incidence X-Ray Diffraction and First-Principles Calculations. *Phys. Rev. B* **2007**, *76* (23), 235322.

(30) Yoshida, H.; Inaba, K.; Sato, N. X-Ray Diffraction Reciprocal Space Mapping Study of the Thin Film Phase of Pentacene. *Appl. Phys. Lett.* **2007**, *90* (18), 181930.

(31) Yoshida, H.; Sato, N. Grazing-Incidence X-Ray Diffraction Study of Pentacene Thin Films with the Bulk Phase Structure. *Appl. Phys. Lett.* **2006**, *89* (10), 101919.

(32) Kowarik, S.; Gerlach, A.; Leitenberger, W.; Hu, J.; Witte, G.; Wöll, C.; Pietsch, U.; Schreiber, F. Energy-Dispersive X-Ray Reflectivity and GID for Real-Time Growth Studies of Pentacene Thin Films. *Thin Solid Films* **2007**, *515* (14), 5606–5610.

(33) Drummy, L. F.; Martin, D. C. Thickness-Driven Orthorhombic to Triclinic Phase Transformation in Pentacene Thin Films. *Adv. Mat.* **2005**, *17* (7), 903–

907.

(34) Watanabe, T.; Hosokai, T.; Koganezawa, T.; Yoshimoto, N. In Situ Real-Time X-Ray Diffraction During Thin Film Growth of Pentacene. *Mol. Cryst. Liq. Cryst.* **2012**, *566* (1), 18–21.

CHAPTER 5

FASTER IS SMOOTHER AND SO IS LOWER TEMPERATURE: THE CURIOUS CASE OF THIN FILM GROWTH OF TETRACENE ON SILICON DIOXIDE*

5.1 Abstract

We have examined the effect of growth rate on the growth mode of thin films of tetracene on SiO_2 at a substrate temperature of 0 °C. For a preponderance of conditions examined here, only the thin-film phase is formed. From a combination of *in situ* real-time synchrotron X-ray scattering and *ex situ* atomic force microscopy, we have observed a transition from 3D growth to 2D layer-by-layer (LbL) growth as the rate of growth is increased, similar to previous results obtained at a substrate temperature of 30 °C. For this lower substrate temperature, however, we find that this transition occurs at a much lower growth rate. We attribute this to the lower temperature significantly diminishing the rate of upward step-edge crossing transport, which competes with the rate of attachment at island edges, and results in 2D LbL growth. By examining the effects of both the rate of growth and the substrate temperature, we can assign an activation energy of ~ 19 kcal-mol^{-1} to these upward set-edge crossing events.

---

* Nahm, R. K.; Bullen, H. J.; Suh, T.; Engstrom, J. R. Faster Is Smoother and So Is Lower Temperature: The Curious Case of Thin Film Growth of Tetracene on SiO2. *J. Phys. Chem. C* **2017**, *121* (15), 8464–8472.

5.2 Introduction

Organic semiconductors have gained much attention for their potential uses in organic-based electronics that could supplant inorganic devices in certain applications.[1,2] Unlike thin films of inorganic materials, where atoms are bound to each other by strong covalent, metallic, or ionic bonds, thin films of organic molecules are held together *via* weaker van der Waals interactions. In addition, in the latter case, the building blocks themselves are typically more complex and of lower symmetry. Nevertheless, many of the same atomic and molecular scale processes known to play important roles in inorganic thin-film growth also do so in organic systems: adsorption, intra- and interlayer transport, cluster formation, among others.[3–7] All of these processes, except possibly adsorption, are expected to be strongly dependent on the substrate temperature. The rates of these processes can greatly influence the morphology of a thin film; for example, does the film grow in a smooth 2D layer-by-layer fashion or are 3D islands formed? These processes can also affect the shapes of islands, as molecular scale events such as attachment at island edges, and diffusion along the edge of an island can also be activated.[6]

We have previously reported that the growth mode of tetracene on SiO_2 displayed an unusual dependence on the rate of thin film growth, where lower growth rates result in 3D growth, and higher growth rates give 2D layer-by-layer (LbL) growth.[8] There, we proposed that this transition was a consequence of two competing rates: the rate at which molecules arrived at the edges of islands (and attached), and the rate at which these molecules could move "upwards" at the step edges. At the lower rates of growth, the rate that molecules could undergo upwards transport was greater than the rate that molecules arrived at the island edges, leading to 3D growth. At sufficiently high rates of growth, however, attachment at island edges can compete

with the rates of upward transport, and 2D LbL growth results. Underlying these observations is the fact that tetracene possesses a higher surface energy than the SiO_2 substrate on which the thin films are grown, thus there is a thermodynamic driving force for upward transport and de-wetting.

If these phenomena as we have described are indeed true, then we expect that the behavior will also be dependent on the substrate temperature, as step-crossing events (both upward and downward) are strongly activated. If the transition from 3D islanded to 2D LbL growth is dependent on the rate of growth, then we should observe a similar transition with the substrate temperature at a fixed rate of growth. In this work, we explore the possibility that 2D LbL growth could be incited by decreasing the rate of upward transport. We will present the results from our investigation of the dependence of the growth mode on growth rate at a lower substrate temperature. We make use of *in situ* X-ray scattering at Cornell High Energy Synchrotron Source (CHESS) to observe the behavior of thin-film growth in real time. We further make use of *ex situ* atomic force microscopy (AFM) and grazing incidence diffraction (GID) to show that lowering substrate temperature does indeed affect the rate of upward transport and has a significant impact on the growth mode .

5.3 Experimental Procedures

Thin-film deposition and *in situ* X-ray scattering measurements were performed in a custom-designed UHV chamber fitted with Be windows, detailed elsewhere,[9] in the G3 station at CHESS. We deposit tetracene *via* a supersonic molecular beam source onto clean SiO_2 samples held at a nominal temperature of T_s = 0 °C. Details regarding the preparation of samples, and measurement of the incident

kinetic energy of tetracene (2.5-2.6 eV) can be found in a previous study of the growth tetracene on SiO_2 at T_s = 30 °C.[8] Briefly, the molecular beam is formed by flowing the carrier gas, He, over a heated crucible containing tetracene. The beam is expanded through a 150 μm diameter nozzle into a UHV source chamber (base pressure ~ 5×10^{-9} Torr), where it passes through a trumpet-shaped skimmer, a differentially pumped ante-chamber, and finally a beam-defining aperture, before entering the main growth chamber and striking the substrate. During deposition, thin-film growth was monitored *in situ* using real-time X-ray reflectivity (XRR) at the anti-Bragg condition, where $q_z = ½q_{(001)}$. This powerful technique provides insight into the nature of growth, i.e., 2D LbL vs. 3D islanded growth.[10,11] The energy of the incident X-ray beam was 11.55 keV, and measurements of the scattered X-ray beam during thin-film deposition were made using a DECTRIS Pilatus 100 K area detector (DECTRIS, Ltd.). After deposition, the samples were removed from UHV, and were characterized *ex situ* with a Bruker Innova AFM (Bruker Corp.) operated in tapping mode. They were also characterized with *ex situ* GID in the G2 station at CHESS.

5.4 Results

In Figure 5-1(a), we display the intensity of the scattered X-ray beam collected at the anti-Bragg condition as a function of time during deposition of tetracene on SiO_2 at T_s = 0 °C. For 2D LbL growth, the scattered intensity will show oscillations, or, for 3D growth, the scattered intensity will show a monotonic decrease.[10,11] Here, we observe two oscillations (local minima near ~ 5 and 9 s), indicative of 2D LbL growth. We fit this data to a simplified version of a mean-field rate-equation model developed by Trofimov *et al*.[12–15] We have previously found this model to accurately

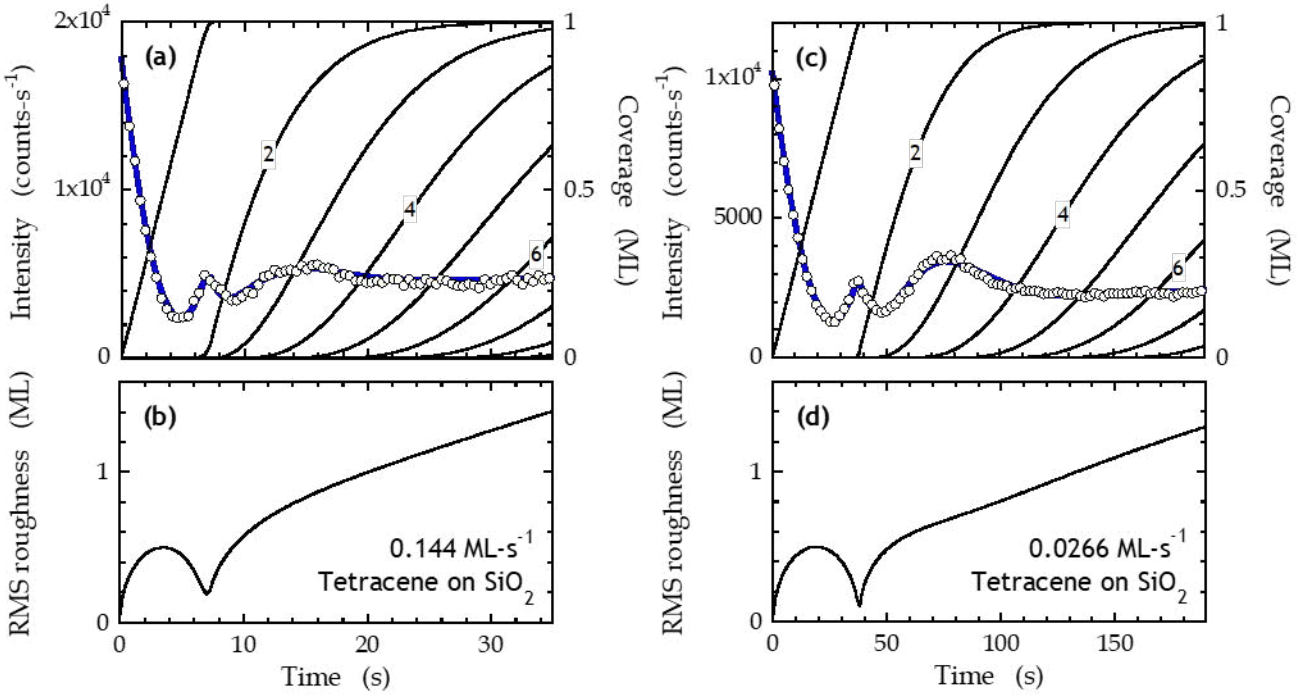

Figure 5-1: **(a)** Scattered X-ray intensity at the anti-Bragg condition as a function of time for a thin film of tetracene grown on SiO_2 at 0.144 ML-s^{-1} and T_s = 0 °C, represented by the open circles (left ordinate, every 2nd data point shown for visibility). The solid blue line (left ordinate) represents a fit of the model to the data, and the solid black curves (right ordinate) represent predicted layer coverages of the individual layers. **(b)** RMS roughness as predicted by the fit of the data shown in **(a)**. A similar set of figures is shown for growth at 0.0266 ML-s^{-1} in **(c)** and **(d)**.

describe the growth of pentacene and diindenoperylene (DIP) on SiO_2, correctly predicting thin-film thickness, layer coverages, and roughness, verified by separate measurements using AFM.[10] We present the fit and the layer coverages predicted by the model in Figure 5-1(a). The fit matches the data closely, capturing the behavior of the local extrema, and the predicted layer coverages indeed show 2D LbL behavior for the first, and part of the second monolayer. We can further extract growth rate and RMS roughness from the model. The growth rate for this set of data is 0.144 ML-s^{-1}, and here, unlike other small molecule systems we have examined,[16–19] this rate does not depend on the coverage. We also display the RMS roughness predicted by the model as a function of time in Figure 5-1(b). There is a sharp, local minimum in the RMS at ~7 s, as would be expected for 2D LbL growth. In Figures 5-1(c)-(d), we show a similar set of results for a growth rate of 0.0266 ML-s^{-1} [a factor of ~5 slower than that shown in Figures 5-1(a)-1(b)]. Again, we observe oscillations in the intensity of the scattered X-ray beam, indicating 2D LbL growth, as well as a sharp, local minimum in RMS roughness at ~ 38 s. The similarity of the two sets of results shown in Figure 5-1 is quite evident.

In Figure 5-2(a), we display the intensity of the scattered X-ray beam at the anti-Bragg condition as a function of time for the thin-film growth of tetracene on SiO_2 at 0.0141 ML-s^{-1} [a factor of ~2 slower than for the case shown in Figures 5-1(c)-(d)] and T_s = 0 °C. We also show the fit to the data in Figure 5-2(a), and also the predicted RMS roughness in Figure 5-2(b). Here, we again observe the presence of an oscillation, but the two local minima are much less pronounced than the two cases we considered in Figure 5-1. In addition, we note that the second monolayer nucleates and grows at a smaller coverage (~ 0.5-0.6 ML) of the first monolayer than in the two cases we considered in Figure 5-1 (> 0.9 ML). This is also reflected in the local minimum in the RMS roughness, which is not as sharp as that observed at the high

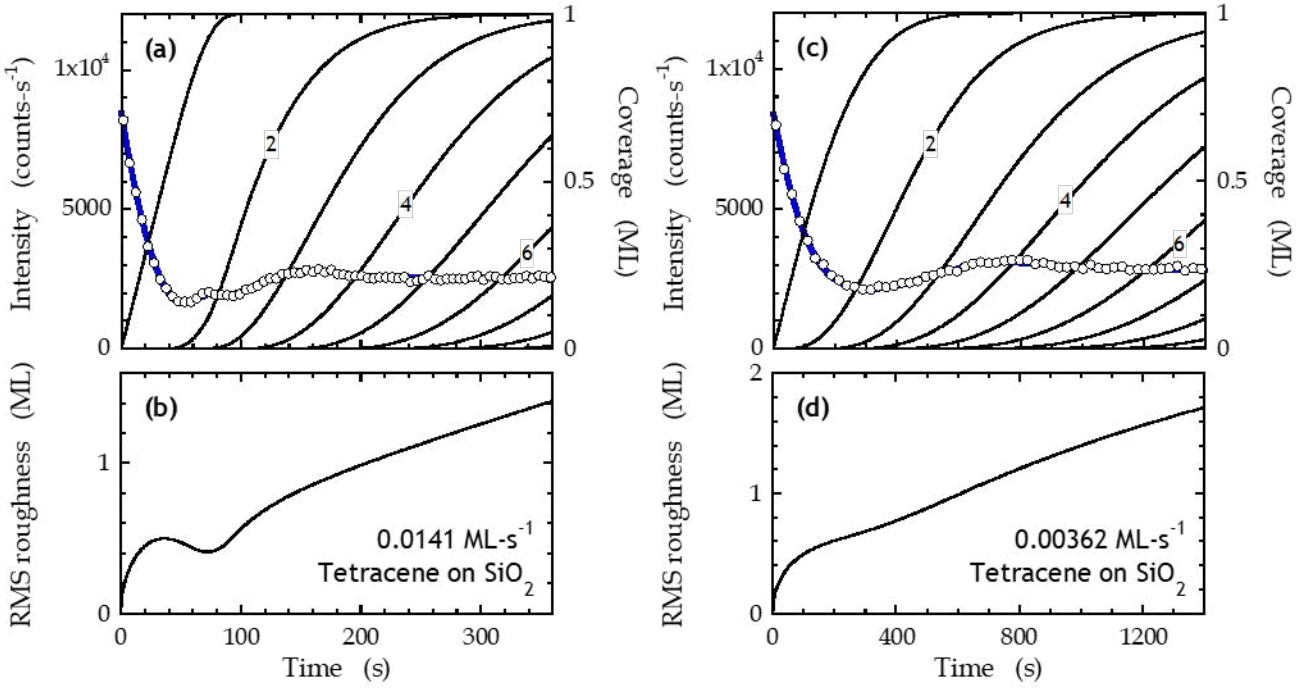

Figure 5-2: **(a)** Scattered X-ray intensity at the anti-Bragg condition as a function of time for a thin film of tetracene grown on SiO_2 at 0.0141 ML-s^{-1} and T_s = 0 °C, represented by the open circles (left ordinate, every 5th data point shown for visibility). The solid blue line (left ordinate) represents a fit of the model to the data, and the solid black curves (right ordinate) represent predicted layer coverages of the individual layers. **(b)** RMS roughness as predicted by the fit of the data shown in **(a)**. A similar set of figures is shown for growth at 0.00362 ML-s^{-1} in **(c)** and **(d)**.

growth rates due to simultaneous growth of the first two monolayers after the deposition of 0.5 ML. Clearly, the growth behavior is becoming more 3D-like. In Figure 5-2(c)-(d), we present a similar set of results for an even slower growth rate of 0.00362 ML-s^{-1} [a factor of ~4 slower than that shown in Figure 5-2(a)-2(b), and a factor of ~ 40 than that shown in Figure 5-1(a)-1(b)]. For this slow growth rate, there is only one broad oscillation, exhibiting only a single local minimum. Moreover, the fit to the data clearly indicates 3D growth.

We have presented results demonstrating a transition from 2D LbL to 3D growth as the growth rate is decreased. Do results from AFM support this conclusion as well? In Figure 5-3, we present AF micrographs of four thin films of tetracene grown on SiO_2 at the conditions discussed above. These AF micrographs were obtained *ex situ* and at room temperature, after growth at T_s = 0 °C. In Figure 5-3(a), we display a micrograph of the thin film of tetracene grown at 0.144 ML-s^{-1}. From the fit to the data, the thickness is predicted to be 12.1 ML. From AFM, we estimate a (mean) thickness of 11.1 ML, where we assumed the lowest areas represented bare substrate [this is more evident in Figures 5-3(b)-3(d)]. The RMS roughness from AFM is 2.59 ML, which matches well with the RMS roughness predicted by the model: 2.51 ML. As can be seen in the micrograph, the grains are small with only a few areas of bare substrate, suggesting good coverage of the substrate. In Figure 5-3(b), we display a micrograph of the thin film of tetracene grown at 0.0266 ML-s^{-1}, predicted by the fit to be a thickness of 10.4 ML, with a roughness of 1.97 ML. For this case, the thickness and RMS roughness from AFM are 12.0 ML and 2.90 ML, respectively. We now observe larger grains, as well as more apparent bare areas of the substrate between grains, suggesting incomplete coverage of the substrate.

As the growth rate decreases, the change in morphology becomes more dramatic. In Figure 5-3(c), we display a micrograph of the thin film of tetracene

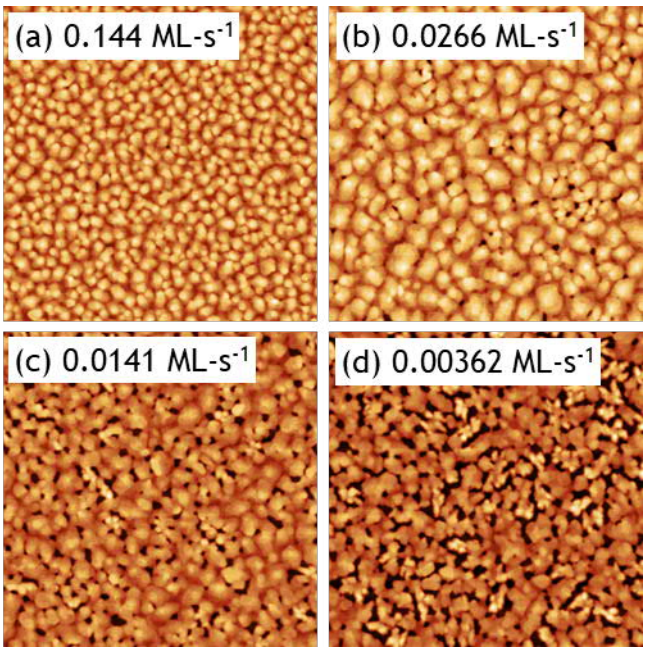

Figure 5-3: 5×5 μm^2 AF micrographs of thin films of tetracene grown on SiO_2 at: **(a)** 0.144 ML-s^{-1} (12.1 ML); **(b)** 0.0266 ML-s^{-1} (10.4 ML), **(c)** 0.0141 ML-s^{-1} (10.7 ML), and **(d)** 0.00362 ML-s^{-1} (12.3 ML). All growths were conducted at T_s = 0 °C.

grown at 0.0141 ML-s^{-1} to a predicted thickness of 10.7 ML, with a roughness of 2.31 ML. Analysis of the AF micrograph gives a thickness of 13.0 ML and a roughness of 3.73 ML. Finally, in Figure 5-3(d), we display a micrograph of the thin film of tetracene grown at 0.00362 ML-s^{-1} to a predicted thickness of 12.3 ML with a roughness of 2.66 ML. For this thin film, we determine from AFM a thickness of 11.7 ML and an RMS roughness of 4.99 ML. In Figures 5-3(c)-(d), we note a transition in morphology from Figures 5-3(a)-(b). Figure 5-3(d) reveals more exposed substrate, as well as some dendritic features. Figure 5-3(c) shows a combination of these types of structures as well as mounds. Can we quantify the changes in the lateral size of these features and identify any effect of the growth rate?

We use 1D power spectral density (1D PSD) analysis, which is a well-established technique to determine the correlation length, ξ, from the AF micrographs.[20–23] We present a summary of the results of this analysis for all rates of growth examined, along with the associated thicknesses and roughness predicted by the fit to the data, as well as those by AFM, in Table 5-1. For the three slowest growth rates, we note that roughness from AFM exceeds that predicted by the model, and in fact even exceeds the roughness that would arise from stochastic growth [where roughness scales with the square-root of total coverage, *cf.* Figure 5-4(a)]. This suggests that there must be some upward transport which occurs either during growth or as a result of post-deposition reorganization.[24] Examination of the correlation lengths for the three slowest rates of growth (< 0.02 ML-s^{-1}) does not reveal any obvious trend with growth rate. Analysis shows that for the three highest rates of growth examined here (> 0.02 ML-s^{-1}), in contrast, the roughness measured with AFM does not exceed the limit from stochastic growth, thus we need not invoke upward transport for these cases. Furthermore, for these three cases, concerning correlation lengths, we do observe what appears to be a dependence on the rate of growth, where

Table 5-1: A tabulated summary of the rates of growth investigated here, thicknesses and roughnesses derived from the fits to the intensity at the anti-Bragg condition, and from AFM, and the correlation length from analysis of the 1D PSD.

Growth rate (ML-s^{-1})	**Predicted thickness (ML)**	**AFM thickness (ML)**	**Predicted RMS roughness (ML)**	**AFM RMS roughness (ML)**	**ξ (nm)**
0.144	12.1	11.1	2.51	2.60	38.6
0.0626	11.1	12.4	2.66	2.66	46.8
0.0266	10.4	12.1	1.97	2.91	56.8
0.0141	10.7	13.0	2.31	3.74	43.5
0.00713	12.1	12.7	3.36	5.53	45.5
0.00362	12.3	11.8	2.66	5.00	39.2

the correlation length increases by a factor of ~ 1.5 or 50%, as the rate of growth is reduced by a factor of ~ 5.4.

In Figure 5-4(a) we plot the results of our analyses: the RMS roughness measured from AFM, the correlation length, and the roughness expected from purely stochastic roughening, as a function of growth rate. First, for the lowest three growth rates, as discussed above, significant thin film reorganization is indicated. Here it is difficult to assign much, if any, significance to the observed correlation lengths, and the apparent weak or no dependence on growth rate. On the other hand, for the three highest growth rates, we may be able to make an observation. If we assume that the density of the features indicated by the PSD analysis directly reflect the density of islands in the sub-monolayer regime, we can plot the log of the density (i.e., $1/\xi^2$) vs. the log of the growth rate to obtain the scaling exponent describing nucleation. We plot the results of this analysis in Figure 5-4(b), where we find a very good correlation with a power law, with an exponent of 0.46. Assuming that nucleation is homogenous, 2D complete,[3] this exponent gives a critical nucleus of $i^* = 1.7$, or ~ 2. Previous work on the nucleation of tetracene *at room temperature* has reported a critical nucleus of $i^* \sim 3$.[25] Interestingly, concerning the nucleation of a similar acene, pentacene on SiO_2, it has been reported that there is a change in the size of the critical nucleus, from a value of $i^* \sim 3$ for $T_s > -15$ °C, to a value of $i^* \sim 2$ for $T_s < -15$ °C.[26] Thus, our results are very consistent with the general expectation that the size of the critical nucleus should decrease with decreasing substrate temperature.

Thus far, we have provided results from both X-ray scattering at the anti-Bragg condition, and *ex situ* AFM, that there is a transition from 3D islanded to 2D LbL growth as the rate of thin film growth is increased. In addition to growth mode and thin film morphology, the exact nature of the crystalline forms of tetracene that are

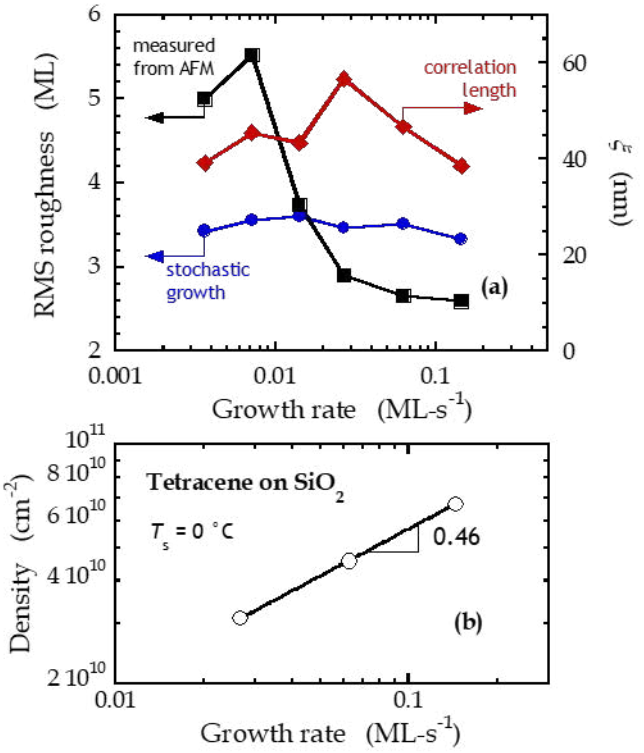

Figure 5-4: **(a)** Correlation length (left ordinate) and RMS roughness (right ordinate) as a function of growth rate, deduced from analysis of the images shown in Figure 5-3 and other similar ones. **(b)** Density of islands/characteristic features as a function of the rate of growth for conditions where 2D LbL growth is achieved.

deposited are of interest. For example, previous studies have shown the presence of two phases in thin films of tetracene, a thin-film phase, and the bulk phase.[27–31] Indeed, we have also examined this issue concerning the growth of tetracene on SiO_2 at T_s = 30 °C, and have found that the two phases do not grow simultaneously.[32] Rather, the thin-film phase grows first, and the bulk phase grows on top of the thin-film phase after some thickness has been deposited, depending on the local coverage. What do we observe concerning the growth of tetracene SiO_2 at T_s = 0 °C? We make use of GID to answer this question.

In Figure 5-5, we consider results from GID for two rates of growth and two thicknesses each, where the growth rates are similar to those we considered in Figure 5-1(c) and 5-1(d), 5-2(c) and 5-2(d), and 5-3(b) and 5-3(d). Thus, they represent rates where growth is clearly 2D LbL for the first few layers for one, but is 3D for the other. In Figures 5-5(a) and 5-5(b), we display results from GID for thin films with thicknesses of (a) ~10 ML and (b) ~ 20 ML deposited at a rate of ~ 0.03 ML-s^{-1}, corresponding to conditions where we observe strong oscillations at the anti-Bragg point and 2D LbL growth for the first few layers [*cf*. Figures 5-1(c), 5-1(d) and 5-3(b)]. As may be seen, in both of these diffraction patterns, we observe the diffraction peaks expected for the thin film phase only. For example, the (021) peak for the thin-film phase appears as expected at q_{xy} = 1.66 $Å^{-1}$, and q_z = 0.204 $Å^{-1}$. The bulk phase peak, expected at q_{xy} = 1.59 $Å^{-1}$, and q_z = 0.175 $Å^{-1}$., is essentially absent, although there may be a faint streak for the 20 ML thin film. On the other hand, there is no evidence of the bulk phase for the 10 ML thin film.

In Figures 5-5(c) and 5-5(d), we display a similar set of results from GID, except for thin films with thicknesses of (a) ~10 ML and (b) ~ 20 ML deposited at a rate of ~ 0.003 ML-s^{-1}. These data correspond to conditions where we observed a single shallow minimum in the anti-Bragg intensity consistent with almost immediate

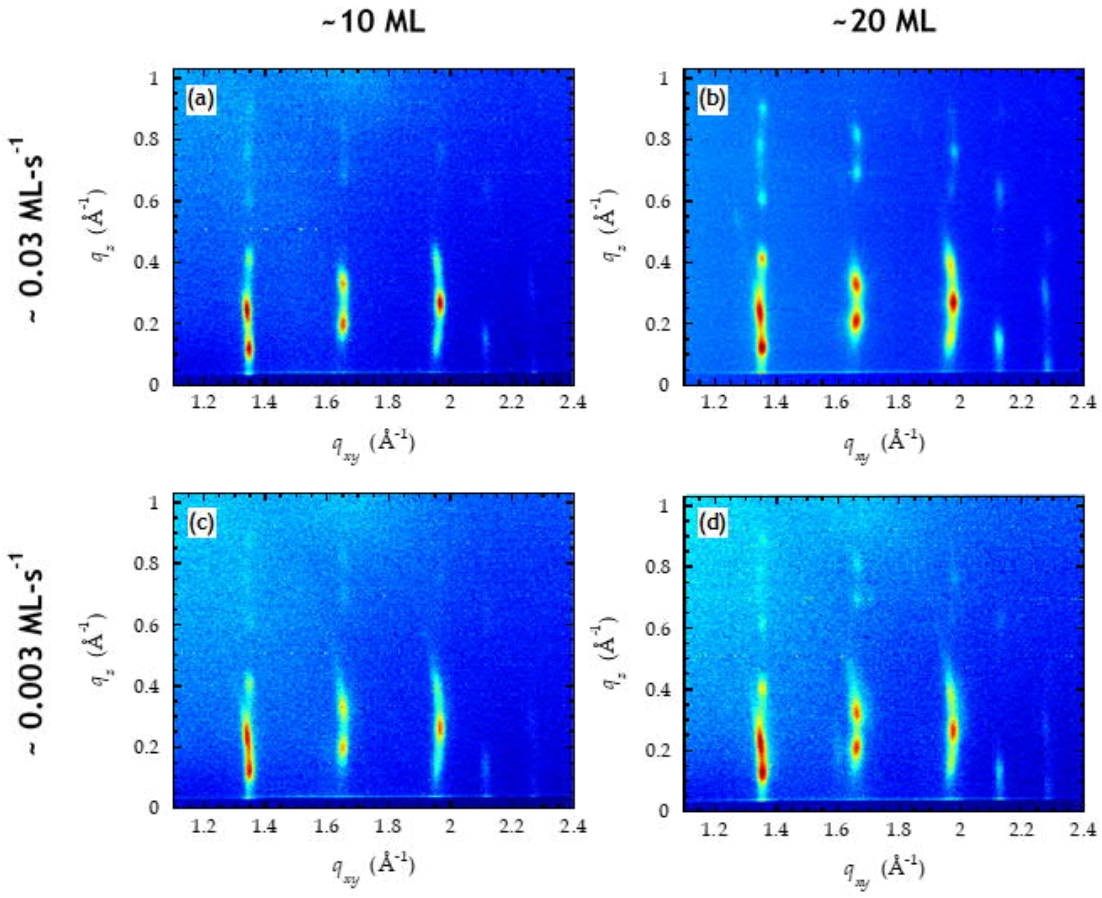

Figure 5-5: Grazing incidence diffraction for thin films of tetracene: **(a)** 10 ML and **(b)** 20.7 ML thick thin films deposited at ~ 0.03 ML-s^{-1}, and **(c)** 10 ML and **(d)** 22.2 ML thick thin films deposited at ~ 0.003 ML-s^{-1}. All growths were conducted at T_s = 0 °C.

3D growth [*cf*. Figures 5-2(c), 5-2(d) and 5-3(d)]. These results are quite similar to those we observed at the higher rate of deposition: essentially only peaks for the thin-film phase, and the appearance of a faint streak for the (021) peak of the bulk phase at a thickness of ~ 20 ML.

5.5 Discussion

We have examined the thin-film growth of tetracene on SiO_2 at T_s = 0 °C to determine the effect of substrate temperature on the mode of growth, and its dependence on the rate of growth. Similar to our previous work, we find that the rate of growth affects the mode of growth. For growth rates ≥ 0.0266ML-s^{-1}, we observed 2D LbL growth, while for growth rates ≤ 0.0141 ML-s^{-1}, there is a short-lived (sub-monolayer) period of 2D LbL growth and an eventual transition to 3D growth. This work expands upon our previous investigation on the growth of tetracene on SiO_2 performed at T_s = 30 °C. There, we observed a short-lived (sub-monolayer) period of 2D LbL growth for rates ≥ 0.21 ML-s^{-1}, while for growth rates ≤ 0.12 ML-s^{-1}, growth became 3D quickly, and, indeed, at a deposition rate of ~ 0.0277 ML-s^{-1} growth is 3D essentially immediately.[8]

First, as discussed in the Introduction, we recognize that based on the surface energies of tetracene [~ 84 mJ-m^{-2} for the (001) face][33,34] and the SiO_2 substrate (~ 60 mJ-m^{-2})[24] there is a driving force for "upward" transport, or de-wetting. We have postulated that this unexpected transition from 3D growth to 2D LbL growth as the growth rate *increases* involves a competition between two different processes: the rate of upward transport of tetracene at an island edge, and the rate of attachment of tetracene at these same island edges. The former is activated, and will exhibit a strong

dependence on temperature, while the latter may be activated, but will certainly scale with the rate of growth. The former process determines the residence time of molecules at the step edge, while the latter process converts step edge molecules to ones representing the interior terrace regions, which are essentially unable to move upward to the next layer. If the rate of the former is greater than the latter, upward transport at step edges will prevail, and the growth mode will be 3D. If the opposite is true, then the growth mode will become more 2D LbL. In this scenario, the transition from 3D to 2D LbL growth will depend on *both* the rate of growth *and* the substrate temperature.

In Figure 5-6, we display results for the thin-film growth of tetracene on SiO_2 at T_s = 30 °C representing two different rates of growth: (a,b) 0.467 ML-s^{-1} and (c,d) 0.0277 ML-s^{-1}. In Figure 5-6(a), we present the intensity of scattered X-rays at the anti-Bragg condition for a growth rate of 0.467 ML-s^{-1}. We note the presence of oscillations, indicating 2D LbL behavior, but the cusp corresponding to growth of ~ 1 ML is not as nearly sharp as what we observe here at T_s = 0 °C and rates of growth of 0.0266 and 0.144 ML-s^{-1} [*cf*. Figures 5-1(a) and 5-1(c)]. Indeed, the predicted layer coverages shown in Figure 5-6(a) indicate that the first monolayer is *ca*. 50% complete when the second monolayer begins to grow. This is distinctly different from the results we have just referenced at T_s = 0 °C [*cf*. Figures 5-1(a) and 5-1(c)], where the first monolayer is nearly entirely filled before the second monolayer begins to grow. Indeed, the behavior displayed in Figure 5-6(a) is most similar in nature to the growth shown in Figure 5-2(a), where T_s = 0 °C and the rate of growth was 0.0141 ML-s^{-1}.

We show an AF micrograph of the thin film of tetracene grown at T_s = 30 °C and 0.467 ML-s^{-1} in Figure 5-6(b). Here the thin film was ~ 12.2 ML thick, with an

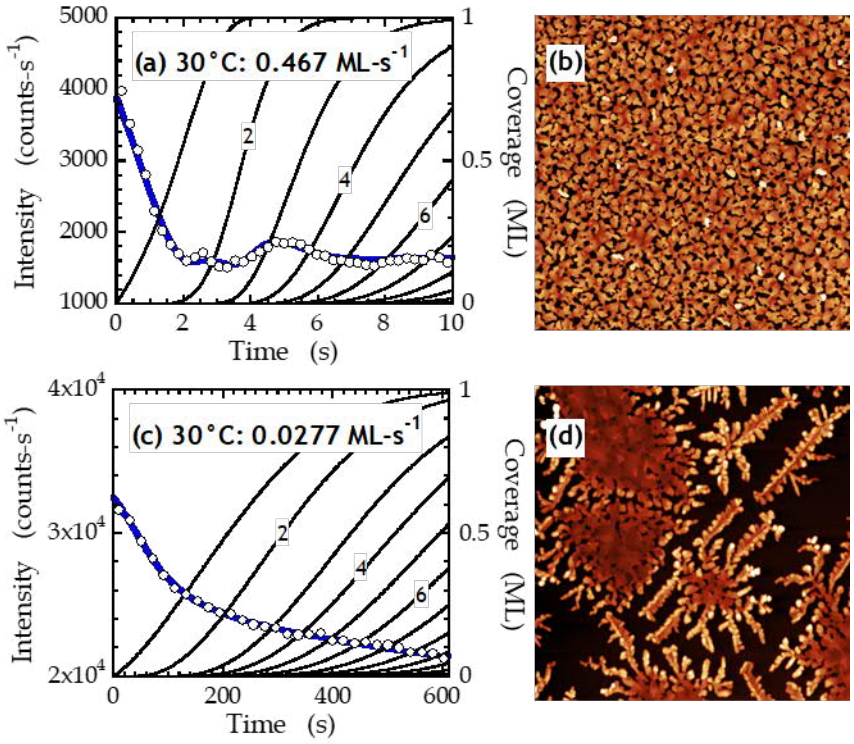

Figure 5-6: **(a)** Scattered X-ray intensity at the anti-Bragg condition, the fit to the data, and predicted layer coverages for a thin film of tetracene grown on SiO_2 at 30 °C at a rate of 0.467 ML-s^{-1}. Plotted in the same fashion as those in Figures 5-1 and 5-2. **(b)** AF micrograph (20 × 20 μm^2) of a 12.2 ML thick thin film grown at the rate considered in **(a)**. Similar figures for a growth rate of 0.0277 ML-s^{-1}, T_s = 30 °C, and a thickness of 17 ML are shown in **(c)** and **(d)**.

RMS roughness of ~ 7 ML. We note that this roughness exceeds those for all the results we report here for growth at T_s = 0 °C (*cf.* Figure 5-4 and Table 5-1). Some of this increase in roughness could be assigned to post-deposition re-organization, as the dependence of the intensity at the anti-Bragg condition is quite similar to growth at 0.0141 ML-s^{-1} and T_s = 0 °C, where we found an RMS roughness of 3.74 ML.

We display in Figures 5-6(c,d) another set of results at T_s = 30 °C, but for a lower growth rate of 0.0277 ML-s^{-1}. In Figure 5-6(c), we observe that the scattered X-ray intensity at the anti-Bragg point decreases monotonically, indicative of purely 3D growth. This behavior is distinct from what we observed here at T_s = 30 °C and for the lowest growth rate (0.00362 ML-s^{-1}), which is a factor of ~ 8 lower than that considered in Figure 5-6(c). An AF micrograph of this thin film grown at 0.0277 ML-s^{-1} is displayed in Figure 5-6(d). The islands here, spanning several microns, are much larger than any cases considered in the previous section. These islands also exhibited edges that were taller than the interiors of the islands—features that are not seen in the thin films considered in the previous section.

As indicated above, we observe similarities in the intensities at the anti-Bragg condition for T_s = 0 °C and a rate of growth of 0.0141 ML-s^{-1}, and what we have observed previously and reproduced here for T_s = 30 °C and a rate of growth of 0.467 ML-s^{-1}. We can make another comparison of these two data sets if we plot the layer occupancies vs. the total coverage that is predicted by the fits to the intensities at the anti-Bragg condition. We display this data in Figure 5-7. As may be seen, we observe two sets of results that are very similar to each other, indicating that the combination of the rate of growth and the substrate temperature has produced essentially the same behavior.

We consider further these effects of growth rate and substrate temperature on the growth mode in the form of an Arrhenius plot in Figure 5-8., where we consider all

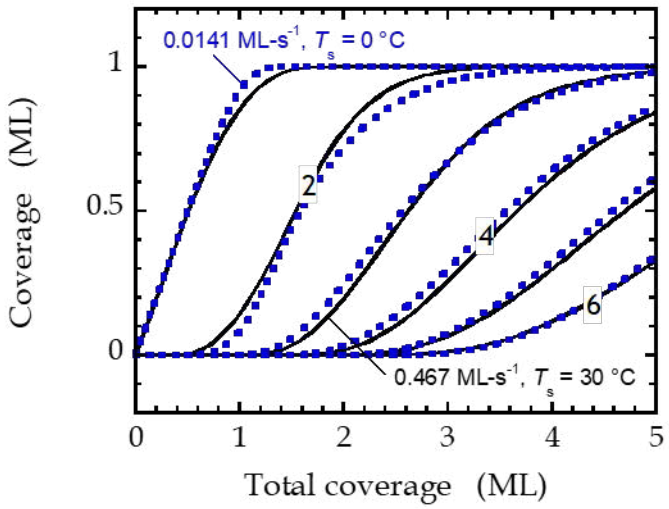

Figure 5-7: Predicted layer coverages for growth of tetracene on SiO_2 at 0.0141 ML-s^{-1} and T_s = 0 °C (smooth black curves), and at 0.467 ML-s^{-1} and T_s = 30 °C (dashed blue curves).

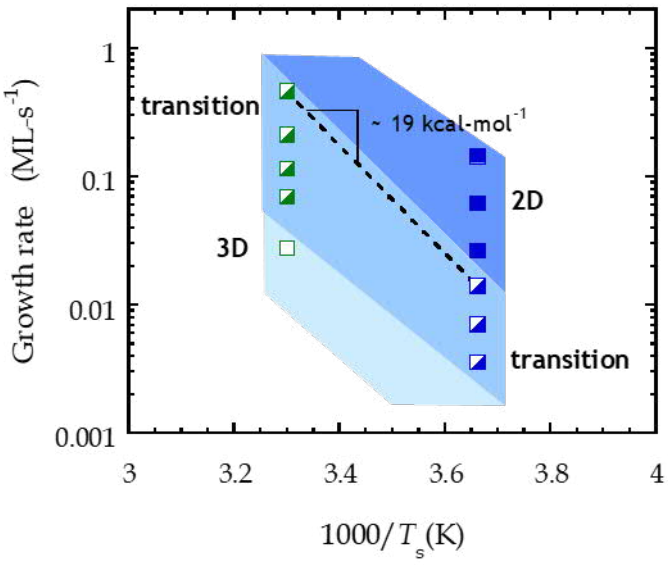

Figure 5-8: A plot of the growth modes as a function of the rate of growth and the inverse substrate temperature. Open symbols represent fully 3D growth, half-filled represent a transition regime, and filled represent 2D LbL growth. The shaded areas represent the approximate regions of phase space for growth.

results we have found at both T_s = 0 and 30 °C. Here we use symbols to indicate the mode of growth. An open square represents complete 3D growth, such as we have shown in Figure 5-6(c,d). The full squares represent what we designate as 2D LbL growth, such as we have shown in Figure 5-1(a-d). In these cases, growth of the 1st monolayer is essentially complete before the second layer nucleates. Finally, the half-filled squares represent what we designate as transition, such as is shown in Figures 5-2(a-d) and 5-6(a,b). Here, we observe an oscillation in the intensity at the anti-Bragg condition, and a significant fraction of the 1st monolayer grows before the 2nd monolayer nucleates. To guide the eye, we have shaded these three regions defining the mode of growth. In addition, we fit a straight line to the two data points we considered previously in Figure 5-7, where the line as shown represents an activation energy of 19 kcal-mol^{-1}. The pre-exponential factor (which has units of ML-s^{-1}), which should be related to an attempt frequency for step up events is within expectations, ~ 3×10^{13} ML-s^{-1}.

Is the activation energy indicated in Figure 5-8 plausible for a step-up event for tetracene? Previously we have discussed how one can use estimates for the binding energy of tetracene to a (001) terrace, the barrier for a step-down event (i.e., the Ehrlich Schwoebel barrier[35]), and the binding energy of a molecule at a step edge (~ equal to crystal cohesive energy) to compute this quantity.[8] Here, we acknowledge that we are ignoring any possible effect of a barrier to attachment at the step edge (e.g., due to molecular reorientation[36]). If we make use of values calculated elsewhere in a study using empirical molecular mechanics (MM3π) potentials,[35] we estimate a barrier for a step-up event of ~ 17.7 kcal-mol^{-1}, close to the value of 19 kcal-mol^{-1} that we report here. A flaw in this study using molecular mechanics potentials is that it consistently underestimated the most well-known experimentally determined number—the crystal cohesive energy—by approximately ~ 21% (for anthracene,

tetracene and pentacene).[37] If we correct for this shortcoming we estimate a barrier for the step-up event of ~ 23.6 kcal-mol^{-1}, which is also close to the value we display in Figure 5-8. From these observations, we reinforce our interpretation of the events that control the 3D to 2D transition involve a competition between attachment at step edges, and step-up edge crossing events. We note that a similar phenomenon was observed by Forrest and co-workers when studying the thin-film growth of perylene-3,4,9,10-tetracarboxylic dianhydride (PTCDA) on Au(111).[4] On the whole, our results presented here strengthen the supposition that 3D growth is driven by upward transport in systems where the rate of upward transport is competitive with the rate at which admolecules attach to a step edge, and also that 2D LbL growth can be achieved by increasing growth rate. We recognize, of course, that at much lower substrate temperatures (and possibly much higher rates of growth), that this picture will eventually break down, as the rates of step-edge crossing (upwards or downwards) will become vanishingly small, resulting in possibly stochastic roughening, or the formation of amorphous thin films.

One final issue we consider involves the fact that tetracene forms both a thin film and a bulk phase. In Figure 5-5 we displayed results from GID for the growth of thin films of ~ 10 and 20 ML in thickness at two rates of growth of ~ 0.03 and ~ 0.003 ML-s^{-1}. In a previous study,[32] we found a correlation with the onset of the bulk phase and the rate of growth—as the rate of growth increased a larger amount of the thin-film phase could be deposited before any appearance of the bulk phase. We have argued that this is a consequence of the local coverage/thickness produced at different growth rates. For example, if a critical thickness exists to nucleate the bulk phase, this thickness is reached at a smaller (mean) thickness if the thin film is rougher, which occurs at lower growth rates due to upward transport.

In Figure 5-9 we plot the thickness of thin film that can be deposited before the appearance of the bulk phase as a function of the rate of growth. We show both data obtained from an analysis of real time GID at T_s = 30 °C,[32] and results we find here for T_s = 0 °C. In the latter case, our results are not from real time GID, arguably the best method to determine the appearance of the bulk phase, but represent "snapshots" of the thin film structure, taken *ex situ*, and after growth. Thus, the comparison is not perfect. However, we would argue that, if anything, post deposition reorganization would favor the thermodynamically favored phase: the bulk phase. Thus, the results from *ex situ* GID likely provide a minimum concerning the amount of the bulk phase formed in real time. As may be seen from the figure, a "universal" relationship between the onset thickness and the growth rate is not observed. This is of course a consequence of the fact that at comparable growth rates, but different substrate temperatures, the thin films are smoother at lower substrate temperature. We argued above that a change in the substrate temperature of 30 to 0 °C, could be compensated by a change in the growth rate from 0.467 to 0.0141 ML-s^{-1}, or a factor of 33. We have sketched in a horizontal line in Figure 5-9 that would represent just such a change in the rate of growth. We see that such a shift would result in a data set better represented by a single universal curve. Although there is considerable uncertainty in our assignment of the appearance of the bulk phase at T_s = 0 °C, these results would argue against a dominant role played by the substrate temperature concerning the appearance of the bulk phase at least for the range of conditions we have considered here.

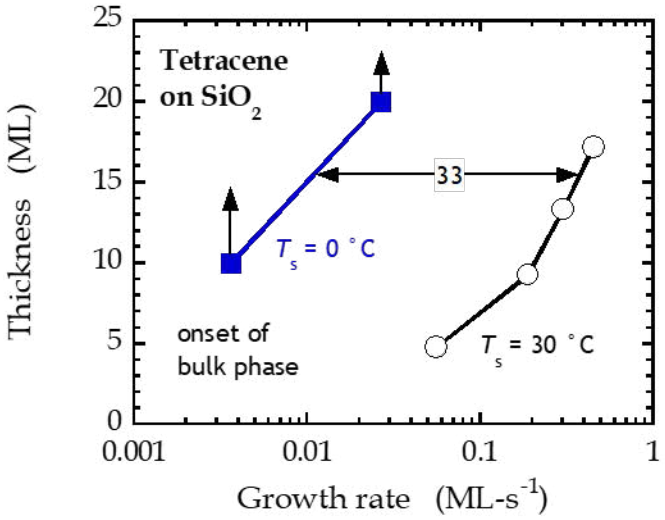

Figure 5-9: The minimum thickness for the appearance of the bulk phase as a function of the rate of growth and the substrate temperature for the growth of tetracene on SiO_2.

5.6 Conclusions

We have investigated the effect of growth rate on the growth mode of thin films of tetracene on SiO_2 at a substrate temperature $T_s = 0$ °C. From *in situ* real-time X-ray scattering and *ex situ* AFM, we have found that thin films of tetracene develop in a 2D LbL mode for growth rates ≥ 0.0266 ML-s^{-1}, where growth of the 1st monolayer is essentially complete before the second layer nucleates. As the rate of growth decreases, for rates ≤ 0.0141 ML-s^{-1}, there is a short-lived (sub-monolayer) period of 2D LbL growth and an eventual transition to 3D growth. The thin films that are grown in the 2D LbL regime display mound-like features, whereas those grown in the 3D regime exhibit some mounds, but also more dendritic features. Analysis of the dependence of the characteristic size of the mounds on the rate of growth in the 2D LbL regime implicates a size of the critical nucleus of $\sim i^* = 1.7$, or ~ 2. Finally, GID also reveals that thin films of tetracene grown on SiO_2 grown at 0 °C in the investigated range of growth rates nearly entirely adopt the thin-film phase.

We have compared the results presented here to results we have presented previously for tetracene grown on SiO_2 at 30 °C. In particular, we have found that there is a significant effect of substrate temperature on the transition from 2D LbL to 3D growth as the rate of growth is decreased. We find that transition to 3D growth occurs at a lower growth rate at the low substrate temperature. This supports our previously made interpretation that the transition is controlled by a competition between attachment at island edges (determined predominantly by the rate of growth) and "upward" step-edge crossing (determined predominantly by the substrate temperature). Using a set of results representing both different growth rates and substrate temperatures, yet giving essentially the same evolution of the thin film

morphology, we derive an activation energy for upward step-edge crossing of ~ 19 kcal-mol^{-1}.

Finally, we did observe the appearance of the bulk phase for one set of growth conditions and a thickness of ~ 20 ML. Again, comparing to our previous work at T_s = 30 °C, at comparable growth rates the appearance of the bulk phase was delayed at T_s = 0 °C. This is best interpreted as not reflecting some intrinsic dependence of the transition from the thin-film to the bulk phase on substrate temperature. Rather, as we have argued before,[32] the appearance of the bulk phase is dependent on the local coverage, where a critical minimum value is required to nucleate the bulk phase. This value is reached quicker for thin films that are rougher, which form at lower rates of growth and higher substrate temperatures. Viewing our results as a whole, it is clear that the growth mode and morphology of thin films of tetracene, and by extension other organic molecules, can be strongly influenced, in unexpected ways, by the growth rate and the substrate temperature—two variables that are typically under the precise control of the crystal grower.

5.7 Acknowledgements

We would like to thank Arthur R. Woll for invaluable technical contributions. This work made use of the Nanobiotechnology Center shared research facilities at Cornell, and is based upon research conducted at the Cornell High Energy Synchrotron Source (CHESS), which is supported by the National Science Foundation under NSF award DMR-1332208.

5.8 References

(1) Forrest, S. R. The Path to Ubiquitous and Low-Cost Organic Electronic Appliances on Plastic. *Nature* **2004**, *428* (6986), 911–918.

(2) Witte, G.; Wöll, C. Growth of Aromatic Molecules on Solid Substrates for Applications in Organic Electronics. *J. Mater. Res.* **2004**, *19* (7), 1889–1916.

(3) Venables, J. A.; Spiller, G. D. T.; Hanbucken, M. Nucleation and Growth of Thin Films. *Rep. Prog. Phys.* **1984**, *47* (4), 399–459.

(4) Forrest, S. R. Ultrathin Organic Films Grown by Organic Molecular Beam Deposition and Related Techniques. *Chem. Rev.* **1997**, *97* (6), 1793–1896.

(5) Schreiber, F. Self-Assembled Monolayers: From Simple Model Systems to Biofunctionalized Interfaces. *J. Phys.-Condens. Mat.* **2004**, *16* (28), R881–R900.

(6) Meyer zu Heringdorf, F. J.; Reuter, M. C.; Tromp, R. M. Growth Dynamics of Pentacene Thin Films. *Nature* **2001**, *412* (6846), 517–520.

(7) Meyer zu Heringdorf, F.-J.; Reuter, M. C.; Tromp, R. M. The Nucleation of Pentacene Thin Films. *Appl. Phys. A-Mater.* **2004**, *78* (6), 787–791.

(8) Nahm, R. K.; Engstrom, J. R. Unexpected Effects of the Rate of Deposition on the Mode of Growth and Morphology of Thin Films of Tetracene Grown on SiO 2. *J. Phys. Chem. C* **2016**, *120* (13), 7183–7191.

(9) Schroeder, T. W. Dissertation: Thin Film Deposition Employing Supersonic Molecular Beams: Nucleation and Growth of Silicon, Silicon Germanium and Pentacene, Cornell University, 2004.

(10) Woll, A. R.; Desai, T. V.; Engstrom, J. R. Quantitative Modeling of in Situ X-Ray Reflectivity during Organic Molecule Thin Film Growth. *Phys. Rev. B* **2011**, *84* (7), 075479/1-075479/14.

(11) Kowarik, S.; Gerlach, A.; Skoda, M. W. A.; Sellner, S.; Schreiber, F. Real-Time Studies of Thin Film Growth: Measurement and Analysis of X-Ray Growth Oscillations beyond the Anti-Bragg Point. *Eur. Phys. J. Spec. Top.* **2009**, *167* (1), 11–18.

(12) Trofimov, V. I.; Mokerov, V. G.; Shumyankov, A. G. Kinetic Model for Molecular Beam Epitaxial Growth on a Singular Surface. *Thin Solid Films* **1997**, *306* (1), 105–111.

(13) Trofimov, V. I.; Mokerov, V. G. Rate Equations Model for Layer Epitaxial Growth Kinetics. *Thin Solid Films* **2003**, *428* (1–2), 66–71.

(14) Trofimov, V. I.; Kim, J.; Bae, S. Influence of Two Different Adatom Mobilities on the Initial Heteroepitaxial Growth Kinetics. *Surf. Sci.* **2007**, *601* (18), 4465–4469.

(15) Trofimov, V. I.; Kim, J.; Bae, S. Temperature Behavior of the Growth Mechanism during Layer Epitaxial Growth. *J. Phys. Conf. Ser.* **2008**, *100* (8), 82005.

(16) Amassian, A.; Desai, T. V.; Kowarik, S.; Hong, S.; Woll, A. R.; Malliaras, G. G.; Schreiber, F.; Engstrom, J. R. Coverage Dependent Adsorption Dynamics in Hyperthermal Organic Thin Film Growth. *J. Chem. Phys.* **2009**, *130* (12), 124701/1-124701/9.

(17) Goose, J. E.; Killampalli, A. S.; Clancy, P.; Engstrom, J. R. Molecular-Scale Events in Hyperthermal Deposition of Organic Semiconductors Implicated from Experiment and Molecular Simulation. *J. Phys. Chem. C* **2009**, *113* (15), 6068–6073.

(18) Desai, T. V.; Hong, S.; Woll, A. R.; Hughes, K. J.; Kaushik, A. P.; Clancy, P.; Engstrom, J. R. Hyperthermal Organic Thin Film Growth on Surfaces Terminated with Self-Assembled Monolayers. I. The Dynamics of Trapping. *J. Chem. Phys.* **2011**, *134* (22), 224702/1-224702/13.

(19) Desai, T. V.; Kish, E. R.; Woll, A. R.; Engstrom, J. R. Hyperthermal Growth of N , N′ -Ditridecylperylene-3,4,9,10-Tetracarboxylic Diimide on Self-Assembled Monolayers: Adsorption Dynamics and Sub- and Multilayer Thin Film Growth. *J. Phys. Chem. C* **2011**, 18221–18234.

(20) Biscarini, F.; Samorí, P.; Greco, O.; Zamboni, R. Scaling Behavior of Anisotropic Organic Thin Films Grown in High Vacuum. *Phys. Rev. Lett.* **1997**, *78* (12), 2389–2392.

(21) Collins, G. W.; Letts, S. A.; Fearon, E. M.; McEachern, R. L.; Bernat, T. P. Surface Roughness Scaling of Plasma Polymer Films. *Phys. Rev. Lett.* **1994**, *73* (5), 708–711.

(22) Papadimitratos, A.; Amassian, A.; Killampalli, A. S.; Mack, J. L.; Malliaras, G. G.; Engstrom, J. R. Organic Thin-Film Transistors of Pentacene Films Fabricated from a Supersonic Molecular Beam Source. *Appl. Phys. A-Mater.* **2008**, *95* (1), 29–35.

(23) Desai, T. V.; Woll, A. R.; Engstrom, J. R. Thin Film Growth of Pentacene on Polymeric Dielectrics: Unexpected Changes in the Evolution of Surface Morphology with Substrate. *J. Phys. Chem. C* **2012**, *116* (23), 12541–12552.

(24) Amassian, A.; Pozdin, V. A.; Desai, T. V.; Hong, S.; Woll, A. R.; Ferguson, J. D.; Brock, J. D.; Malliaras, G. G.; Engstrom, J. R. Post-Deposition Reorganization of Pentacene Films Deposited on Low-Energy Surfaces. *J. Mater. Chem.* **2009**, *19* (31),

5580–5592.

(25) Shi, J.; Qin, X. Nucleation and Growth of Tetracene Films on Silicon Oxide. *Phys. Rev. B* **2008**, *78* (11), 115412.

(26) Tejima, M.; Kita, K.; Kyuno, K.; Toriumi, A. Study on the Growth Mechanism of Pentacene Thin Films by the Analysis of Island Density and Island Size Distribution. *Appl. Phys. Lett.* **2004**, *85* (17), 3746–3748.

(27) Gompf, B.; Faltermeier, D.; Redling, C.; Dressel, M.; Pflaum, J. Tetracene Film Morphology: Comparative Atomic Force Microscopy, X-Ray Diffraction and Ellipsometry Investigations. *Eur. Phys. J. E* **2008**, *27* (4), 421–424.

(28) Milita, S.; Servidori, M.; Cicoira, F.; Santato, C.; Pifferi, A. Synchrotron X-Ray Investigation of Tetracene Thin Films Grown at Different Deposition Fluxes. *Nucl. Instrum. Meth. B* **2006**, *246* (1), 101–105.

(29) Milita, S.; Santato, C.; Cicoira, F. Structural Investigation of Thin Tetracene Films on Flexible Substrate by Synchrotron X-Ray Diffraction. *Appl. Surf. Sci.* **2006**, *252* (22), 8022–8027.

(30) Wünsche, J.; Tarabella, G.; Bertolazzi, S.; Bocoum, M.; Coppedè, N.; Barba, L.; Arrighetti, G.; Lutterotti, L.; Iannotta, S.; Cicoira, F.; Santato, C. The Correlation between Gate Dielectric, Film Growth, and Charge Transport in Organic Thin Film Transistors: The Case of Vacuum-Sublimed Tetracene Thin Films. *J. Mater. Chem. C* **2013**, *1* (5), 967.

(31) Moriguchi, N.; Nishikawa, T.; Anezaki, T.; Unno, A.; Tachibana, M.; Kojima, K. Carrier Mobility and Crystal Perfection of Tetracene Thin Film FET. *Phys. B* **2006**, *376–377*, 276–279.

(32) Nahm, R. K.; Engstrom, J. R. Who's on First? Tracking in Real Time the Growth of Multiple Crystalline Phases of an Organic Semiconductor: Tetracene on SiO2. *J. Chem. Phys.* **2017**, *146* (5), 52815.

(33) Knieling, T.; Lang, W.; Benecke, W. Gas Phase Hydrophobisation of MEMS Silicon Structures with Self-Assembling Monolayers for Avoiding in-Use Sticking. *Sens. Actuat. B-Chem.* **2007**, *126* (1), 13–17.

(34) Kawai, A.; Kawakami, J. Characterization of SiO2 Surface Treated by HMDS Vapor and O2 Plasma with AFM Tip. *J. Photopolym. Sci. Tec.* **2003**, *16* (5), 665–668.

(35) Goose, J. E.; First, E. L.; Clancy, P. Nature of Step-Edge Barriers for Small Organic Molecules. *Phys. Rev. B* **2010**, *81* (May), 10–12.

(36) Desai, T. V.; Woll, A. R.; Schreiber, F.; Engstrom, J. R. Nucleation and

Growth of Perfluoropentacene on Self-Assembled Monolayers: Significant Changes in Island Density and Shape with Surface Termination. *J. Phys. Chem. C* **2010**, *114* (47), 20120–20129.

(37) Roux, M. V.; Temprado, M.; Chickos, J. S.; Nagano, Y. Critically Evaluated Thermochemical Properties of Polycyclic Aromatic Hydrocarbons. *J. Phys. Chem. Ref. Data* **2008**, *37* (4), 1855–1996.

CHAPTER 6

THE ROLE OF SURFACE ENERGY IN THE GROWTH OF THIN FILMS OF TETRACENE ON THIN FILMS OF PENTACENE ON SILICON DIOXIDE

6.1 Abstract

We report on our investigations on the growth of thin films of tetracene on pre-deposited 1, 2, and 3 ML-thick thin-films of pentacene, a surface which is more similarly matched in surface energy to tetracene. Using synchrotron X-ray radiation techniques and atomic force microscopy, we find that tetracene grows initially 2D layer-by-layer and then 3D on 1 ML-thick pentacene and on SiO_2, but growth is more 3D in the case of SiO_2. On 2 ML and 3 ML-thick thin films of pentacene, growth may be layer-by-layer initially but is more 3D than on 1 ML of pentacene. Thin films of tetracene on pentacene possess a morphology similar to that of tetracene on SiO_2 grown at faster rates, signifying a slower rate of upward transport facilitated by the better-matched surface energies. However, in all cases, we see roughening that exceeds the limit by stochastic growth, indicating that there must still be significant reorganization. Our results make clear that matching the surface energies of the substrate and tetracene are not wholly sufficient to give rise to 2D layer-by-layer growth.

6.2 Introduction

The formation of high-quality organic-organic heterostructures remains an intense area of interest as researchers strive toward controlling interfaces in organic electronics and solar cells.[1] Simple planar heterojunctions and superstructures derived from repeating planar heterojunctions represent important architectures for different devices such as solar cells and quantum wells[2,3] and allow for control over the thickness of the different layers to accommodate varying exciton diffusion lengths.[4] Such heterostructures have been demonstrated for a variety of combinations, including perfluoropentacene (PFP) and diindenoperylene (DIP),[5,6] pentacene and PFP,[5] C_{60} and DIP,[7] 3,4,9,10-perylenetetraccarboxylic dianhydride (PTCDA) and copper phthalocyanine (CuPc),[8] among others.[9,10] We have also recently reported on our investigations of the heterostructure formation of a variety of perylene derivatives (PTCDI-C_n) and pentacene, where we find that the order of deposition is extremely important in the resulting morphology due to surface energies.[11] There, we demonstrate that surface energies must be matched in order to grow high-quality interfaces of differing organic molecules.

Here, we investigate the heterostructure formation of tetracene on pentacene. We have previously found that tetracene undergoes significant reorganization on SiO_2 due to uphill transport driven by differences in the surface energies between tetracene and the substrate.[12] Tetracene and pentacene possess very similar crystal structures[13–15] and are predicted to have similar surface energies on their respective (001) planes.[16] We explore the effect of matching the surface energy of the substrate with tetracene by first depositing a thin film of pentacene. In this paper, we report on our findings concerning the thin-film growth of tetracene on 1, 2, and 3 MLs of pentacene

monitored with *in situ* and *ex situ* synchrotron X-ray techniques and *ex situ* atomic force microscopy (AFM) and compare this to growth on SiO_2.

6.3 Experimental Procedures

Thin-film deposition occurred in a custom-designed UHV chamber fitted with Be windows, detailed elsewhere,[17] in the G3 station at Cornell High Energy Synchrotron Source (CHESS). A supersonic molecular beam was used to deposit tetracene. A supersonic beam of tetracene is generated by passing He carrier gas over a heated vessel containing tetracene (99.99%, Sigma-Aldrich) and expanding this gas through a 150 μm nozzle into a UHV source chamber with a base pressure of $\sim 5 \times 10^{-9}$ Torr. The beam then passes through a trumpet-shaped skimmer, a differentially pumped ante-chamber, and finally a beam-defining aperture before striking the sample in the main scattering chamber. This beam is modulated by a shutter, located just upstream of the aperture, that is mounted on a pneumatically controlled, linear translator. A conventional thermal evaporation source (CreaTec Fischer & Co. GmbH) was used to deposit pentacene. The molecular beam of pentacene is modulated by a separate shutter, and there is a separate translatable beam-defining mask that confines deposition of pentacene to line-of-sight to the substrate. Thus, tetracene and pentacene may be sequentially deposited on the same area of a sample in quick succession. In these experiments, tetracene was deposited typically <1 hour after deposition of pentacene. We vary the growth rate of tetracene and pentacene by controlling the temperatures of the heated vessel with tetracene and the crucible with pentacene, respectively. For the experiments described here, the heated vessel containing tetracene was held at the same temperature for all experiments. The

samples, in all cases, were at a nominal temperature of T_s = 30 °C. Further details concerning the estimated kinetic energy (2.5-2.6 eV) and sample preparation are detailed elsewhere.[12]

Thin-film growth was monitored *in situ* with real-time X-ray scattering at the anti-Bragg condition. Thin-films of pentacene were grown to nominal thicknesses of 1, 2, and 3 MLs, determined by the oscillations in the scattered X-ray intensity at the anti-Bragg point for pentacene (q_z = 0.204 for d_z = 1.54 nm) – a method we had previously validated using AFM.[18] Thin-film growth of tetracene was also monitored using the same technique, but at the anti-Bragg point for tetracene (q_z = 0.243 for d_z = 1.293 nm). The energy of the X-ray beam was 10.06 keV, and the intensity of the scattered X-ray beam was measured using a DECTRIS Pilatus 100K area detector (DECTRIS, Ltd.) with one second exposures per frame. The thin films were then characterized *ex situ* using a Bruker Innova AFM (Bruker Corp.) operated in tapping mode, and with X-ray reflectivity (XRR) in the G2 station at CHESS.

6.4 Results and Discussion

First, we examine the thin-film growth of tetracene on 1 ML of pentacene on SiO_2. Based on our previous work concerning the thin-film growth of pentacene on SiO_2, we expect the occupancy of the first monolayer of pentacene to be 0.99 ML and the occupancy of the second monolayer to be 0.01 ML.[18] The intensity of the scattered X-rays at the anti-Bragg condition during the thin-film growth of tetracene on this nominally 1 ML of pentacene is shown as a function of time in Figure 6-1(a). Here, there is a clear oscillation at ~22 s and what appears to be a dampened oscillation at ~11 s. We can fit this data to a simplified version of a mean-field

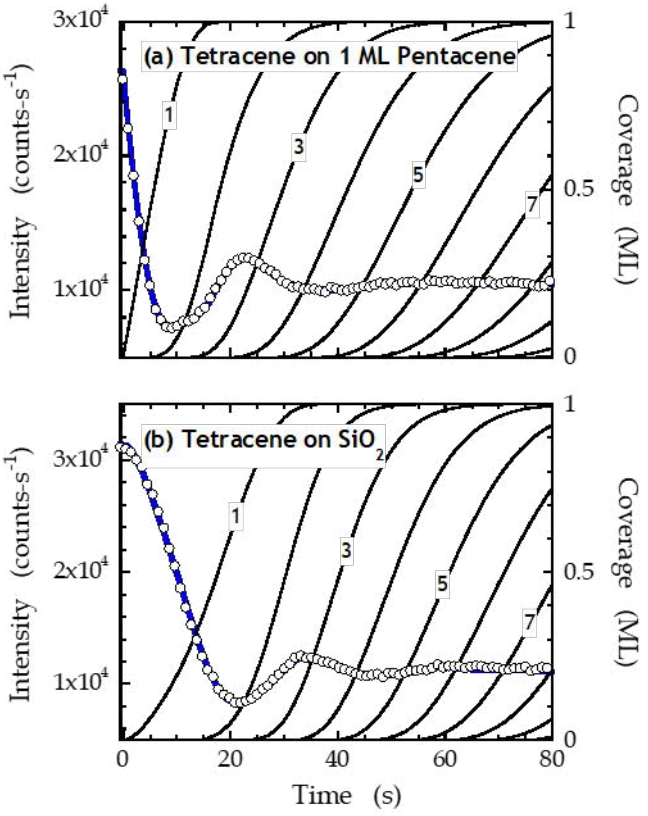

Figure 6-1: (a) Scattered X-ray intensity at the anti-Bragg condition as a function of time for a thin film of tetracene grown on **(a)** a nominally 1 ML pentacene on SiO_2 and **(b)** SiO_2, represented by the open circles (left ordinate). The solid blue line (left ordinate) represents a fit of the model to the data, and the solid black curves (right ordinate) represent predicted layer coverages of the individual layers. Data up to 80 s (of a total 172 s) shown for clarity.

rate-equation model developed by Trofimov *et al*.[19,20] This model has been found to accurately describe the growth of pentacene and other small organic semiconductors on a variety of surfaces[21–25] and AFM has been used to verify that the model's predictions of layer coverages, thin-film thickness, and roughness.[18] The fit of the model to this data is shown by the blue line in Figure 6-1(a) and is in good agreement with the experimental data. The predicted layer coverages are indicative of 2D LbL for the first monolayer, as it is nearly filled before the second monolayer begins to grow. After the first monolayer, growth becomes more 3D in nature. The fit of the model to the data predicts a growth rate of 0.084 ML-s^{-1}. We expect the model to reasonably capture the behavior of tetracene growing on 1 ML of pentacene because this layer is nearly complete with very few islands of pentacene in what would be the second monolayer, and so this can be treated as a uniform interfacial layer as we have done with self-assembled monolayers in the past.[23]

In Figure 6-1(b), we display similar data as in Figure 6-1(a) but for growth of tetracene on SiO_2 under nominally the same conditions of growth (e.g., flux). Here, one dampened oscillation is visible, but the growth is clearly more 3D than growth on 1 ML of pentacene. The fit of the model to the data gives a growth rate of 0.099 ML-s^{-1}, which is higher than the growth rate on 1 ML of pentacene. We can in see in Figure 6-2 that the predicted roughness of tetracene grown on 1 ML of pentacene is lower than that on SiO_2. The evolution of RMS roughness also shows that, for the growth of tetracene on 1 ML of pentacene, there is a local minimum in roughness at ~14 s, coinciding with the completion of the first monolayer of tetracene. A similar behavior is not predicted for the growth of tetracene on SiO_2, which is consistent with growth on SiO_2 being more 3D. While the model predicts that the roughness of the thin film of tetracene grown on SiO_2 is initially smoother than that grown on 1 ML of pentacene, the former is eventually predicted to exceed the latter at longer times.

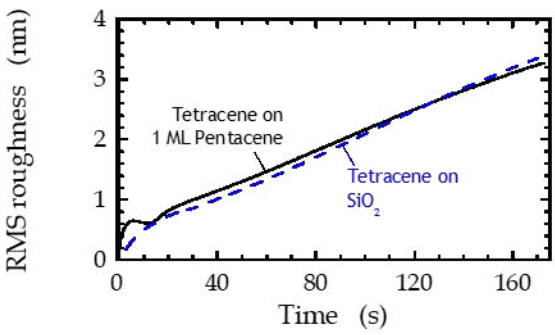

Figure 6-2: RMS roughness as predicted by the fit to the data shown in **Figure 6-1(a,b)**.

The morphologies of these thin films, grown on SiO_2 and on 1 ML of pentacene under the same conditions and for the same duration (172 s), are starkly different, as we show by AFM and associated line scans in Figures 6-3(a-d). The thin film on SiO_2, with an RMS roughness of 5.55 ML and a thickness of 14.4 ML (by AFM), is similar to what we reported in our previous study of tetracene on SiO_2 at comparable growth rates. The thin film on 1 ML of pentacene has an RMS roughness of 7.34 ML and a thickness of 17.9 ML (by AFM). This is opposite of the predicted trend for roughness. Moreover, the thicknesses of these thin films differ slightly from the predicted thickness of 15.54 ML for the thin film on SiO_2 and 14.48 ML for the thin film on 1 ML of pentacene. This may be due to the models inadequately describing long-time growth as there are no critical features past the first couple of monolayers. In both of these cases, however, the roughness measured by AFM exceeds the limit for stochastic roughness: 3.79 ML for the thin film on SiO_2 and 4.23 ML for the thin film on 1 ML of pentacene.

We note that this thin film on 1 ML of pentacene possesses a morphology similar to the 2D growth seen on SiO_2 at a high growth rate of 0.47 ML-s^{-1} (0.61 nm-s^{-1}) – nearly ~5 times greater than the growth rates considered in this study.[26] How could this be possible? We previously discussed the competition between the rate of upward transport and the rate of attachment to the edges of islands leading to morphologies like the one shown in Figure 6-3(c). The rate of upward transport is driven by the surface energy between the substrate and the growing thin film.[26] Ambrosch-Draxl *et al.* calculated surface energies for the (001) faces for bulk phase of tetracene and the thin-film phase of pentacene to be 84 mJ-m^{-2} and 91 mJ-m^{-2}, respectively.[16] For comparison, we note that the surface energy of clean, unmodified SiO_2 has been reported to have a surface energy of 50-60 mJ-m^{-2}.[27] On 1 ML of pentacene, the surface energy is much better matched with tetracene than with SiO_2 as

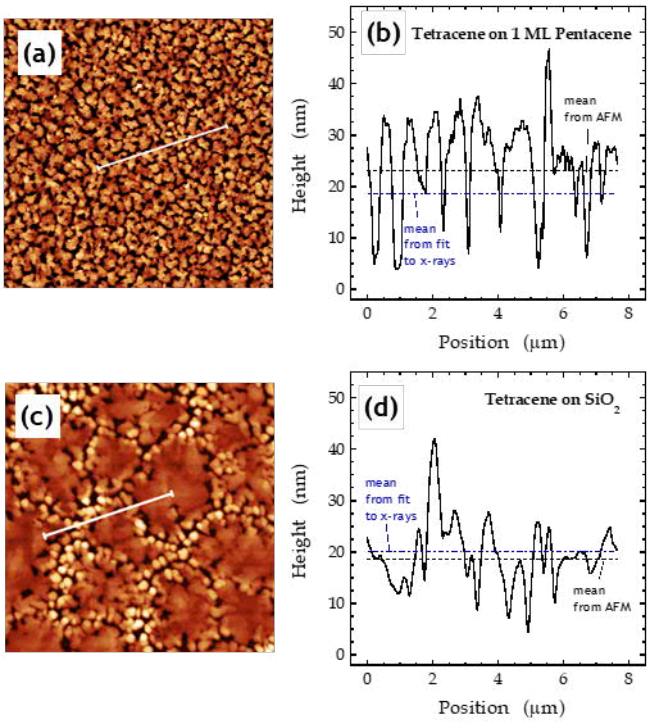

Figure 6-3: **(a)** A 15×15 μm^2 AF micrograph of a ~17.9 ML thin film of tetracene grown on nominally 1 ML pentacene on SiO_2. **(b)** A line scan from **(a)**. **(c)** A 15×15 μm^2 AF micrograph of a ~14.4 ML thin film of tetracene grown on SiO_2. **(d)** A line scan from **(c)**.

the substrate. Consequently, the rate of upward transport is lowered on 1 ML of pentacene and the net effect is a morphology that is like the case on SiO_2 at high growth rates where the rate of edge attachment is increased relative to the rate of upward transport. Despite this, we can deduce that there still is a significant amount of upward transport as there is no other way for the thin films to be rougher than the stochastic limit without reorganization.

We prepared substrates with nominally 2 ML and 3 ML of pentacene on SiO_2. Like with 1 ML of pentacene, we know the occupancies of each layer in these thin films.[18] In the case of 2 ML of pentacene, we expect the first monolayer to be completely occupied, the second monolayer to have 0.89 occupancy, the third monolayer to have 0.12 occupancy, and the fourth monolayer may have some nuclei. In the case of 3 ML of pentacene, we expect the first two monolayers to be completed filled, the third monolayer to have 0.76 occupancy, the fourth monolayer to have 0.24 occupancy, and the fifth monolayer may contain some nuclei. In Figure 6-4(a,b), we show the intensity of the scattered X-rays at the anti-Bragg condition for thin films of tetracene grown on 2 ML and 3 ML of pentacene. For 2 ML of pentacene, there is one oscillation at ~10 s, whereas for 3 ML of pentacene, there is an initial rise in intensity followed by a plateau and no oscillations. Because the layer occupancies of the thin films of pentacene are fractional, we did not apply the same model used for the growth of tetracene on SiO_2 and 1 ML of pentacene (*vide supra*). That model accounts for flat and uniform surfaces and interfacial layers, but not fractional coverages by a molecule distinct from the one that is actively being deposited.

We display AF micrographs of thin films of tetracene on 2 ML and 3 ML of pentacene and associated line scans in Figure 6-5(a-d). The thin film on 2 ML of pentacene is estimated by AFM to be 18.2 ML thick with a roughness of 6.9 ML. The thin film on 3 ML of pentacene is 21.0 ML thick with a roughness of 6.7 ML. The

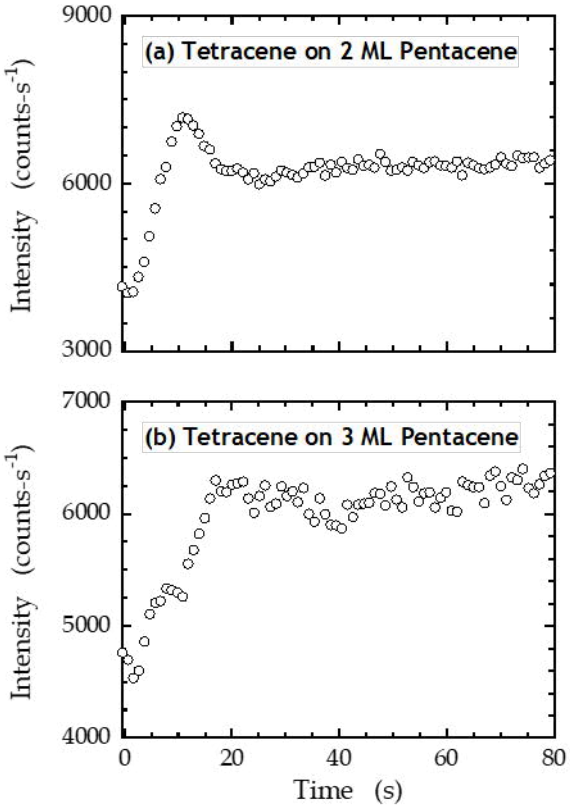

Figure 6-4: Scattered X-ray intensity at the anti-Bragg condition as a function of time for thin films of tetracene grown on **(a)** nominally 2 ML pentacene on SiO_2 and **(b)** nominally 3 ML pentacene on SiO_2, represented by the open circles.

morphology of these thin films is similar to tetracene on 1 ML of pentacene, and the roughness for both exceeds the stochastic limits of 4.27 ML for tetracene on 2 ML of pentacene and 4.58 ML for tetracene on 3 ML of pentacene. Therefore, the implications remain the same: the rate of upward transport on these surfaces is still lower than on SiO_2.

We present XRR of thin films of tetracene grown on 1, 2, and 3 ML thick thin films of pentacene in Figure 6-6(a,b,c). These thin films are estimated (by AFM) to be 149 ML, 140 ML, and 127 ML thick, respectively. The XRR shows three Bragg peaks belonging to the expected phases of pentacene and tetracene: one thin film phase of pentacene (d_z = 1.54 nm), a thin film phase of tetracene (d_z = 1.293 nm), and a bulk phase of tetracene (d_z = 1.219 nm).[28] The peaks from pentacene become more prominent as the thin film of pentacene becomes thicker, consistent with the presence of more material from which to scatter. From this data alone, we only know that tetracene does indeed for both a thin film phase and a bulk phase. We cannot tell if the underlying pentacene has any effect on *when* these phases nucleate and begin to grow relative to each other.

6.5 Conclusions

We have examined the thin-film growth of tetracene on 1, 2, and 3 MLs of pentacene on SiO_2 using a combination of *in situ* and *ex situ* synchrotron X-ray radiation techniques, as well as *ex situ* AFM. *In situ* X-ray scattering at the anti-Bragg condition revealed that growth of tetracene, at the rate considered here, on SiO_2 is immediately 3D, but, for the growth of tetracene on 1 ML of pentacene, growth is initially 2D for one monolayer before becoming 3D. On 2 and 3 MLs of pentacene,

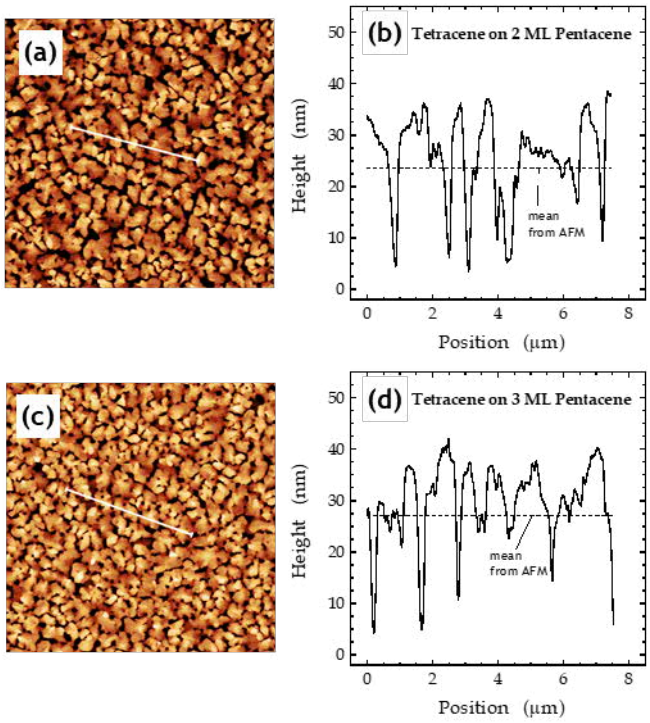

Figure 6-5: **(a)** A 15×15 μm^2 AF micrograph of a ~18.2 ML thin film of tetracene grown on nominally 2 ML pentacene on SiO_2. **(b)** A line scan from **(a)**. **(c)** A 15×15 μm^2 AF micrograph of a ~21.0 ML thin film of tetracene grown on SiO_2. **(d)** A line scan from **(c)**.

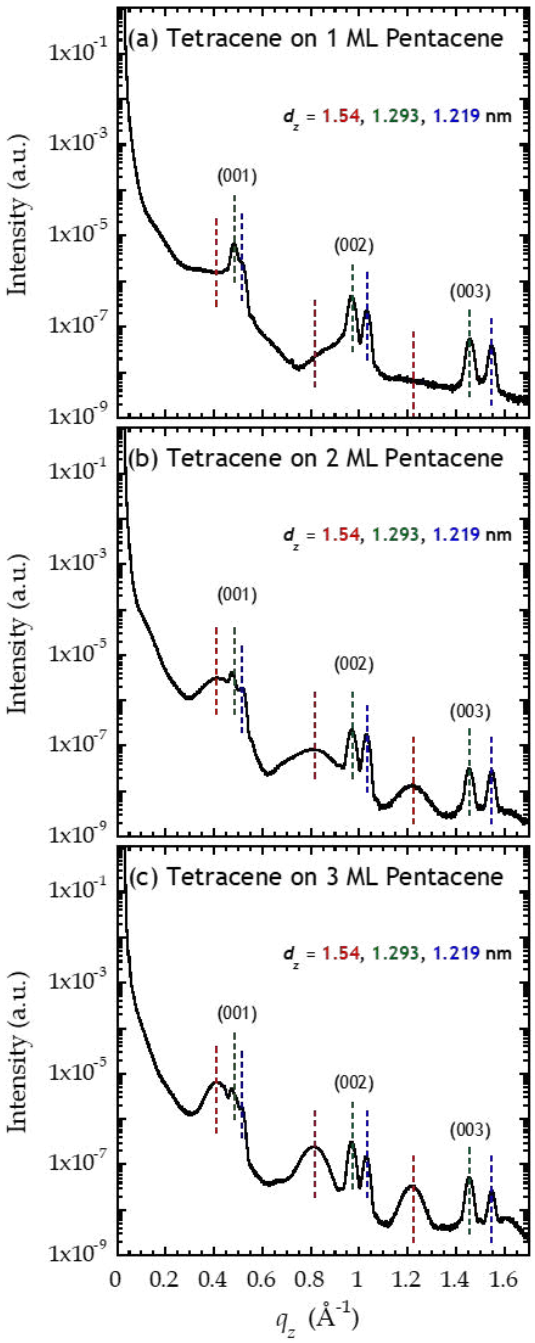

Figure 6-6: XRR of the thin films: **(a)** ~127 ML tetracene on 1 ML of pentacene, **(b)** ~140 ML tetracene on 2 ML of pentacene, **(c)** ~149 ML tetracene on 3 ML of pentacene. The colored, dashed lines represent the expected Bragg peaks (from left to right) for the thin-film phase of pentacene, the thin-film phase of tetracene, and the bulk phase of tetracene.

growth appears to be more 3D. For the growth rate considered in this study, AFM shows a similar morphology for tetracene grown on 1, 2, and 3 MLs of pentacene, and this morphology is similar to that seen previously for thin films of tetracene on SiO_2 grown at a rate ~5 times greater. Moreover, AFM reveals that there is reorganization of the thin film. Our results show that even in the situation where the surface energies between two organic molecules may be similar, kinetics still plays a large enough role to allow for significant upward transport, potentially influencing the ability to form well-ordered heterostructures.

6.6 Acknowledgements

We would like to thank Arthur R. Woll for invaluable technical contributions. We would also like to thank Jade M. Noble for technical contributions. This work made use of the Nanobiotechnology Center shared research facilities at Cornell, and is based upon research conducted at the Cornell High Energy Synchrotron Source (CHESS), which is supported by the National Science Foundation under NSF award DMR-1332208.

6.7 References

(1) Hinderhofer, A.; Schreiber, F. Organic-Organic Heterostructures: Concepts and Applications. *Chemphyschem* **2012**, *13* (3), 628–643.

(2) So, F.; Forrest, S. Evidence for Exciton Confinement in Crystalline Organic Multiple Quantum Wells. *Phys. Rev. Lett.* **1991**, *66* (20), 2649–2652.

(3) So, F. F.; Forrest, S. R.; Shi, Y. Q.; Steier, W. H. Quasi-Epitaxial Growth of Organic Multiple Quantum Well Structures by Organic Molecular Beam Deposition. *Appl. Phys. Lett.* **1990**, *56* (7), 674.

(4) Lunt, R. R.; Giebink, N. C.; Belak, A. A.; Benziger, J. B.; Forrest, S. R. Exciton Diffusion Lengths of Organic Semiconductor Thin Films Measured by Spectrally Resolved Photoluminescence Quenching. *J. Appl. Phys.* **2009**, *105* (5), 053711/1–053711/7.

(5) Hinderhofer, A.; Gerlach, A.; Kowarik, S.; Zontone, F.; Krug, J.; Schreiber, F. Smoothing and Coherent Structure Formation in Organic-Organic Heterostructure Growth. *Eur. Lett.* **2010**, *91* (5), 56002/1–56002/5.

(6) Hinderhofer, A.; Hosokai, T.; Frank, C.; Novák, J.; Gerlach, A.; Schreiber, F. Templating Effect for Organic Heterostructure Film Growth: Perfluoropentacene on Diindenoperylene. *J. Phys. Chem. C* **2011**, *115* (32), 16155–16160.

(7) Hinderhofer, A.; Gerlach, A.; Broch, K.; Hosokai, T.; Yonezawa, K.; Kato, K.; Kera, S.; Ueno, N.; Schreiber, F. Geometric and Electronic Structure of Templated C 60 on Diindenoperylene Thin Films. *J. Phys. Chem. C* **2013**, *117* (2), 1053–1058.

(8) Lunt, R. R.; Benziger, J. B.; Forrest, S. R. Growth of an Ordered Crystalline Organic Heterojunction. *Adv. Mat.* **2007**, *19* (23), 4229–4233.

(9) Lunt, R. R.; Sun, K.; Kröger, M.; Benziger, J. B.; Forrest, S. R. Ordered Organic-Organic Multilayer Growth. *Phys. Rev. B* **2011**, *83* (6), 064114/1–064114/7.

(10) Forrest, S.; Burrows, P.; Haskal, E.; So, F. Ultrahigh-Vacuum Quasiepitaxial Growth of Model van Der Waals Thin Films. II. Experiment. *Phys. Rev. B* **1994**, *49* (16), 11309–11321.

(11) Kish, E. R.; Nahm, R. K.; Woll, A. R.; Engstrom, J. R. When the Sequence of Thin Film Deposition Matters: Examination of Organic-on-Organic

Heterostructure Formation Using Molecular Beam Techniques and in Situ Real Time X-Ray Synchrotron Radiation. *J. Phys. Chem. C* **2016**, acs.jpcc.6b01717.

(12) Nahm, R. K.; Engstrom, J. R. Unexpected Effects of the Rate of Deposition on the Mode of Growth and Morphology of Thin Films of Tetracene Grown on SiO 2. *J. Phys. Chem. C* **2016**, *120* (13), 7183–7191.

(13) Holmes, D.; Kumaraswamy, S.; Matzger, A. J.; Vollhardt, K. P. C. On the Nature of Nonplanarity in the [N]Phenylenes. *Chem.-Eur. J.* **1999**, *5* (11), 3399–3412.

(14) Campbell, R. B.; Robertson, J. M.; Trotter, J. The Crystal Structure of Hexacene, and a Revision of the Crystallographic Data for Tetracene. *Acta Crystallogr.* **1962**, *15* (3), 289–290.

(15) Nabok, D.; Puschnig, P.; Ambrosch-Draxl, C.; Werzer, O.; Resel, R.; Smilgies, D.-M. Crystal and Electronic Structures of Pentacene Thin Films from Grazing-Incidence X-Ray Diffraction and First-Principles Calculations. *Phys. Rev. B* **2007**, *76* (23), 235322.

(16) Ambrosch-Draxl, C.; Nabok, D.; Puschnig, P.; Meisenbichler, C. The Role of Polymorphism in Organic Thin Films: Oligoacenes Investigated from First Principles. *New J. Phys.* **2009**, *11* (12), 125010.

(17) Schroeder, T. W. Dissertation: Thin Film Deposition Employing Supersonic Molecular Beams: Nucleation and Growth of Silicon, Silicon Germanium and Pentacene, Cornell University, 2004.

(18) Woll, A. R.; Desai, T. V.; Engstrom, J. R. Quantitative Modeling of in Situ X-Ray Reflectivity during Organic Molecule Thin Film Growth. *Phys. Rev. B* **2011**, *84* (7), 075479/1–075479/14.

(19) Trofimov, V. I.; Mokerov, V. G.; Shumyankov, A. G. Kinetic Model for Molecular Beam Epitaxial Growth on a Singular Surface. *Thin Solid Films* **1997**, *306* (1), 105–111.

(20) Trofimov, V. I.; Mokerov, V. G. Rate Equations Model for Layer Epitaxial Growth Kinetics. *Thin Solid Films* **2003**, *428* (1-2), 66–71.

(21) Hong, S.; Amassian, A.; Woll, A. R.; Bhargava, S.; Ferguson, J. D.; Malliaras, G. G.; Brock, J. D.; Engstrom, J. R. Real Time Monitoring of Pentacene Growth on SiO2 from a Supersonic Source. *Appl. Phys. Lett.* **2008**, *92* (25), 253304/1–253301/3.

(22) Amassian, A.; Desai, T. V.; Kowarik, S.; Hong, S.; Woll, A. R.; Malliaras, G. G.; Schreiber, F.; Engstrom, J. R. Coverage Dependent Adsorption Dynamics in

Hyperthermal Organic Thin Film Growth. *J. Chem. Phys.* **2009**, *130* (12), 124701/1–124701/9.

(23) Desai, T. V.; Hong, S.; Woll, A. R.; Hughes, K. J.; Kaushik, A. P.; Clancy, P.; Engstrom, J. R. Hyperthermal Organic Thin Film Growth on Surfaces Terminated with Self-Assembled Monolayers. I. The Dynamics of Trapping. *J. Chem. Phys.* **2011**, *134* (22), 224702/1–224702/13.

(24) Desai, T. V.; Kish, E. R.; Woll, A. R.; Engstrom, J. R. Hyperthermal Growth of N , N′ -Ditridecylperylene-3,4,9,10-Tetracarboxylic Diimide on Self-Assembled Monolayers: Adsorption Dynamics and Sub- and Multilayer Thin Film Growth. *J. Phys. Chem. C* **2011**, 18221–18234.

(25) Desai, T. V.; Woll, A. R.; Engstrom, J. R. Thin Film Growth of Pentacene on Polymeric Dielectrics: Unexpected Changes in the Evolution of Surface Morphology with Substrate. *J. Phys. Chem. C* **2012**, *116* (23), 12541–12552.

(26) Amassian, A.; Pozdin, V. A.; Desai, T. V.; Hong, S.; Woll, A. R.; Ferguson, J. D.; Brock, J. D.; Malliaras, G. G.; Engstrom, J. R. Post-Deposition Reorganization of Pentacene Films Deposited on Low-Energy Surfaces. *J. Mater. Chem.* **2009**, *19* (31), 5580–5592.

CHAPTER 7

CONCLUSIONS AND FUTURE WORK

In this dissertation, we have presented the results of our investigations on the thin-film growth of tetracene obtained using synchrotron X-ray scattering. We have found that the nature of thin-film growth on SiO_2 for tetracene is unusually different from that of pentacene, despite their similar structures. While other researchers had reported some of these unusual behaviors, none had studied these using *in situ* techniques. We have successfully done so and have proposed mechanisms for these effects. At a substrate temperature of nominally $T_s \sim 30$ °C, we observe two unusual phenomena concerning growth.

First, we have observed a transition from 3D island growth to 2D LbL growth of tetracene as the growth rate is increased. We determined this using *in situ* X-ray reflectivity at the anti-Bragg condition as well as *ex situ* atomic force microscopy to determine that upward transport drives 3D island growth. There is a competition between the rate of admolecule attachment at the tetracene island/SiO_2 substrate edges and the rate of upward step-edge transport. The transition from 3D growth to 2D growth occurs when the former, which is related to growth rate, effectively outcompetes the latter.

Second, we observed a transition from growth of only a thin-film phase to growth of a bulk phase using *in situ* grazing incidence X-ray diffraction. We found that the bulk phase appears at lower thickness for slower growth rates than for faster growth rates. Furthermore, we found that there is a lower contribution of the thin-film phase for slower growth rates than for faster growth rates. This is due to significant reorganization at slower growth rates as previously determined, resulting in molecules

traveling upwards on island edges and escaping the influence of the substrate and relaxing into the bulk phase.

Third, we found that at a nominal temperature of $T_s \sim 0$ °C, the transition from 3D to 2D growth occurs at a much lower growth rate than at $T_s \sim 30$ °C. Additionally, we observe a lack of evidence for bulk-phase growth. These observations suggest that the rate of upward transport is sufficiently decreased at lower temperatures to perhaps enable the growth of higher quality thin-films of tetracene.

Finally, we grew thin films of tetracene atop pre-deposited thin films of pentacene and found that tetracene grows 2D LbL for 1 ML on 1 ML-thick pentacene and grows in a 3D fashion on 2 and 3 ML-thick thin-films of pentacene. This highlights the fact that even with a lower driving force for reorganization, the roughness of the initial surface and kinetics of the processes involved in reorganization must still be considered. On the whole, these results concerning the thin-film growth of tetracene likely extend to other organic molecules and provide additional insight into the complexities arising in the thin-film growth of small molecule organic thin films.

There remain unanswered questions that could be addressed in future experiments. This dissertation has only examined two temperatures and two initial surfaces for growth. Further work can be done to determine how low the temperature can be before downward transport is arrested and growth becomes immediately 3D. Such a phenomenon has been reported for the growth of PTCDA.[1] More work can also be done to test the effect of surface energy and initial roughness of the substrate. Possible experiments include modifying SiO_2 with SAMs, which would provide, in general, very low energy surfaces compared to SiO_2. Instead of thermal oxide, we could instead use a chemical oxide with a high density of silanol groups on the surface, making this surface more hydrophilic, or perhaps use clean, annealed silicon.

More experiments can also be carried out to grow superlattices of tetracene and pentacene. Growth of tetracene has been shown on pentacene at $T_s \sim 30$ °C, but not for $T_s \sim 0$ °C, where tetracene has been shown to grow in a more 2D LbL fashion.

1.4 References

(1) Krause, B.; Schreiber, F.; Dosch, H.; Pimpinelli, A.; Seeck, O. H. Temperature Dependence of the 2D-3D Transition in the Growth of PTCDA on Ag(111): A Real-Time X-Ray and Kinetic Monte Carlo Study. *Eur. Lett.* **2004**, *65* (3), 372–378.

APPENDIX

A.1 SAMPLE COOLING IN THE G-LINE CHAMBER

The G-line chamber is fitted with a sample mount from Thermionics that enables us to heat and cool the sample. In Chapter 5, we explored the growth of tetracene on SiO_2 at nominally 0 °C. To achieve this, we used pressurized LN2 from a dewar (~60 psig) to cool and the Thermionics pBN heater to heat (push-pull). A Neslab RTE-7 water chiller at a set-point of 18.0 °C was used to cool the sample manipulator as current was applied to the sample heater. The pressurized dewar was connected to the sample manipulator's inlet for LN2 via insulated pipes, and the outlet of the LN2 from the sample manipulator was insulated and fed into the general gas exhaust with a branch for a pressure relief valve.

We measured the temperature of the substrate by using a thermocouple that mounts onto the transfer arm and touches the substrate (pictured below). Note that the "T" of the thermocouple assembly for the transfer arm was later removed, and the thermocouple was clamped directly to the transfer arm. We then compared this temperature to the reference temperature of the heater on the sample manipulator. The latter used by a Eurotherm controller for feedback control. Reference data is shown below.

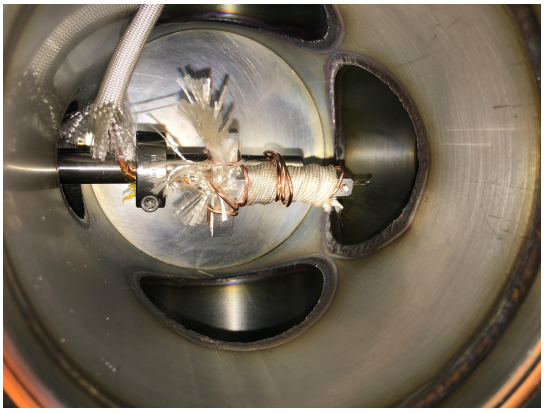

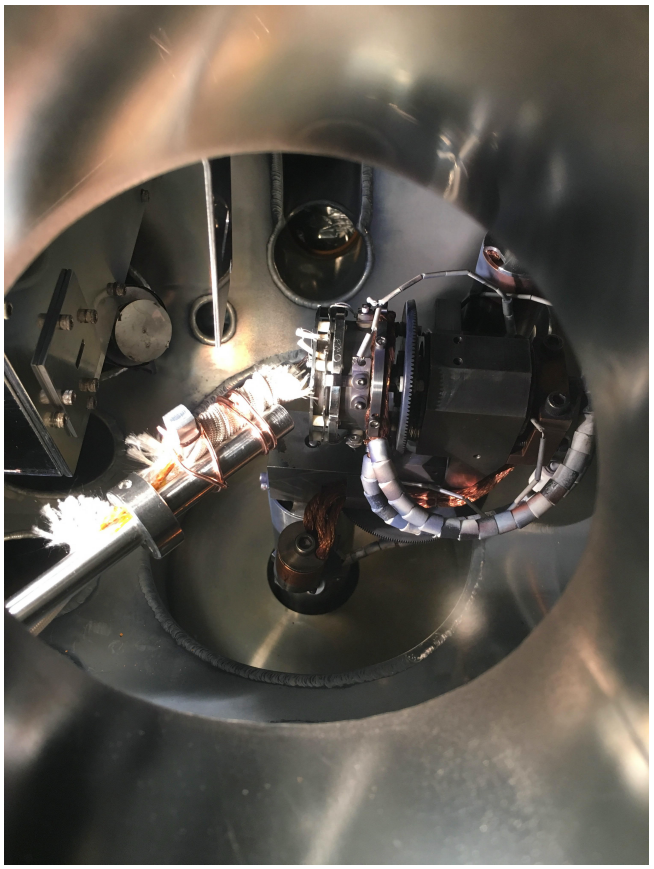

Time (min)	**$T_{transfer}$ (°C)**	**$T_{manip.}$ (°C)**	**P_{dewar} (psig)**	**Notes**
0	30.9	26.6	71	LN2 opened and cooling water on.
5	30.6	26.7	69	Sample heater set to on with set-point of T_{manip} = 0 °C.
11	29.6	26.6	67	
15	27.9	26.5	61	
20	25.5	26.2	60	
25	22.0	25.6	60	
30	18.1	24.6	60	
35	14.5	23.5	59	
40	11.1	22.0	59	
46	8.6	20.6	53	Adjusted position of thermocouple on transfer arm
50	4.2	20.1		
55	6.4	22.7		Sample heater began supplying power at this time. Position of thermocouple adjusted slightly.
60	5.4	28.1	51	
68	3.8	26.5	50	
80	2.7	19.2	49.5	
95	2.2	13.2	49	
105	1.7	10.1	49	
115	1.1	8.0	48	
127	0.6	6.1	48	
140	0.3	4.8	45	
149	0.2	4.0	44	

A.2 FITTING PSEUDO-VOIGT FUNCTIONAL TO GID IN MATLAB

To quantify the 2D GID data taken in real-time by a PILATUS 100K detector, we need to fit the diffraction peaks using a pseudo-Voigt functional. This is a combination of a Gaussian and a Lorentzian distribution. Through this exercise, we can fit the peak position and width, and then track these parameters with time. The functional form used in Chapter 4 is:

$$GG = \frac{e^{-4\ln 2(1-m)\left[\frac{(x-x_0)^2}{F_{xx}^2}+\frac{(y-y_0)^2}{F_{yy}^2}\right]}}{\left[1 + 4m\left(\frac{(x-x_0)^2}{F_x^{\,2}} + \frac{(y-y_0)^2}{F_y^{\,2}}\right)\right]}$$

where:

m = the ratio of Gaussian to Lorentzian (bounded 0-1)

x_0, y_0 = the x and y coordinates of the peak, respectively

F_x, F_y = the widths of the peaks at full-width half maximum (FWHM)

Using MATLAB, one can use the curve fitting function (‘fit’) to iteratively fit this function to each frame taken during an experiment.